STRUCTURE AND FUNCTION OF THE HUMAN INSULIN RECEPTOR: QUATERNARY 3D RECONSTRUCTION OF THE INSULIN-INSULIN RECEPTOR COMPLEX AND THE STRUCTURAL LOCALIZATION OF THE INSULIN-BINDING SITE

A Thesis

Submitted to
The School of Graduate Studies
of
The University of Toronto

By

ROBERT ZHAO-TIAN LUO

In partial fulfillment of requirements
for the degree of
Doctor of Philosophy

TABLE OF CONTENTS

LIST OF FIGURES

Chapter 1 **Page**

Chapter 2

Chapter 3

LIST OF ABBREVIATION

°C	degree Celsius
2D	two-dimensional
3D	three-dimensional
AZAP	azedo-phenylazo-aminopropyl
BBpa	biotinyl-benzoylphenoalanine
BES	baculovirus expressing system
BI	bovine insulin
BSA	bovine serum albumin
CD	connecting domain
CNBr	cyanogen bromide
CR	cysteine-rich domain
DAG	diacylglycerol
DBI	di-boc-insulin
DIPEA	di-iso-propylenthylamine
DMA	bimethylacetamide
EGF	epidermal growth factor
ELISA	enzyme-linked immunosorbant assay
EM	electron microscope
FGF	fibroblast growth factor
Fn1	fibronectin type III repeat 1
Fn2	fibronectin type III repeat 2
FPLC	fast performance liquid chromatography
g	gram
HGF	hepatocyte growth factor
hIR	human insulin receptor
hIRα	human insulin receptor extracellular domain
HPLC	high performance liquid chromatography
ID	insert domain
IGF-I	insulin-like growth factor I
IGF-II	insulin-like growth factor II
IGF-I R	insulin-like growth factor I receptor
IQAD	iterative quaternary-assisted angular determination
IR	insulin receptor
IRS-1	insulin receptor substrate-1
IRR	insulin receptor related receptor
kDa	kiloDalton
kV	kilovolts
L1	large homologous domain 1
L1-CR-L2	L1-Cysteine-rich-L2 domain
L2	large homologous domain 2
LDL	low density lipoprotein
M	molar
MABI	monoazido-benzoyl-insulin

MALTI-TOF	matrix-assisted laser desorption/ionization time-of –flight
mg	miligram
µg	microgram
MIP	molloscan insulin-like peptide
ml	milliliter
µl	microliter
mM	minimolar
MOI	multiplicity of infection
Mr	molecular weight
NG	nanogold
NGBI	nanogold-bovine insulin
NGF	nerve growth factor
nm	nanometers
NMR	nuclear magnetic resonance
PAGE	polyacrylamide gel electrophoresis
PBS	phosphate buffer solution
PDB	protein data bank
PDGF	platelet-derived growth factor
PTK	protein-tyrosine kinase
RPTK	receptor protein-tyrosine kinase
SDS	sodium doedecyl sulfate
SEM	scanning electron microscope
SH2	Src homology 2
SK	serine/threonine kinase
STEM	scanning transmission electron microscope
TEM	transmission electron microscope
TK	tyrosine kinase
TM	transmembrane domain

ACKNOWLEDGEMENT

My greatest thanks are due to my thesis supervisor, Dr. Cecil C. Yip. It is Cecil's invaluable, enthusiastic inspiration, and never ending guidance that made my research experience at the University of Toronto most wonderful. Through his dedication and persistence to scientific research, Cecil not only showed me how to conduct great science but also taught me how to be a human being with great integrity. I am also exceedingly grateful to my thesis co-supervisor Dr. F. Peter Ottensmeyer for his excellent guidance, encouragement and giving me the opportunity to access the state of the art STEM and computer image processing technique in his lab.

I am deeply grateful to other members of my graduate committee: Dr. Daniel Drucker and Dr. Jennifer Dorrington. I appreciate their contributions and critical suggestions to the fruition of this research.

I would particularly thank Dr. Margaret Moule for her helpful discussion, encouragement, enthusiastically reviewing my thesis and her expertise in research during the project. I would like to thank other colleagues and members in Dr. Yip's lab: Helga Hsu, Guoqing Zhong, Christine Mirtsos, Elaine Jack and Dr. Teresa Tallerico-Melnyk. Their consistent encouragement, technical assistance and friendship helped me finish my program. I would also like to thank colleagues and members in Dr. Ottensmeyer's lab: Allen Fernandes, Dr. Yongyi Mao, Michael Burke, Dr. Daniel Beniac, Brenda Rutherford, Yew Meng Heng and David McAlduff. Without their technical assistance, inspiring discussion and noble friendship, my project would not get any progress.

I acknowledge the financial support from the University Toronto, the Ontario Government and the Medical Research Council of Canada.

Finally, I would like to give my special thanks to my lovely wife, Dr. Hongqi Peng and daughter Nancy, for their endless support and companionship. Without their sacrifice, I wouldn't be able to stand where I am. I am extremely grateful to my parents, parents-in-law, brothers and sister for their long time encouragement and support.

STRUCTURE AND FUNCTION OF THE HUMAN INSULIN RECEPTOR: QUATERNARY 3D RECONSTRUCTION OF THE INSULIN-INSULIN RECEPTOR COMPLEX AND THE STRUCTURAL LOCALIZATION OF THE INSULIN-BINDING SITE

Ph.D. Thesis, Robert Zhao-Tian Luo, Institute of Medical Science, University of Toronto, 2000

ABSTRACT

The elucidation of the mechanism of cellular signal transduction is one of the key challenges in biology. The first step in this pathway has been particularly refractory to study. In the case of insulin action, it is the binding of insulin to its cell surface receptor, a large integral transmembrane glycoprotein. The binding of insulin results in the activation of the cytoplasmic domain of the receptor as a tyrosine kinase. While much is known about the interaction of the activated receptor with its substrates leading to down-stream signal transduction, how the binding of insulin to the extracellular domain of the receptor can lead to receptor activation remains unknown. The specific goal of this study is to localize the insulin-binding site of the insulin receptor (IR), and, if possible, to elucidate in molecular details the insulin-IR interaction and the structure-function relationship of the insulin receptor.

To achieve this goal with biochemical approach, I used the baculovirus expression system to produce in large quantity the extracellular domain of the human insulin receptor, and used various specific photoaffinity probes to identify the insulin-contacting sites. Peptide identification methods of high sensitivity were developed to detect the labeled IR fragment containing the putative insulin-binding site by HPLC peptide mapping analysis. A small fragment of 1-3 kDa that might contain the putative insulin-

binding or contacting site on the receptor α subunit was detected. However, partly due to the lack of an insulin photoprobe with a high efficiency of cross-linking, and a high efficiency peptide mapping method, I failed to obtain a sufficient quantity of the fragment for amino acid sequencing.

In an alternative approach, using gold-labeled insulin as a ligand, and sets of electron micrographs obtained by low-dose low temperature dark field scanning transmission electron microscopy (STEM) of the insulin-IR complex, I successfully reconstructed the 3D quaternary structure of the whole 480-kDa human insulin receptor (HIR), complexed with insulin, at a resolution of 20 Å. Contiguous high densities within the 3D structure indicated a two-fold symmetry for this dimeric receptor and the presence of subdomain structures which begin with the extracellular subdomain involved in insulin binding and terminate with the intracellular tyrosine kinase subdomains. These subdomains were confirmed by fitting known high-resolution crystal domain substructures. In addition, the 3D insulin-HIR complex provides evidence for the involvement of only a single insulin molecule in receptor activation. It also explains many of the known characteristics of insulin binding to its receptor and many biochemical findings in the studies of the insulin receptor.

CHAPTER 1

INTRODUCTION

1. INTERCELLULAR COMMUNICATION

In multicellular organisms communications are crucial to coordinate their function in responding to the environment and maintaining homeostasis. The growth, migration and differentiation of cells in the embryo, and their organization into specific tissues, depend on signals transmitted from one cell to another. In the adult, cell signaling orchestrates normal cellular behavior and responses to external stimuli. The basis for the intercellular communication can be viewed as ligand-receptor interaction. The receptors, either intracellular or cell surface, are expressed by cells to enable them to detect signal molecules such as hormones and growth factors in their microenvironment. Signal molecules such as neurotransmitters or growth factors may be limited to interacting with the receptors on their own cells or neighboring cells. Alternatively, many secreted signal molecules, including insulin and many hormones, circulate in the blood and interact with their target cells elsewhere in the organism. An extracellular ligand binds to a specific receptor on a target cell and converts the receptor to an active state. The activated receptor then subsequently stimulates intracellular biochemical pathways leading to an appropriate cellular response, which may involve changes in cellular gene expression, protein trafficking and metabolism. For example, the binding of insulin to its receptor activates the receptor on the cell surface, and subsequently the signal is transmitted to the cell interior to activate various intracellular pathways to elicit the proper biological responses. Alterations of these signaling pathways have been found in the pathogenesis of many diseases such as cancer, diabetes mellitus and disorders of immune and cardiovascular systems.

There are generally two categories of receptors for the circulating signals based on the lipid solubility of the ligands. Steroids, thyroid hormones as well as retinoids are lipid

soluble signaling molecules. They usually induce slower, longer-lasting responses in their target cells, which are crucial in the regulation of cell growth and differentiation. Lipid-soluble molecules can cross the plasma membrane and bind to the cytosolic receptors that function as ligand-dependent transcription factors. On the other hand, water-soluble polypeptide signal molecules, such as insulin and growth factors, are not able to cross the plasma membrane freely. They must bind to the specific cell surface receptors on the plasma membrane of the target tissues and signal via the transmembrane receptors. These glycoprotein receptors are structurally and biochemically very diverse, but they all have an extracellular ligand-binding domain, through which the polypeptide signal molecule is recognized, and an internal effector domain. The effector may function as an enzyme, such as a kinase, or a transporter, or it may interact with a cellular constituent like the subunit of G-protein, or an ion channel. The first response of the ligand-receptor interaction may involve the production of second messengers intracellularly, typically small molecules like cAMP, cGMP, diacylglycerol (DAG) and Ca^{2+}, or, in the case of the insulin receptor, the activation of the protein kinase system. The kinase cascade systems or channel activities act as switches and amplifiers of one or more biochemical pathways controlling cell metabolism, gene expression, cell cycle or cell fate (Baulieu, 1990; Fuller, 1991; Ullrich and Schlessinger, 1990).

Three major types of structurally and functionally distinct receptors have been intensively studied. They are the G-protein-coupled receptors, receptors with guanylyl cyclase activity, and receptor protein-tyrosine kinases (RPTKs). Members of the G-protein-coupled receptor superfamily feature seven transmembrane loops and comprise a big receptor family of approximately 80% of known hormones and neurotransmitters (Kobilka, 1992). Ligand-induced activation of these receptors results in the dissociation of the α- and $\beta\gamma$- subunits of the heterotrimeric G protein, leading to the activation of intracellular effector molecules for signal propagation (Clapham and Neer, 1993). The receptors with guanylyl cyclase activity have been found to bind natriuretic peptide

hormones. The downstream signal transduction of these receptors is still not very clear but an increased cGMP level was found following the activation of the receptor (Garbers and Lowe, 1994). The third group of the receptors, which bind many polypeptide hormones and growth factors, such as insulin and epidermal growth factor (EGF), have an intrinsic, ligand-sensitive, protein-tyrosine kinase (PTK) activity (Ullrich and Schlessinger, 1990; van der Geer, 1994). These structurally related glycoprotein receptors belong to a superfamily of receptor-type PTKs (RPTKs). They feature a large extracellular ligand binding domain, a single transmembrane region and an internal tyrosine kinase domain. Ligand binding to the receptor leads to the autophosphorylation of its kinase domain followed by the phosphorylation of the substrate proteins. Activation of these receptors induces diverse biochemical pathways including the generation of second messengers, alteration of enzymatic activity, and/or expression of specific genes.

As a principal polypeptide hormone controlling cell metabolism and growth, insulin has pleiotropic effects on cells and in the whole organism. Insulin acts on cells to stimulate glucose, protein, and lipid metabolism. In addition, it stimulates RNA and DNA synthesis, by modifying the expression or activity of a variety of enzymes and transport processes. The glucoregulatory effects of insulin at a whole body level are predominantly exerted by its action on liver, fat, and muscle. Insulin stimulates glucose incorporation into glycogen and inhibits the production of glucose by glycogenolysis and gluconeogenesis in liver. By affecting glycogen metabolism and gluconeogenesis in those tissues insulin regulates glucose homeostasis. Insulin also stimulates amino acid uptake in liver and muscle to increase protein synthesis. As well insulin acts as a growth factor to modify or augment the action of other regulators of cellular metabolism. Altered insulin action, such as insulin resistance, plays an important role in the pathogenesis of many disorders, including diabetes mellitus, obesity, hypertension and atherosclerosis.

In the years since the discovery of insulin by Banting and Best in 1921, much work has been done in an attempt to understand the molecular mechanism of insulin action.

(Goldfine, 1987; Kahn, 1994; White and Kahn, 1994). The identification of the insulin receptor (Yip et al., 1978, 1980; Yip and Moule, 1983; Pilch and Czech 1979), the elucidation of its primary structure (Ebina et al., 1985; Ullrich et al., 1985) and its characterization as a tyrosine kinase (Kasuga et al., 1982) served as the basis to clarify the molecular mechanism of insulin action. This was followed by the identification of downstream transducers (White et al., 1985; Sun et al., 1991). The binding of insulin to the extracellular domain of the receptor results in conformational changes leading to the activation of a tyrosine kinase in the cytoplasmic domain of the receptor. Activation of the kinase is mediated by tyrosine phosphorylation of the receptor itself. The level of tyrosine kinase activity reflects the serum concentration of insulin. The activated receptor in turn phosphorylates a substrate called insulin receptor substrate-1 (IRS-1). The multiple phosphotyrosine residues in IRS-1 serve as docking sites for the signal transduction proteins in the signaling cascade (White, 1994, Sun et al., 1995). Many signal transduction proteins, such as PI3'-kinase, SH-PTP-2, GRB-2, Syp and Nck, containing a specific recognition domain, termed Src homology 2 (SH2) domain, can specifically recognize and bind to the phosphorylated tyrosines of IRS-1. The interactions between activated receptors and SH2-containing proteins amplify the signal produced by the binding of insulin to its receptor and link insulin signaling to other kinase cascades involving serine/threonine kinases and other signal transduction pathways, such as the ras pathway. Ultimately, this process leads to stimulation of glycogen, lipid and protein synthesis, as well as translocation of insulin-sensitive glucose transporters to the surface of muscle and fat cells (Haring, 1991; White and Kahn, 1994). Malfunction of this signaling pathway, from the first step of ligand binding, through receptor autophosphorylation, to any of the postreceptor signal transducing steps, will lead to the manifestation of metabolic disorders in non-insulin dependent diabetes mellitus.

In this section, I will review the current knowledge of the insulin receptor family in terms of insulin-activated signal transduction, focusing on the structure of the receptor and the ligand-receptor interaction.

2. THE INSULIN FAMILY OF PEPTIDES

Insulin is a member of a family of hormones, growth factors and neuropeptides, found in both vertebrates and invertebrates. In addition to insulin, the family includes insulin-like growth factor I (IGF-I), and insulin-like growth factor II (IGF-II) as well as the more distantly related peptides, the relaxins, the bombysins and the molloscan insulin-like peptides (MIPs). All members of the family share a high degree of sequence homology and probably, a common "insulin fold" in the structures. Apart from the IGFs, all comprise A and B chains, joined by disulfide bonds, following the cleavage of the connecting (C) peptide in the processing of their precursors. Since the C peptides in the precursors of IGFs are retained, the IGFs are analogous to proinsulin, with the C peptide linking the C-terminal of the B chain to the A chain N-terminus (Fig.1-1).

These hormones, though sharing very similar primary sequence and structure, act quite differently, with some overlaps, in their physiologic effects. While insulin is primarily involved in regulating carbohydrate, fat and protein metabolism, the IGFs act mainly as regulators of growth, development and differentiation. IGF-I and IGF-II, but not insulin, circulate as complexes with specific binding proteins. The action of each hormone is mediated by its distinct, specific high-affinity cell-surface receptor with intrinsic tyrosine kinase activity (Czech 1982; Humbel, 1990).

2.1. Insulin

Insulin is produced exclusively by the β cells of pancreas and has a remarkable array of biological effects. Although liver, muscle and fat tissue are considered as its primary physiologic targets, insulin exerts some regulatory effects on virtually all cell

types. These effects include the mobilization of transport systems for hexoses, amino acids, ions, the acute modulation of enzyme systems such as the hormone-sensitive lipase in adipocytes, and the modulation of the transcription of specific genes, such as those encoding phosphoenolpyruvate carboxykinase. The time of onset of these effects can vary from rapid (seconds to minutes) for alterations of enzyme activities to slow (hours) for the synthesis of protein, lipid, and nucleic acid, and cell proliferation. Insulin acts through its specific insulin receptors expressed by almost all cell types, normally at a level of 10^2 to 10^5 receptor molecules per cell. The amino acid sequence of the insulin receptor has been deduced from the nucleotide sequence of its cDNA (Ebina et al., 1985; Ullrich et al, 1985).

One of the structural characteristics of insulin is that it is composed of two polypeptide chains linked by two disulfide bridges. The shorter chain, called the A chain because of its relatively acidic nature, has 21 amino acids residues and an internal disulfide bridge. The less acidic and longer B chain has 29-31 amino acids, depending on the species. There are 30 amino acids in the B chain of human insulin. This dual-chain structure and the positions of the three disulfide bridges are invariant in all the different species of insulin that have been isolated and characterized (Blundell and Wood, 1975). Within the "insulin fold" framework, the amino acid sequences of the A and B chains are highly conserved as well. For example, human insulin differs from porcine insulin by only one, and from bovine by three amino acids.

The genes encoding insulin have been sequenced and analyzed from several species, including human. The immediate translation product of the gene is a single polypeptide, preproinsulin. It contains a signal peptide at the N-terminus, which facilitates transit of the precursor into the endoplasmic reticulum. The signal peptide is cleaved away during the process. The resultant molecule, proinsulin, consisting of linked B, C, and A chains,

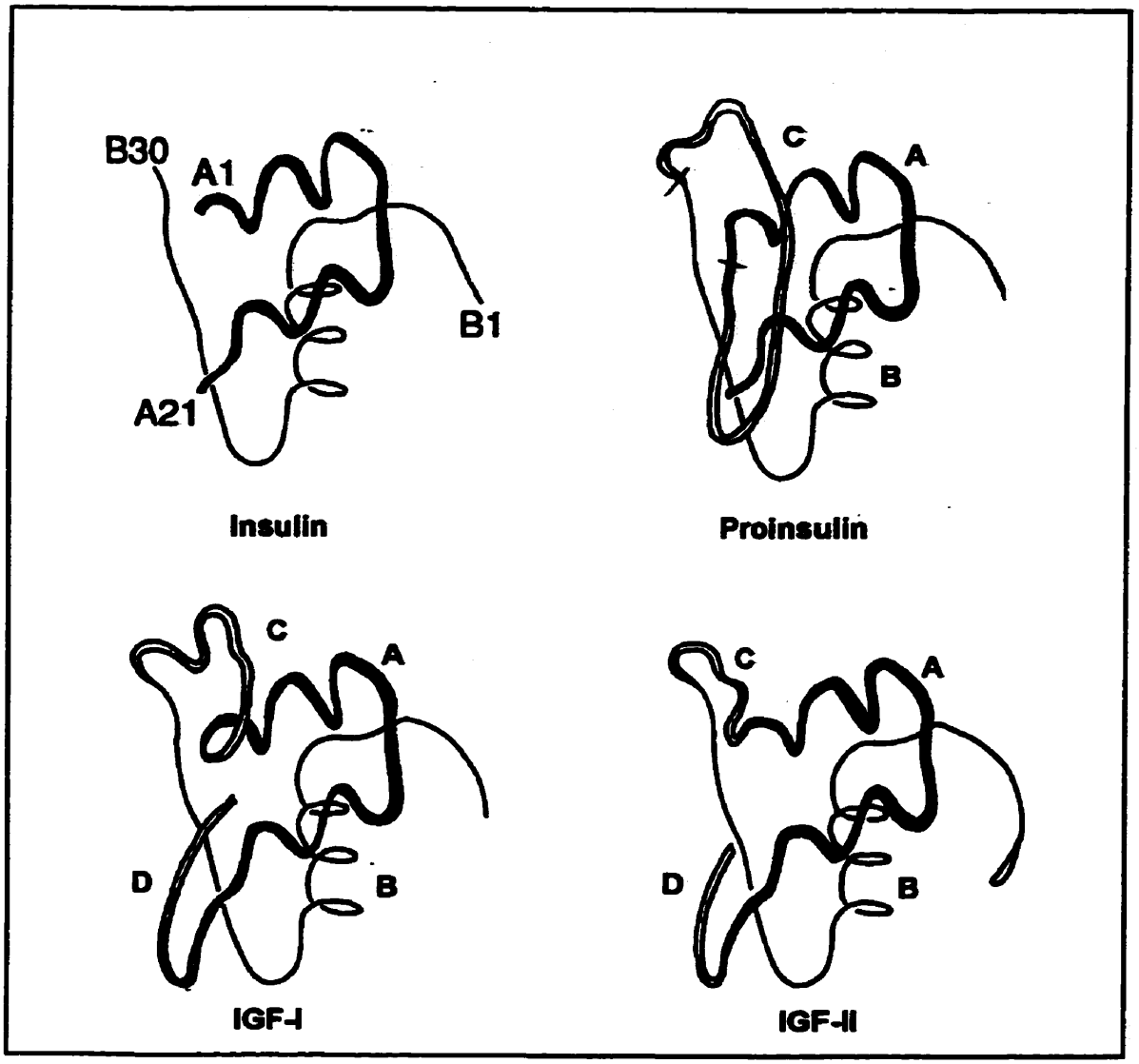

From D LeRoith et al., 1994

Fig. 1-1. Predicted tertiary structures of the insulin family of peptides. All peptides are presented to contain folding similar to that of insulin as formed by its A and B chain. The heavy line and the light line represent respectively the A chain and the B chain in insulin. Double lines represent the C chain joining the A and B chains in proinsulin, or the D extension of the A chain found in the IGFs.

is further processed into the mature insulin, a disulfide-linked polypeptide with a molecular weight of about 6 kDa.

Since the amino acid sequence of insulin was determined by Sanger and co-workers more than 40 years ago (Brown et al., 1955), our knowledge of insulin has greatly increased. In 1969, determination of the X-ray crystal structure of 2-zinc porcine insulin provided the first direct experimental evidence for the insulin fold (Adams et al., 1969). In this structure, insulin protomers form a hexamer composed of three identical dimers assembled around a three-fold axis. In the dimer the two monomers have their A and B chains folded to form compact globular structures with a number of common features (Fig. 1-2a). These include (Fig. 1-2B): 1. an A chain with 2 helices (A2-7 and A13-19), joined by an extended loop (A8-12); 2. a B chain with an extended N-terminus, followed by a helix (B9-19), a sharp turn (B20-23) and an extended C-terminal section; 3. three disulfide bridges (A6-A11, A7-B7, A20-B19); and 4. a hydrophobic core.

The crystal, and the later NMR structures, as well as the studies of insulin sequences, mutagenesis and chemical modifications have contributed to our understanding of the molecular mechanisms of receptor binding. Insulin binding to its receptor exhibits a curvilinear Scatchard plot which indicates the presence of at least two classes of binding sites or negative cooperativity between sites. It suggests that insulin, as a non-symmetric molecule, may contact its receptor at different surface sites. By analyzing the interaction of insulin analogues with the insulin receptor, Schaffer proposed a model for insulin binding to the insulin receptor (Fig. 1-2 C) (Schaffer, 1994). He hypothesized that insulin has two binding domains to contact its receptor. Binding site one is the classical binding site, studied by most investigators and comprising a number of residues (including B24, B25, A1 and A21) in the dimer-forming surface of the insulin molecule. The second binding site consists of B17 and A13, located in the hexamer-

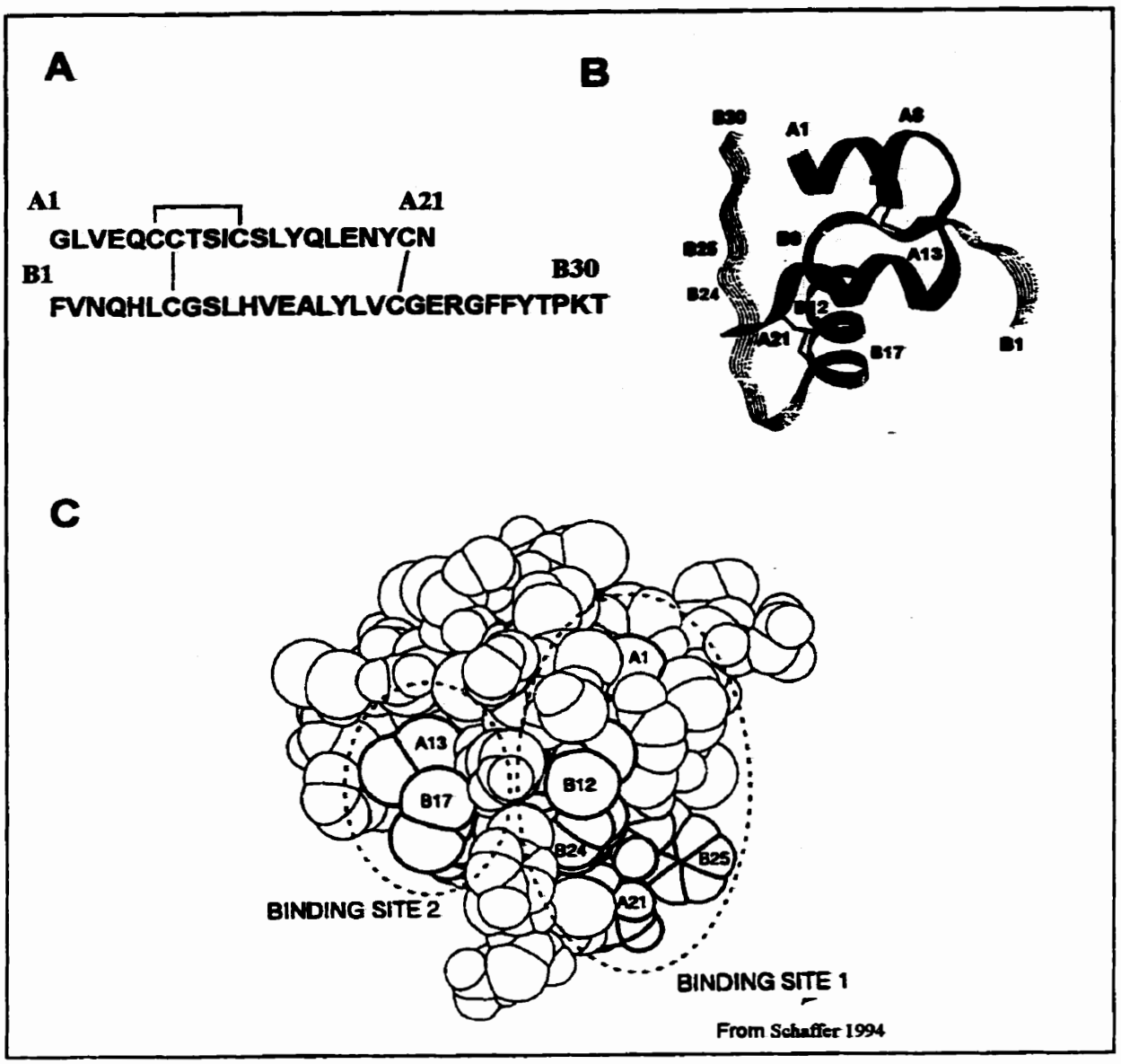

Fig. 1-2. **The primary structure (A), the 3D crystal structure (B) and the 3D space-filling model (C) of human insulin.** The 3D model (C) shows the putative receptor contacting sites (BINDING SITE 1 and 2). These two binding sites located on two separate surfaces of the insulin molecule may be involved in the the high affinity binding of insulin to the IR.

forming surface on the opposite side of the molecule from the classical binding site. Substitutions of these residues would dramatically decrease insulin affinity to its receptor. Thus, a high-affinity binding of insulin to its receptor may require the insulin receptor to contact a different binding region on the insulin molecule.

2.2. Insulin-Like Growth Factors

Unlike other members of insulin family, IGF-I and IGF-II are single-chain polypeptides of about 7.5 kDa but share similar tertiary structure and amino acid homologies with insulin (LeRoith et al., 1992). Genes encoding the IGFs have been cloned and analyzed from several species (Brissenden et al., 1984; Humbel, 1990). The mature form of IGF is a single-chain polypeptide of about 70 amino acid residues divided into contiguous B, C, A and D domains. Its structure is analogous to that of proinsulin as shown by computer-assisted molecular modeling and NMR analysis (Fig. 1-1). The A and B domain exhibit about 42% amino acid identity to the corresponding A and B chains of insulin. The C domain is analogous to the connecting (C) peptide of proinsulin. A short D domain, which is not found in proinsulin, extends at the C-terminus.

IGF-I and IGF-II, though sharing many structural properties with insulin, differ significantly with respect to their sites of synthesis and biological effects. The origin of the circulating IGF-I is the liver, where its expression is under the control of growth hormone. In the blood stream, the IGFs circulate at 1000 times higher concentration than insulin but, unlike insulin, most if not all of the circulating IGFs are complexed with specific binding proteins which are believed to modulate the action of the IGFs and to prevent hypoglycemia by lowering their effective free concentration in the circulation. In addition, IGF-I is also expressed at lower concentration in most tissues, both prenatally and postnatally, and thus functions as an important paracrine or autocrine growth factor. It is clear that IGF-I, by interacting with its own high-affinity receptor, mediates most of the effect of growth hormone on longitudinal growth. The IGFs also show insulin-like

metabolic effects *in vitro* and *in vivo*, such as glucose transport, in adipose and muscle tissue, but only at relatively high concentrations (Froesch et al., 1985). Like insulin, IGF-I also plays a role in embryogenesis. It is expressed even before the development of the embryonic liver. As in the insulin signaling system, the effects of IGF-I are mediated by a specific high-affinity IGF-I receptor which is a tyrosine kinase highly homologous to the insulin receptor.

Though IGF-II mimics most of IGF-I effects in vitro, its biological roles are still not clear. It has been suggested that IGF-II may be involved in the fetal development since its expression dramatically decreases just before birth in both amount and the range of tissue distribution. In contrast to IGF-I, IGF-II receptor has no structural similarity to either the insulin or IGF-I receptor. This receptor is in fact the same molecule as the cation-dependent mannose-6-phosphate (Man-6-P) receptor, a protein that targets the Man-6-P-containing proteins to lysosome (Massague et al., 1982), and its role in the action of IGF-II remains unknown. It has been proposed that most of IGF-II effects are mediated through IGF-I or insulin receptors (Czech, 1989).

2.3. Other members of the Insulin family

Several other polypeptides with highly homologous sequences to insulin have been discovered. Some have been found in the vertebrates and others have been identified in proto-chordates, insects and molluscs. They are bombyxins, relaxins and MIPs. The sequence data suggest that they share similar three-dimensional structures and conformation. Unlike insulin and the IGFs, these distantly related members show more divergence. Interestingly, most residues in the extended receptor-binding region of insulin are well conserved in these family members, which suggests possible heterologous ligand-receptor interactions. Relaxin has been identified in several species, including human. In human, relaxin has been identified mainly as a paracrine/autocrine hormone regulating activities in the uro-reproductive system (Schwabe et al., 1994). The

interaction of relaxin with its receptor at the molecular level is still poorly understood, and the receptor itself has not been well characterized.

3. MOLECULAR AND CELL BIOLOGY OF THE INSULIN AND IGF-I RECEPTORS

As the proteins primarily responsible for transducing the signals for insulin and IGF-I, the insulin and IGF-I receptors, like their ligands, are the products of homologous genes (Abbott et al., 1992). The characterization of cDNAs encoding the insulin and IGF-I receptors revealed a high degree of similarity in the primary nucleotide and amino acid sequences, their overall structures, and enzymatic activities. Both receptors are glycosylated heterotetramers, composed of two α subunits of ~130 kDa and two β subunits of ~90 kDa linked by disulfide bonds. The α subunit, which is entirely extracellular, contains the ligand-binding domain, while the β subunit consists of an extracellular domain, a transmembrane domain, and a tyrosine kinase (TK) domain. Among the similarities between the insulin receptor (IR) and IGF-I receptor (IGF-I R), the highest amino acid homology (84%) is found in their TK domains, while the overall amino acid homology between their β subunits is only 44-60%. Both IR and IGF-I R belong to a membrane receptor superfamily called the receptor tyrosine kinase (RTK). Members of this superfamily possess intrinsic tyrosine kinase activity and are structurally similar.

3.1. The Receptor Tyrosine Kinase Superfamily

Tyrosine Kinase and Receptor Tyrosine Kinase

Insulin and IGF-I receptors were among the first RTKs identified in the early 1980s due to their ligand-stimulated autophosphorylation (Kasuga et al, 1982). More than 100 proteins with the consensus sequences characteristic of TK have been cloned and characterized from a variety of eukaryotic species (Hunter and Cooper, 1985). Acting as

an on/off switch in signal transduction, the protein phosphorylation/ dephosphorylation cycle plays a key role in controlling various cellular processes. Protein kinases catalyze the transfer of a phosphate group from a donor, usually the γ phosphate of ATP, to an acceptor amino acid in a substrate protein. Serine/threonine kinases (SKs) phosphorylate serine or threonine residues of substrate proteins whereas tyrosine kinases (TK) specifically phosphorylate protein substrates on their tyrosine residues. Hunter et al have demonstrated the existence also of protein-histidine kinases that phosphorylate histidine residues of substrate proteins (Hunter, 1991). Some protein kinases are able to phosphorylate all three hydroxy amino acid residues.

Members of the protein kinase family share highly conserved amino acid sequences in their catalytic domain. Based on their cellular location they can be divided into two classes: cytoplasmic and membrane bound. Cytoplasmic enzymes serve as molecules of signal transduction inside the cells. Transmembrane kinases, such as the insulin receptor family, transfer signals across the cell membrane and activate cytosolic kinases. It is interesting that TKs are found only in multi-cellular organisms, whereas SKs are found in both single cell and multi-cellular organisms. This suggests that the tyrosine specificity may have been an evolutionary development related to the acquisition of multi-cellularity and cell-cell communication.

The overall architecture of all RTKs is very similar: a large glycosylated extracellular domain that binds the polypeptide ligand; a single hydrophobic transmembrane domain; and an intracellular domain containing a highly conserved TK catalytic region. Interestingly, some cytoplasmic TKs are not transmembrane but anchor at the inner surface of the plasma membrane and are coupled to transmembrane glycoprotein receptors which do not have cytoplasmic kinase domain. This coupling allows them function like a transmembrane RTK. T cell antigen receptor-fyn, growth hormone receptor-Jak2, and interleukin-jaks are examples.

Based on the comprehensive analysis of the primary sequences, RTKs are subdivided into many subfamilies according to their unique and shared structural features (Fantl et al., 1993; van der Geer et al., 1994). More than ten subfamilies have been classified over the last few years. The best characterized subfamily members include: epidermal growth factor (EGF) receptor, platelet-derived growth factor (PDGF) receptor, insulin and IGF-I receptors, nerve growth factor (NGF) receptor, fibroblast growth factor (FGF) receptor, and hepatocyte growth factor (HGF) receptor (c-met). Most of the RTK family members are single-chain polypeptide receptors, except for the insulin receptor subfamily. Members of the insulin receptor subfamily include insulin receptor, IGF-I receptor and insulin receptor related receptor (IRR) with their unique $\alpha_2\beta_2$ tetrameric structure. The structural similarities within a subfamiliy suggest that receptors in a subfamily share similar mechanisms of molecular regulation and signal transduction pathways, as in the case of insulin and IGF-I receptors.

The catalytic domains of protein kinases are 250-300 amino acid residues in length mostly located near the carboxyl terminus or as a subunit of multi-subunit enzymes (Hanks et al., 1988; 1991). The three-dimensional structure of the TK domain of the insulin receptor exhibits a highly conserved bi-lobular structure (Hubbard et al., 1994; Hubbard, 1997). In the large lobe of the TK domain, an extended sequence containing Tyr1158, Tyr1162 and Tyr1163 forms a flexible loop, called the activation loop (A–loop). During activation, the A-loop undergoes a major conformational change upon autophosphorylation of the three tyrosine residues within the loop, resulting in unrestricted access of ATP and protein substrates to the kinase active sites. Although both SKs and TKs share a basic structure, TKs have the extended A-loop sequence in the larger lobe. It may explain the specificity for tyrosine since serine and threonine hydroxyls may be too short to reach the phospho-transfer site within the catalytic center (Hubbard et al., 1994).

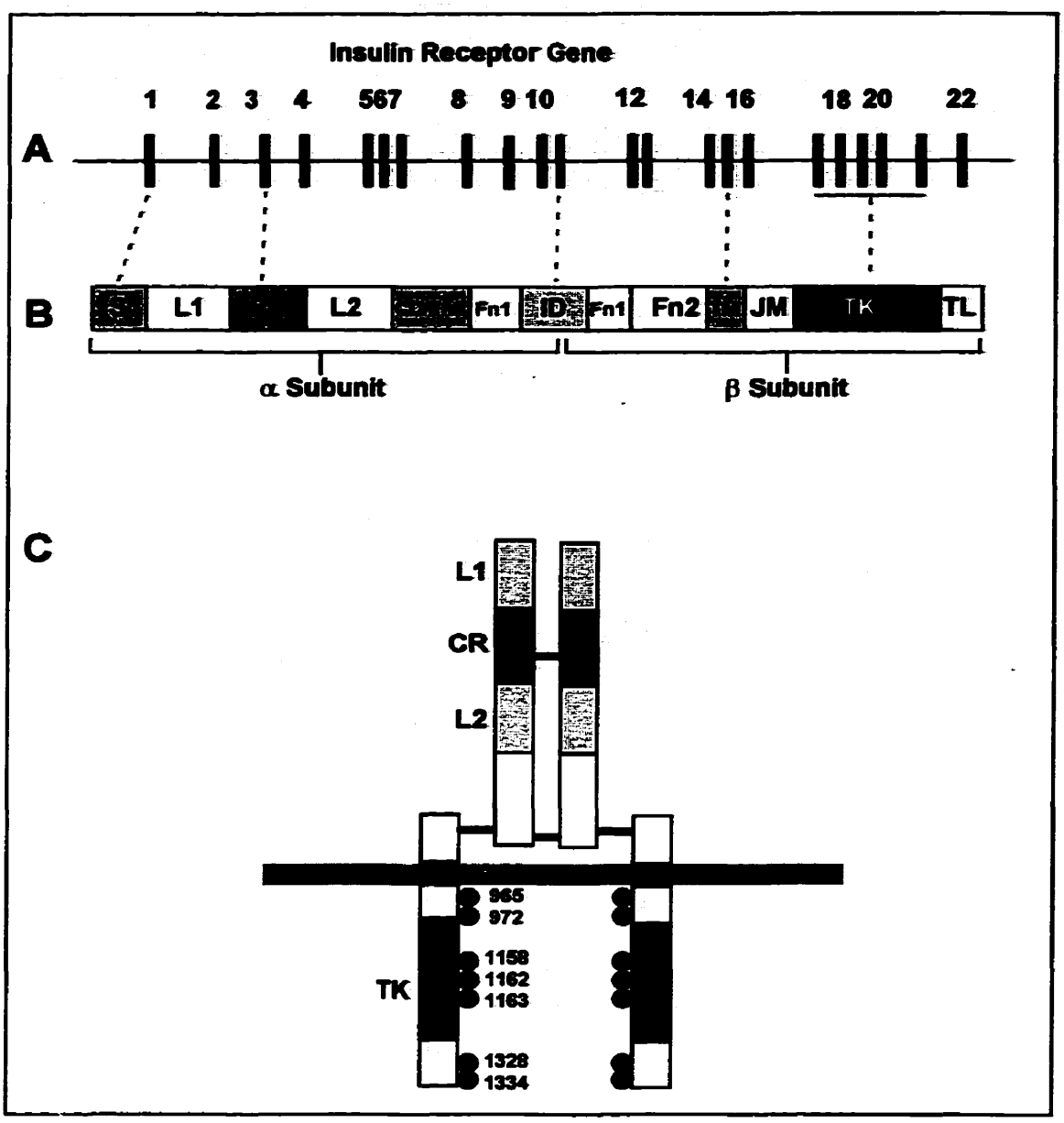

Fig. 1-3. Schematic representation of the insulin receptor gene (A) and the primary (B) and secondary (C) structure of hIR. Receptor domains encoded by specific exons are indicated (A and B). Labels: S=signal peptide, L1,L2=L1 and L2 domains, CR=cysteine-rich domain, CD/Fn0=connecting domain or fibronectin III repeat, Fn1,Fn2= fibronectin III repeats, ID=insert domain, TM=transmembrane domain, JM=juxtamembrane domain, TK tyrosine kinase domain, TL=C-terminal tail. Disulfide bonds connecting α–α and α–β subunits are indicated by ▬ and possible phosphorylation sites are indicated by ● (C).

3.2. Insulin Receptor

Gene structure and Expression

The insulin receptor (IR) is the product of a single gene located on the short arm of chromosome 19 (19p7) near the gene of the LDL receptor (Yang-Feng et al., 1985). The structure of this gene has been elucidated by both restriction mapping (Muller-Wieland et al., 1989) and genomic cloning (Seino and Bell, 1989; Seino et al., 1990). The human IR gene, composed of more than 150 Kb of DNA, has 22 exons and 21 introns. Exon 1 through 11 are spread over 90 Kb and code for the α subunit. Exons 12 through 22 span 30 Kb and code for the β subunit (Fig. 1-3). The promoter of the IR gene is of the typical GC-rich "housekeeping" type with a few binding sites for enhancer protein (McKeon et al., 1991).

The receptor is synthesized in the rough endoplasmic reticulum (RER) as a single polypeptide chain proreceptor of either 1339 or 1351 amino acids, depending on the differential splicing of exon 11. The pre-receptor has a 27 residue N-terminal signal peptide that assists in the intracellular translocation of the receptor precursor. The signal peptide is subsequently cleaved off. The proreceptor is transported through the Golgi apparatus, where it rapidly undergoes extensive N- and O-linked glycosylation. Two monomeric proreceptors are then linked by the formation of disulfide bonds into a dimeric structure. Proteolytic removal of a tetrabasic amino acid sequence (Arg732-Lys-Arg-Arg735, numbering based on Ebina et al., 1985) from each proreceptor monomer gives rise to the α and β subunit. Further glycosylation takes place before the mature insulin receptor is inserted into the plasma membrane (Olson et al., 1988). The final active mature receptor is a fully glycosylated tetrameric transmembrane protein, composed of two α subunits and two β subunits (Fig. 1-4). Each α subunit is comprised of 719 or 731 amino acids. There are 620 amino acid residues in each β subunit including an extracellular portion of 194 residues, a transmembrane region of 23 amino acids, and a cytoplasmic domain of 403 residues.

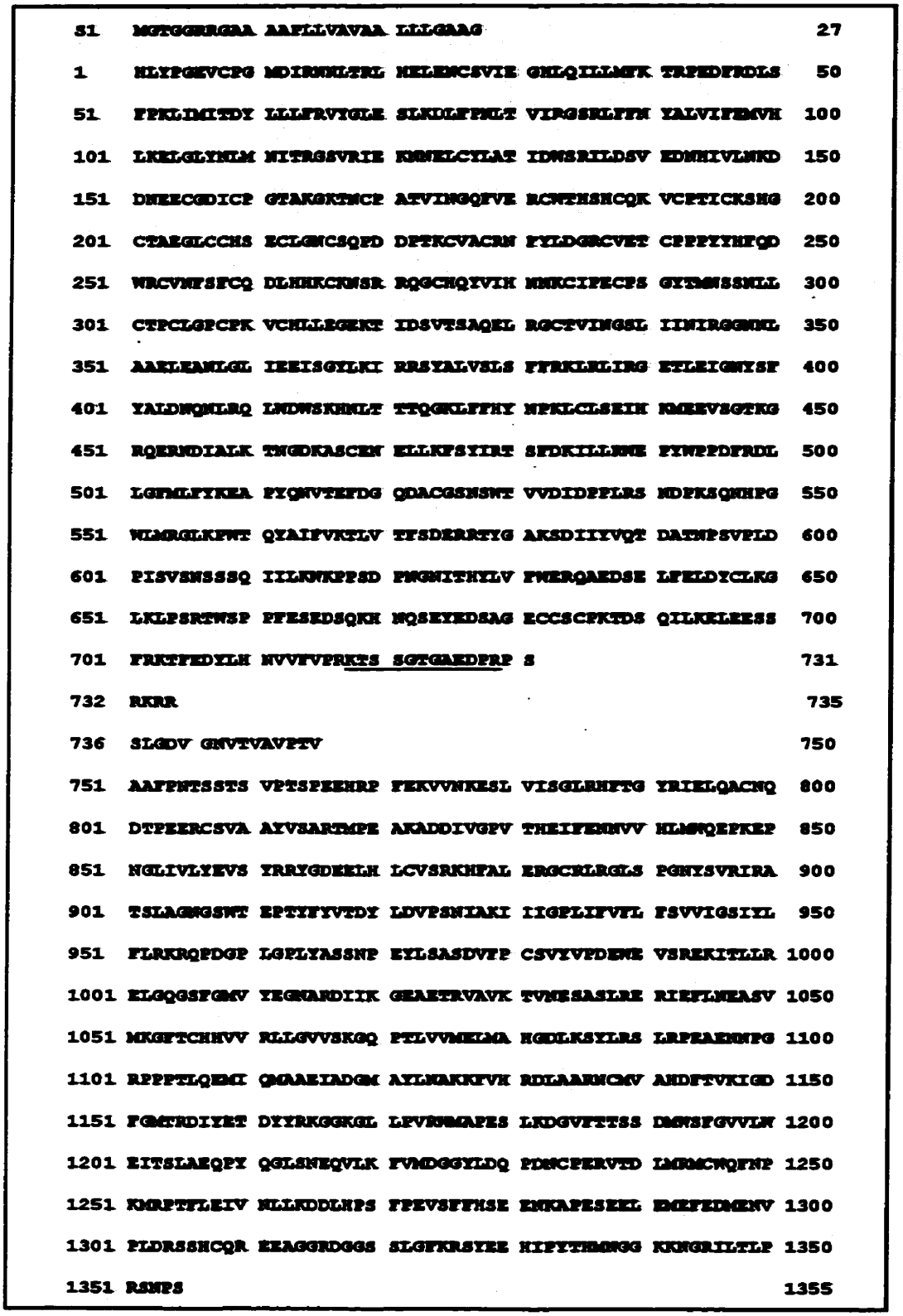

Fig. 1-4. **Human insulin receptor amino acid sequence** (from Ebina et al., 1985) Residues s1 to s27 are the signal sequence. Residues 1 to 731 constitute the α subunit, and residues 735 to 1355 constitute the β subunit. The polybasic residues 732 to 735 are the enzymatic cleavage site to yield the α and the β subunits. Underlined residues are encoded by Exon 11.

Structure and Function

The heterotetramer structure of the insulin receptor was initially elucidated in the late 70s by cross-linking radioactive insulin to either whole cells or plasma membranes (Yip et al., 1978; Pilch et al., 1979). Later, purification of the receptor led to cloning of its cDNA (Ebina et al., 1985; Ullrich et al., 1985). While the primary sequence of the IR has been known for some time (Fig. 1-4), knowledge of the secondary and higher order structures of the receptor are limited. Based on current knowledge of insulin receptor function, and the function of RTK proteins, it seems reasonable to propose that specific functional properties of the IR reside in its separate domains. A major advance in understanding the overall receptor structure was the model proposed by Bajaj and co-workers (Bajaj et al., 1987). They proposed that the N-terminal half of the IR contained two large homologous domains (L1 and L2) separated by the cysteine-rich domain (CR) which itself was comprised of three repeating units each containing eight cysteine residues. A second major development was the observation that the C-terminal portion of the extracellular region of IR contains three fibronectin type III repeats (here designated as Fn0, Fn1 and Fn2) linked to the L2 domain (Marino-Buslje et al., 1998; Mulhern and Booker, 1998; Ward 1999). The first repeat, Fn0, or identified as the connecting domain (CD) by some authors, located in the α subunit consists of 123 amino acid residues. The second repeat (Fn1) is a structure with contributions by both the α and the β subunit, connected with a so-called insert domain (ID) that includes both the α–β cleavage site and the alternative-spliced exon 11 (O'Bryan et al., 1991). The third repeat (Fn2) is part of the β subunit. The extracellular region also provides the two disulfide-bonds that covalently link the $\alpha\beta$ monomers to form the constitutive IR dimer. One of them is in the Fn0 region and the other is located in the α insert domain. The extracellular portion the IR is followed by a short, single transmembrane domain (TM) connected to the intracellular portion of the β subunit that contains the TK domain. The crystallographic

structure of the TK fragment of the β subunit was determined several years ago (Hubbard et al., 1994), but the three dimensional structure of the holoreceptor remains unknown.

The general structural domain layout of the IR agrees with the suggestion that insulin binds to the extracellular domain leading to the transmembrane activation of the intracellular TK of the β subunit.

The α Subunit

The α subunit of the IR is entirely extracellular containing either 719 or 731 amino acids depending on whether or not exon 11 is expressed (Seino and Bell, 1989). A characteristic feature of the α subunit is its cysteine-rich region which contains twenty four of the thirty seven cysteine residues in the α subunit. The function of the cysteine-rich domain is not fully understood, but it has been suggested that it is involved in binding to insulin (Yip et al, 1988, Rafaeloff et al., 1989; Gustafson and Rutter, 1990). Homologous cysteine-rich regions are also seen in the low density lipoprotein (LDL) receptor, IGF-1 receptor and epidermal growth factor (EGF) receptor (Goldstein et al., 1985; Ullrich et al., 1984,1986). These regions in IGF-1 and LDL receptors have been shown to bind to their ligands. However, in the case of the insulin receptor, it is still controversial as to whether the cysteine-rich domain is directly involved in insulin binding.

There are 37 cysteine residues in each α subunit monomer. Most of them appear to form intrachain disulfide bonds within the α subunits, mainly in the Cys-rich region. On the other hand, some cysteine residues form disulfide bonds joining α–α or α–β subunits, which contribute to the important conformation of the functional receptor (Finn et al., 1990). There are two classes of disulfide bonds in the IR. Class 1 disulfide bonds link α–α subunits, while class 2 disulfide bonds join the α–β subunits. The latter is more resistant to reduction than those of class 1. The mature insulin receptor is a disulfide

linked heterotetramer, including one disulfide on each α–β connection and more than one on the α–α cross-linking.

Based on the structural analysis of the IR subjected to mild tryptic proteolysis, the C-terminal 25 kDa fragment of the α subunit was found to be involved in α–β disulfide bonding (Shoelson et al., 1988; Xu et al., 1990). Cys647 located in this region has been reported to be vital to the α–β bond formation (Cheatham and Kahn, 1992). Recently, Sparrow et al confirmed that Cys647 in the Fn1 of the α subunit forms a disulfide bond with Cys872 in the Fn2 of the β subunit (Sparrow et al., 1997).

Until recently the disulfide bonds connecting the two α–α monomers together were unknown. Schaffer and his co-worker first noticed that the Cys524 upstream of the Fn1 domain contributes an α–α interchain disulfide bond (Schaffer and Ljunqvist, 1992). Other investigators (Macaulay et al., 1994; Bilan and Yip, 1994) suggested that additional disulfide bonds exist between the α–α dimer, which is probably located in the cysteine-rich domains. Surprisingly, the second disulfide bond connecting the α–α dimer has been recently localized to one of the cysteine triplet, Cys682, 683, and 685 at the end of the C-terminal region of the α subunit (Sparrow et al, 1997).

Bajaj et al (Bajaj et al, 1987) proposed, in addition to the cys-rich region, two similar but independently folded subdomains, L1 (encoded by exon1-2, residues 1-156) and L2 (encoded by exon 4-6, residues 310-470), each being mainly β-pleated sheet in structure. Between L1 and L2 is the cysteine-rich (CR) domain (residues 157 to 309, encoded by exon 3-4). Based on sequence alignment and secondary structure prediction, Bajaj et al. proposed that the L1 and L2 domains juxtaposed and extended away from the cell membrane, with the CR domain underlying and supporting them (Bajaj et al., 1987). The recently determined crystal structure of a fragment containing the first three domains (L1-CR-L2) of IGF-IR, a receptor closely related to IR (Garrett et al, 1998), shows that the layout of the three domains was quite different from that proposed by Bajaj et al. The remaining regions of the α subunit (residues 471-731, encoded by exon 8 to 11) consist

of a fibronectin III repeat (Fn0, residues 471-593, also called connecting domain (CD)), part of the second fibronectin III repeat (Fn1, residues 594-661) and a 71 residues insert domain (ID) (O'Bryan et al., 1991, Schaefer et al., 1992). L1, L2 and CR domains have been suggested to be involved in insulin binding (Haynes et al., 1986; Yip, 1988,1992,1993; De Meyts, 1994) and in both α–α and α–β disulfide bond formation (Cheatham and Kahn, 1992; Schaffer and Ljunqist; 1992, Bilan and Yip, 1994; Sparrow et al, 1997). Little is known about the function of the insert and connecting domains.

The quaternary structure of IR has not been determined. Schaefer et al. (Schaefer et al., 1992), using electron microscopic image technique, reported that the extracellular domains of the IR (the entire α subunits plus the extracellular domains of the β subunits) in solution had a "Y" shape with globular features at the end of each arm of the "Y". Similar studies also showed the solubilized placenta holoreceptor as a "T" shaped structure (Christiansen et al., 1991). These studies suggest that the receptor has two extracellular arms, each of which may represent a separate α subunit. The authors also suggested that each of the subunits would contribute one independent insulin-binding site. There has been no report of the successful crystallization of the insulin receptor. Its large size (M_r 450 kDa) and its glycoprotein nature may account for the lack of success in its crystallization. It is also too large for NMR analysis.

Early studies using the technique of photoaffinity labeling (Yip et al., 1980) and chemical cross-linking (Pilch and Czech, 1980) have clearly shown that insulin binds to the α subunit of IR. Although the entire α subunit could be involved in contacting insulin, recent studies on insulin-receptor interaction have gradually focused on the L1-CR-L2 region (White and Kahn, 1994). Since no structural information on the IR α subunit or its fragments is available, the structure of the L1-CR-L2 domain of IR now can only be inferred from the x-ray structure of its counterpart of IGF-IR (Garrett et al, 1998). The overall structure of the L1-CR-L2 domains of IGF-IR was shown as a notch shape structure. Each L domain is a single-stranded right-handed β-helix. The cysteine-rich

region is composed of eight disulfide-bonded modules, seven of which form an elongated rod shape domain connecting the L1 and L2 domain. The three domains surround a center space of sufficient size to accommodate a ligand molecule. Although this fragment is incapable of binding to IGF-I, this structure does provide clear information that the L1-CR-L2 region is a putative region for ligand binding.

Two isoforms of the insulin receptor, differing in length by 12 amino acids near the C terminus of the α subunit, are derived from the alternative splicing of exon 11. This results in a smaller A isoform of 1339 amino acids and a larger B isoform of 1351 amino acids (Ullrich et al., 1985; Ebina et al., 1985). Both isoforms (- and + exon 11) are expressed in most tissues in various proportions. The functional differences between the two isoforms are not clear. It seems that isoform A has a relatively higher affinity for both insulin and IGF-I and is more rapidly internalized and down regulated (Mosthaf et al., 1991; Voge et al., 1991; Yamaguchi et al., 1991). The mechanism of this change in affinity by a structural variation distant from the presumed binding site is uncertain. However, mutant insulin receptors with mutations at the cleavage site have been reported with markedly reduced affinity to insulin (Williams et al, 1990; Sasaoka et al., 1993). This suggests that the C-terminal of the α subunit may contribute to a conformation for high affinity ligand binding. Interestingly, Frasca et al recently reported that insulin receptor isoform A binds to IGF II with an affinity close to that of insulin. It actually serves as a high-affinity IGF II receptor affecting growth of fetal and cancer cells (Frasca et al., 1999; Sciacca et al., 1999). This finding also suggested that the small variation in the C-terminal of the α subunit plays an important role in the conformation for high affinity ligand binding.

The β Subunit

The β subunit of the insulin receptor contains an extracellular domain of 193 amino acids, a single transmembrane domain of 23 amino acids, and an intracellular portion of

402 amino acid residues. The intracellular portion of the β subunit can be further subdivided into three functional domains: a juxtamembrane domain, a tyrosine kinase domain and a C-terminal domain. The tyrosine kinase domain has been recently crystallized and its structure determined (Hubbard et al., 1994). The main function of the β subunit is to react to the signal generated by extracellular insulin binding.

Relatively little is known about the function of the extracellular domain of the β subunit. It contains a half (Fn1) and a full (Fn2) fibronectin domain and four cysteine residues. Cys872 in the Fn2 region forms the interchain bonding between the α and β subunits (Cheatham and Kahn, 1992, Sparrow et al., 1997). There are also sites for both N-linked and O-linked glycosylation (Edge et al., 1990). A monoclonal antibody to this region allows normal insulin binding but inhibits receptor autophosphorylation and biological signaling (Gherzi et al., 1987), suggesting that this domain likely plays a role in receptor signal transduction.

Besides the putative signal transduction function, the extracellular domain of the β subunit may play a critical role in the conformation of the high affinity binding site of the α subunits. Schaefer et al. (Schaefer et al., 1990) demonstrated that truncated insulin receptors with all or part of the extracellular domain of the β subunit deleted dramatically lost their insulin-binding affinity. The minimal truncated receptor maintaining full binding affinity is the complete extracellular domain, including both α subunits and the entire extracellular part of the β subunits. They suggested that, even though the β subunits do not directly participate in insulin binding, their existence is critical in forming the right conformation for the high affinity binding site in the α subunits.

The transmembrane domain of the β subunit is a single α–helical segment of 23 residues which links the extracellular and intracellular domains of the receptor. This physical connection between the extracellular and intracellular region of the β subunit is implicitly crucial to signal transduction. However, mutations or replacement of this region with the transmembrane region of other receptor family members did not affect the

function of the receptor (Yamada et al., 1992, Frattali et al., 1991). Thus, it appears that the structural requirements of this region for signal transduction are not restrictive.

The juxtamembrane domain is a short fragment of 48 residues at the beginning of the intracellular portion of the β subunit. Two essential functions have been found for the juxtamembrane domain: receptor internalization and signal transmission. Interestingly, both functions relate to the specific NPXY motif in this region (Feener et al., 1993). They are NPEY at position 969-972 and GPLY at residues 962-965.

The NPXY motif has been indicated to interact with adaptor proteins in coated pits to facilitate receptor endocytosis (Brown and Greene. 1991). Mutagenesis of this domain has shown that the ligand-induced IR endocytosis was abolished. More recently, the NPXY-motif has been identified as the interacting site with insulin receptor substrates, such as IRS-1/IRS-2, and Shc (Keegan et al., 1994; O'Neill et al., 1994). Mutations at or near Tyr 972 inhibit insulin stimulated tyrosine phosphorylation of IRS-1/IRS-2 and Shc (White et al., 1988, White & Khan 1994). The phosphorylation of IRS relies on the engagement of the phosphorylated NPXY-motif in the insulin receptor (Sun et al., 1995; Keegan et al., 1994).

The tyrosine kinase domain is the most conserved region among the family of RTK (White and Kahn. 1986; Ullrich and Schlessinger, 1990). It contains an ATP-binding region and a so-called regulatory or catalytic region. The ATP-binding region composed of an invariant sequence GXGXXGX located at residues 1003-1008 of the insulin receptor, followed by a lysine residue located distally 10 to 20 residues toward the C-terminal. The Lys_{1030} in this region provides an ATP-binding site through a salt bridge. Point mutation of Lys_{1030} disrupts both ATP binding and kinase activity (Maegawa et al., 1988), and leads to severe insulin resistance (Taylor et al. 1992).

There are 13 tyrosine residues in the cytoplasmic portion of each β subunit. Phosphopeptide mapping demonstrated that 8 of the tyrosine residues are critical for exogenous tyrosine kinase activity and insulin receptor biological activities (White et al.,

1988; Kohanski et al., 1993; Feener et al., 1993). These tyrosine residues are located in three clusters in the primary structure: Tyr965, 972, and 984 in the juxtamembrane region, Tyr1158, 1162, and 1163 in the kinase catalytic domain, and Tyr1328 and 1334 in the C-terminal tail. This numbering system includes exon 11. The three tyrosine residues, Tyr1158, Tyr1162, and Tyr1163, lying in the kinase activation loop (A-loop, residues 1149-1170) are the most important site of autophosphorylation of the IR. Autophosphorylation of all three tyrosine residues in the YXXXYY motif of the activation loop occurs within seconds after insulin stimulation and stimulates tyrosine kinase activity by 10-20-fold (White et al. 1988). Mutation of one, two or three tyrosine residues in this region progressively reduces insulin-stimulated kinase activity and results in a parallel loss of biological activity (Vogt et al. 1991; Wilden et al. 1992). The crystal structure of the tyrosine kinase domain of the insulin receptor β-subunit not only shows the fine structure of the kinase domain but also provides important information on the mechanism of kinase activation (Hubbard et al. 1994, Hubbard, 1997). In the inactive state, Tyr1162 in the A-loop competes with protein substrates for binding in the active site. During activation, the A-loop undergoes a major conformational change upon autophosphorylation of Tyr1158, 1162 and 1163, resulting in unrestricted access by ATP and protein substrates to the kinase active site. The crystal structure of the kinase domain also indicates that autophosphorylated Try1163 plays a role in stabilizing the phosphorylated A-loop and suggests that Tyr1158 may provide a docking site for downstream signaling proteins.

The C-terminal region of the IR exhibits maximal divergence between IR and other RTKs (Ullrich et al., 1986). Therefore, it has been proposed that it contributes to specificity in transmembrane signaling. It also contains a second major region of autophosphotylation (Tyr1328, and Tyr1334) in the IR β subunit. However, the exact role of phosphorylations of these tyrosines in insulin action is still not clear since kinase activity in the C-terminal truncated IR is normal (Myers et al. 1991; Takata et al., 1992).

It also contains a few serine/threonine phosphorylation sites stimulated by several stimulators, including insulin. The function of serine/threonine phosphorylation in this region remains controversial (Yonezewa et al., 1991; Hotamisligil et al., 1993).

3.3. IR, IGF-1R and IRR: Similarity and Divergence

Three receptors, insulin receptor (IR), IGF-I receptor (IGF-IR) and insulin receptor-related receptor (IRR), in the RTK family share a high level of overall structural similarity. Although their genes have been mapped to different chromosomes (chromosome 19, 15 and 1, respectively), IR, IGF-IR and IRR have similar amino acid sequences and identical exon/intron organization (Ebina et al. 1985, Ullrich et al. 1986, Shier & Watt. 1989, Abbott et al. 1992). All three receptors are synthesized as a single polypeptide that is processed to yield distinct α and β chains joined by disulfide bonds into a $\alpha_2\beta_2$ heterotetrameric complex. Whereas the IR and IGF-IR have a tetrabasic cleavage site, RKRR, the IRR has an RHRR at this site. All three have a completely extracellular α subunit that contains a region of approximately 150 residues which is particularly rich in cysteines. However, these cysteine-rich regions show a lower sequence homology than surrounding regions (~45% compared to ~65%). This difference has been implicated in some studies as playing a role in determining ligand specificity (Zhang and Roth, 1991; Kjeldsen et al., 1991; LeRoith et al., 1994). The β subunit consists of both extracellular and intracellular domains connected by a transmembrane domain. The intracellular tyrosine kinase domain is highly homologous in all subfamily members.

While the IR and IGF-IR share a very close sequence homology, IRR is less similar. Most notably, the β subunit of IRR is only 551 amino acids long versus 620 and 627 amino acids for that of the IR and IGF-IR, respectively (Shier and Watt, 1989). This size difference is in large part accounted for by the carboxyl-tail of IRR which lacks 48 amino

acids including the two C-terminal tyrosines and the serine/threonin phosphorylation sites present in other two receptors. In contrast to the highly conserved ATP-binding and tyrosine kinase region in all three receptors (79-84% identical), the sequence homology in the carboxyl-tail region of the three receptors is remarkably low (19-44%).

Despite their structural similarities, the insulin and IGF-I receptors mediate different physiological effects. The insulin receptor regulates metabolism as well as some development and growth (Lee and Pilch, 1994). The IGF-I receptor, on the other hand, is noted for mediating the growth-promoting action of IGF-I, as well as some of the effects of IGF-II (Humbel et al., 1990). The ligand for IRR is still unknown. It is interesting that the insulin receptor, besides binding insulin with high affinity, also binds IGF-I and II with about 100-fold weaker affinity (Anderson et al., 1990; LeRoith et al., 1994). However, the IGF-I receptor has a very low affinity for insulin. There is also a small amount of naturally occurring hybrid IGF-I/insulin receptors which contain $\alpha\beta$ halves of both the insulin and IGF-I receptor (Mosthaf et al., 1990, Siddle et al., 1994) with low affinity to either ligand. The function of the hybrid receptor is not clear.

Taking advantage of the similarities and differences in the domain structures and their big difference in affinity for their ligands, especially in the case of IR and IGF-IR, investigators have an opportunity to study the ligand binding sites and specific signaling pathways. Several chimera receptors with switched domains between IR and IGF-I have been studied. These studies have revealed important information in the understanding of the interaction of ligand and receptor (Anderson et al., 1990; Zhang and Roth, 1991; Schumacher et al., 1993).

4. INSULIN BINDING AND SIGNAL TRANSDUCTION

4.1. Affinity and Kinetics of Insulin Binding

Insulin binds to its receptor in a rapid and reversible manner. The affinity constants vary around 10^9 M^{-1}, and dissociation occurs from within minutes to several hours with

increasing insulin concentration. De Meyts noticed twenty years ago that insulin binding to its membrane receptor, as analyzed by Scatchard plots, showed an upwardly curvilinear binding isotherm (De Meyts et al, 1973). These were interpreted as indicative of negatively cooperative binding, suggesting that the affinity of the reaction is not uniform over the saturation range. They proposed that there were two "binding sites" on the receptor and consequently that the IR can bind insulin with high and/or low affinity based on the insulin concentration. The insulin receptor binds one insulin molecule with high affinity (Kd~10^9 M^{-1}) in its high affinity site at physiological concentration of the insulin. At saturation conditions, the receptor can bind another insulin molecule with lower affinity (Kd~10^8 M^{-1}). This interpretation has triggered numerous additional binding studies from many laboratories and resulted in considerable controversy over the years.

De Meyts's model also provided an explanation for the kinetics of insulin binding. When the binding site is empty, the receptor can bind to insulin with high affinity. This binding leads to additional insulin binding occurring with lower affinity and results in a higher dissociation rate.

Considering the fact that the insulin receptor is a functional $\alpha_2\beta_2$ heterotetramer, it is highly possible that high affinity insulin binding requires that insulin be in contact with both α subunits, although the contact region in each α subunit may be different (Yip, 1992; Lee et al., 1993; Schaffer, 1993). Binding of one insulin molecule to the receptor may make it more difficult to bind the second insulin molecule. The exact ligand contact region on the α subunit is still incompletely defined. The mechanism of negative cooperative binding will be better explained when more details of the insulin receptor structure are known.

4.2. Autophosphorylation

Insulin binding to the receptor α subunit rapidly stimulates autophosphorylation and enhances tyrosine kinase activity of the β subunit of the receptor (White et al., 1988). The signal of ligand binding in the extracellular domain is transmitted through the hydrophobic transmembrane domain, possibly by a conformational change. The unoccupied insulin receptor actually inhibits the tyrosine kinase activity of the β subunit (Hubbard et al., 1994).

As mentioned previously, autophosphorylation of the receptor occurs in three distinct regions: the juxtamembrane region Tyr972, and possibly 965 and 984; the kinase catalytic region, Tyr1158, Tyr 1162, and Tyr1163; and the C-terminal region, Tyr1328 and Tyr1334 (White et al., 1988, Kohanski, 1993; White and Kahn, 1994). The mechanism of insulin receptor autophosphorylation likely occurs by mutual transphosphorylation of the β subunits (Lammers et al., 1990; Lee et al., 1993; Taouis et al., 1994) although some *cis*-phosphorylation has been reported. The recent crystal structure of the insulin receptor PTK domain suggests that a *cis*-autoinhibition is found in the inactive kinase. Insulin binding moves two kinase domains closer to enable *trans*-phosphorylation in the presence of ATP by disengaging Tyr1162 from the catalytic loop (Hubbard et al., 1994; Hubbard, 1997).

The intracellular juxtamembrane domain of the insulin receptor β subunit contains at least one phosphorylation site (Tyr972) in a $NPXY^{972}$ motif (Feener et al., 1993). Point mutation at this residue has no effect on the insulin receptor's tyrosine kinase activity but impairs receptor signal transmission (White et al., 1988; Kaburagi et al., 1993). This $NPXY^{972}$ sequence is also the binding site for the insulin substrate IRS-1 and Shc, which transduces the signal intracellularly (Gustafson et al., 1995; Pawson, 1995).

4. 3. Post-Receptor Signal Transduction

The downstream elements responsible for the propagation of extracellular signals through tyrosine kinase messenger systems have attracted much attention and been extensively reviewed (Pawson and Gish, 1992; White and Kahn, 1994; White 1994; 1996). In this section, I briefly summarize the current knowledge about the insulin signaling pathways.

The binding of insulin stimulates the intrinsic tyrosine kinase of the IR, which results in autophosphorylation of the β subunits on tyrosine residues and the subsequent phosphorylation of insulin receptor substrate proteins, including insulin receptor substrate proteins (IRS-1 and IRS-2). IRS-1 and IRS-2 are proteins with molecular weight larger than 180 kDa based on their electrophoretic mobility SDS-PAGE. They are 43% identical in their primary amino acid sequences (Sun et al. 1995). Both of them contain so-called IRS-homology domains: IH1, 2 and 3 (White, 1996). The IH2 domain, sharing 75% homology between IRS-1 and IRS-2, has been found to be similar to the phosphotyrosine binding (PTB) domain in Shc and can bind to the phosphorylated $NPXY^{972}$ sequence in the insulin receptor (Gustafson et al. 1995; Sun et al., 1995). While IH1 and IH2 are important for recognizing and binding to the insulin receptor, IH3 may mediate downstream signals (Gustafson et al. 1995). IRS-proteins contain more than 20 potential tyrosine and 30 serine/threonine phosphorylation sites, including many tyrosine-containing motifs such as YMXM and YXXM recognized by various kinases. Unlike other RTK family members, such as EGF and PDGF receptors, the insulin receptor does not appear to have direct association with SH2-proteins. Instead, in the case of the insulin receptor the phosphorylation sites and motifs in IRS-proteins provide docking sites for SH2-proteins, such as PI-3K, SH-PTP2(Syp), GRB-2 and Nck (White, 1994; 1996), and many other kinases, such as casein kinase II, and MAP kinase (Sun et al., 1993; Tanasijevic et al., 1993). These multi-protein interactions provide a means for signal amplification by eliminating the stoichiometric constraints encountered by receptors that directly recruit SH2-proteins to their autophosphorylation sites.

Interestingly, in addition to interacting with the IR, IRS-proteins are also engaged and phosphorylated by the receptors of IGF-I and various classes of cytokines and growth factors (White et al., 1985; Myers et al., 1993, White, 1994; 1996). The shared use of IRS-proteins by different receptors likely suggests important connections previously unknown, or observed but unexplained, between various hormones and cytokines.

Several intracellular pathways are involved in the insulin signaling system through the phosphorylated IRS-proteins (Fig. 1-5). For example, phosphorylated IRS-protein can associate with and activate PI-3K and SH-PTP2. The activated PI-3K may link to p70 ribosomal S6 kinase and specific isotypes of protein kinase C (Myers et al., 1994). Activated PI-3K was also found to be involved in GLUT4 translocation (Cheatham et al., 1994). In addition, IRS-proteins, mostly IRS-2, can activate Grb-2 which regulates a Ras guanine nucleotide exchange factor called SOS. The Grb-2-activated SOS initiates a mitogen-activated kinase cascade consisting of c-Raf, MAPKK, MAP kinase. This pathway leads to alterations in gene transcription and other cellular activities (Nishida and Gotoh. 1993). It is not yet clear how the metabolic effects of insulin, such as glucose metabolism, are regulated in the insulin-signaling pathway. Although there is evidence that suggests that PI-3 kinase (Cheatham et al., 1994) or a kinase cascade similar to the MAP kinase pathway may be involved in glucose homeostasis (Sutherland et al. 1993), many of the details in this pathway are still to be elucidated.

Protein tyrosine phosphatases (PTPs) also play a critical role in regulating insulin action in part through dephosphorylation of the active (autophosphorylated) form of the insulin receptor and attenuation of its tyrosine kinase activity (Drake and Posner, 1998). Recent studies have shown that PTP1B knockout mice have increased insulin sensitivity and are resistant to obesity, suggesting this PTP is a negative regulator in insulin action and related to the pathogenesis of diabetes and other diseases (Elchebly et al., 1999).

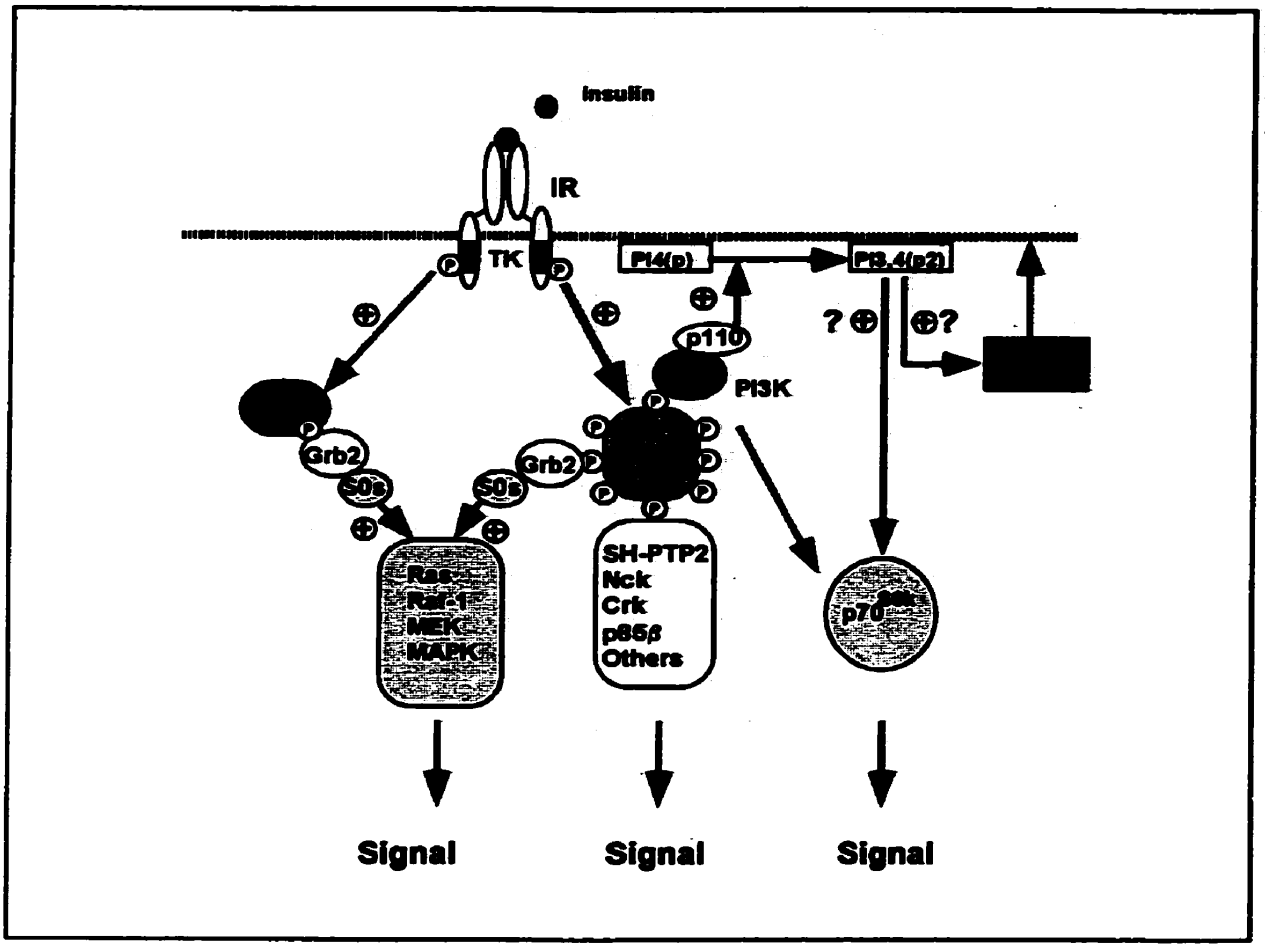

Fig. 1-5. A schematic diagram of the insulin signaling pathways. Insulin receptor contains intrinsic kinase activity that is activated by autophosphorylation after insulin binding. The activated IR then tyrosine-phosphorylates IRS proteins. The activated IRS signaling complex is shown to compose of PI3'-Kinase, GRB-2/SOS/Ras, and SH-PTP2 pathways. The activated IR may also stimulate other signaling pathways.
Ⓟ Phosphorylated Tyrosine. ⊕ Stimulatory effects

Besides the principal IRS substrates, other substrates, such as Shc, might also exist in the insulin-signaling pathway. Alternative pathways of the IR may be responsible for the multiple actions of insulin. Shc is a substrate protein rapidly tyr-phosphorylated by insulin stimulation. Shc contains an N-terminal PTB domain which binds to the phosphorylated $NPXY^{972}$ sequence in the insulin receptor and can also bind Grb-2 to link these signals to Ras activation (Skolnik et al., 1993; Pronk et al. 1994; Gustaffson et al., 1995). It has been suggested that Shc, rather than IRS-1, may be the main mediator of the mitogenic actions of insulin and IGF- II (Yamaguchi and Pessin, 1994).

5. MAPPING THE INSULIN BINDING SITE

As discussed insulin initiates signal transduction in target cells by binding to a specific cell surface receptor. Photoaffinity labeling studies have implicated the α subunit as the location of insulin-insulin receptor interactions (Yip et al., 1978). Subsequently, several regions in the α subunits of the IR have been shown by different techniques to be involved in insulin binding (Yip et al., 1988, 1991; Anderson et al., 1990; Schumacher et al., 1993; Kjeldsen et al., 1991,1994; Schaefer et al., 1992). The molecular details of these events are still obscure and will require a detailed understanding of the structure function relationships of the IR, in particular those of the extracellular domain. The purpose of my study is to explore the structure and function of the IR, and particularly to focus on the localization of the insulin-binding site on the IR. Multiple approaches were used to achieve these goals. The information obtained would greatly help us to understand the mechanism of the insulin-IR interaction and signal transduction, the pathogenesis of diabetes mellitus, and eventually, to assist in designing new medicine to treat diabetic patients.

5.1. Insulin Interaction with the IR

As mentioned previously, human insulin consists of two chains, the A-chain (21 residues) and B-chain (30 residues), and it is assumed to bind to its receptor as a monomer (Brange et al., 1988). The X-ray crystal structure of porcine insulin provided the first direct experimental evidence for the insulin folding (Adams et al., 1969). Subsequent studies have shown that insulin A and B chains fold to form a compact globular structure, stabilized by the two interchain disulfide bridges.

A vast number of insulins from diverse animal species, and chemically or genetically modified insulin analogues have been studied for their biological properties and binding to IR. The results indicate that many residues of the insulin molecule may contact or be involved in the insulin-receptor binding (Baker et al., 1988; Murray-Rust, et al., 1992; Mynarcik et al., 1997). On the putative receptor-binding surface of insulin, GlyA1, IluA2, ValA3,A19, AspA21, ValB12, PheB24 and B25, TyrB26 are the major determinants of the receptor binding site. A few other residues make minor contributions. Meanwhile, the N-terminus of the B chain being the most flexible region of insulin as suggested by X-ray and NMR studies, was considered to be a characteristic of insulin-insulin interaction rather than being directly relevant to receptor binding (Kruger et al., 1990; Murry-Rust et al., 1992). Since mutations in the C-terminal region of the B chain insulin have been reported to be associated with diabetes (Steiner et al., 1990), residues in this region has been suggested to play a critical role in the expression of insulin's biological activity. Many studies have been done to elucidate the role of this region in the interaction with the insulin receptor (Nakagawa and Tager, 1986, 1987, 1993; Mirmira and Tager, 1989, 1991; Mynarcik, 1997). PheB24 and PheB25 have been suggested to provide much of the binding free energy involved in inducing the site-site interaction (De Meyte, et al., 1978). Systemic studies of insulin analogs modified at B24, B25 (Mirmira and Tager, 1989; Nakagawa and Tager, 1986; 1987) have also supported the suggestion that these residues are responsible for the initial interaction with the receptor.

Combining information from the crystal structure of insulin and its biological properties, Schaffer proposed a model for insulin binding to the insulin receptor (Fig. 1-2 b). He hypothesized that high affinity insulin binding required two receptor-binding sites on insulin. The first binding site is the classical binding site, including B24, B25, A1 and A21 in the dimer-forming surface of the insulin molecule. The second binding site consists of B17 and A13, located in the hexamer-forming surface on the opposite side of the molecule from the classical binding site (Schaffer, 1994). Substitutions of these residues would be expected to dramatically decrease insulin affinity to its receptor. Other studies also suggest that insulin binding to its receptor may lead to a conformational change in the C-terminus of the B chain, a region which is essential for high affinity receptor binding. The emerging concept, therefore, is that receptor binding is not a simple collision process, but rather a multiple step process that may involve successively different residues in the transition towards to the active state.

5.2. The Insulin-Binding Domain of the IR

Unlike insulin, the exact regions of the receptor that directly contact its ligand remain incompletely defined and are still the object of much study.

Evidence suggests that the binding of insulin at high affinity involves multiple regions in the α subunit, and even the β subunit of the receptor. The free single α subunit, or the α–β monomer, as well as the α–α subunit dimer, has minimal, or no binding affinity for insulin (Boni-Schnetzler et al., 1986; Schaefer et al., 1990; Roach et al, 1994). The minimal truncated holoreceptor which still maintains the same high affinity for insulin is the solubilized whole extracellular domain of the receptor, including the entire α and all extracellular β subunit linked in tetrameric form (Schaefer et al., 1990). Although there is still a considerable uncertainty about where the receptor binds to insulin, these observations suggest that the high-affinity insulin-binding pocket requires a conformation consisting of the entire extracellular portion of IR. It suggests that the

insulin-IR interaction requires not only multiple specific contact sites but also some supporting regions to keep the proper binding pocket in the right conformation.

Approaches to Study the Insulin-Binding Site

Attempts to localize the specific region for high affinity insulin binding on the α subunit have involved several different approaches, including affinity labeling, recombinant DNA technology, such as site-directed mutagenesis, deletion studies and the construction of chimeric receptors comprised of different domains of the insulin and IGF-1 receptors (Tavare and Siddle, 1993). Although each approach has its advantages and disadvantages, and the results may not agree, these studies do provide useful information about where on the IR insulin binds.

Affinity Labeling Chemical or photoaffinity labeling was one of the earliest methods used to study the insulin-receptor interaction. Photoaffinity labeling (Yip et al., 1978; 1980) and chemical cross-linking techniques (Pilch and Czech, 1979; 1980) have been used to show that insulin primarily binds to the α subunit of the IR. These pioneering experiments also revealed the overall $\alpha_2\beta_2$ subunit structure of the insulin holoreceptor (Yip et al., 1978, 1980, 1982; Pilch and Czech, 1979, 1980; Yeung et al, 1980; Massague et al., 1980). Although they have advantages in the characterization of the structure and function of the IR, the chemical bifunctional reagents or the early photoaffinity labeling reagents for cross-linking of insulin to the receptor have low intrinsic efficiency and/or specificity. The disadvantages include the fact that the cross-linked insulin-receptor complexes are either typically a low percentage of the total IR and the non-specific cross-linking products may increase during attempts to increase cross-linking efficiencies (Waugh et al., 1989). Later attempts to develop reagents with greater efficiency and selectivity have focused primarily on derivatizing the ε- or α-amino groups of LysB29 or PheB1, respectively, with additional modified aryl azides (Brandenburg et al, 1980; Ng and Yip, 1985; Yip et al., 1988; Fabry, et al., 1992). These new reagents

have much higher specificity in cross-linking and can provide more precise information on insulin-receptor interaction, but their efficiencies are usually still below 10%, which limit their usefulness in functional studies. Recently, a novel benzoylphenylalanineB25-insulin photoprobe was reported to have an efficiency of cross-linking as high as 60-100% (Shoelson et al., 1993). This new class of photoaffinity reagents would facilitate the studies of insulin-receptor structure and function.

The technique of photoaffinity labeling has been used to identify the insulin-binding site. The approach includes a photo-cross-linking process followed by isolation of receptor-insulin fragments to allow the identification of the regions where the putative insulin-receptor contact occurs. Using radioactive photoreactive insulin derivatives that maintain more than 75% of the bioactivity of insulin, the laboratory of Yip found that the cysteine-rich domain of the IR α subunit contains the insulin-binding site (Yip et al., 1988, 1991). This finding has been confirmed by another similar study (Waugh et al, 1988) and mutagenesis studies, using either site-directive mutagenesis (Rafaeloff et al., 1989) or HIR/IGF-IR chimeras (Gustafson and Rutter, 1990). However, using different photoprobes, other investigators later found that other regions might also be in contact with insulin. They are the L1 domain, residues 60-90, (Wedekind et al, 1989), the L2 domain, residues 300-390 (Fabry et al, 1992), and the carboxyl terminal region of the α subunit (residues 704-718)(Kurose et al, 1994). This variation in the results indicates the complicated nature of the insulin- binding "pocket" and each of these regions may only represent part of the whole receptor-binding site. The photoaffinity labeling approach theoretically could provide the most accurate information for insulin-receptor contacting sites, but the generally low cross-linking efficiency and the requirement for a large quantities of insulin receptor protein make the post-labeling analysis of the products very difficult.

Recombinant DNA techniques Recombinant DNA techniques have frequently been applied to mapping the insulin-binding site. Taking advantage of the

highly conserved domain structure but a large difference in the affinity to their cognate ligands, domain exchanged chimeric insulin/IGF-I receptors have been extensively studied (Anderson et al., 1990; Schumacher et al., 1993; Kjeldsen et al., 1991,1994; Schaefer et al., 1992). This technique is a useful approach for the study of domain involvement in ligand binding. Results obtained have suggested that various regions of the α subunit are involved in the insulin binding. These include the N-terminal region, residues 1-68 or 1-137 (Schaffer et al., 1993; Kjeldsen et al., 1991, Schumacher et al., 1993), the cysteine-rich region (Gustafson et al., 1990, Anderson et al., 1990), and regions in the L2 domain (Schumacher et al., 1993). Results from several chimeric studies also indicate that the Cysteine-rich region is specific only for high affinity binding of IGF-1 but not of insulin (Anderson et al., 1992; Schumacher et al., 1993; Zhang and Roth, 1991).

Many mutations, both naturally occurring and resulting from site-directed mutagenesis in the α subunit, also provide important information on insulin binding of the IR. Site-directed mutations in the amino acid residues 240-250 of the cysteine-rich domain (Thr-Cys-Pro-Pro-Pro-Tyr-Tyr-His-Phe-Gln-Asp to Thr-Cys-Pro-Arg-Arg-Tyr-Tyr-Asp-Phe-Gln-Asp) has increased the receptor's affinity to insulin (Rafaeloff et al., 1989), while a mutation in Phe 89 of the L1 domain almost abolishes insulin binding (De Meyets et al., 1990). A natural mutation in Ser 323 (the beginning of the L2 domain) in a diabetic patient markedly impairs insulin binding to its receptor, suggesting its critical role in insulin binding (Roach et al., 1994). A series of deletions within the extracellular domain (Schaefer et al., 1990) and alanine-scanning mutagenisis on the whole L1 domain and C-terminal region of the α subunit (Williams et al., 1995, Mynarik et al., 1996) have also provided very useful information about the localization of the insulin-binding site. Mutation analysis also show that glycosylation of the α subunit does not affect insulin binding (Caro et al., 1994).

The observations mentioned above suggest that the insulin-binding site is a complex multiple domain structure. It possibly involves the L1, C-R, L2, and C-terminal regions of the α subunit. Both α subunits seem to be involved in forming the high affinity ligand-binding site, and even the β subunit may play a role in stabilizing the structure.

Cryoelectron Microscopy Recently, with the progress of the electron microscope technology, especially the use of scanning transmission electron microscope (STEM) in biological studies, cryoelectron microscopy has become a new trend in the study of structure. The concept and feasibility of reconstructing three-dimensional images from electron micrographs were introduced 30 years ago (DeRosier and Klug, 1968). A convergence of technical advances in cryoelectron microscopy and computing image processing has now allowed this technique to be used to analyze biomolecular structure without crystallization. It is clear that the electron cryomicroscopic and image processing technique are an ideal and powerful tool to elucidate the structure of large proteins that are quite difficult for "conventional" techniques, like x-ray crystallography or NMR. This technique also can be used to map out the functional domains in a large complex and to study their conformational variations in different functional states. There is considerable evidence that high resolution cryoelectron microscopy is able to provide the structure resolution at below 10 Å level (Bottcher et al., 1997; Conway et al., 1997; Chiu and Schmid, 1997; Cheng et al., 1997; Walz et al., 1997). It is especially useful in studying large proteins, such as the insulin receptor, which are very difficult to analyze by x-ray crystallization or NMR spectroscopy. This technique also has been successfully applied to structurally localize the ligand or substrate binding site in protein-protein / protein-virus interaction (Zhou et al., 1998; Paredes et al., 1998; Wagenknecht et al., 1994). This new technique gives us a powerful approach in the study of the insulin receptor structure and function.

6. THESIS OVERVIEW

During the course of my Ph.D program I have tried biochemical and biophysical methods to elucidate the structure and function of the human insulin receptor, focusing on the insulin-insulin receptor interaction. In Chapter 2, I describe my attempts to use the conventional biochemical approaches to localize the insulin-binding site on the human insulin receptor. A baculovurus expressing system has also been established to overproduce the functional extracellular domain of the HIR. Different photoaffinity labeling and limited proteolysis, as well as various peptide-mapping methods were used in an attempt to identify the primary site(s) of the insulin-IR interaction. In Chapter 3, using cryoelectron microscopy and computer image processing technique, I determined the quaternary structure of the IR and where the insulin receptor binds to its ligand. A Nanogold-bovine insulin derivative was used as a marker to localize the insulin-binding site on the 3D reconstruction of IR. We have successfully obtained the 3D structure of human insulin receptor and localized insulin in the 3D insulin-insulin receptor complex. Finally, in the last Chapter I discuss the significance and future perspectives on my thesis work.

CHAPTER 2

LOCALIZATION OF INSULIN-BINDING SITE(S) ON THE HUMAN INSULIN RECEPTOR BY BIOCHEMICAL APPROACHES

1. INTRODUCTION

As described in Chapter 1, the mature human insulin receptor (HIR) consists of two α and two β subunits linked by disulfide bonds, with a mass of approximately 450 kDa (Yip, 1988; Kahn and White, 1988). Previous affinity cross-linking studies using photoreactive probes or bifunctional reagents have identified relatively large receptor fragments as putative insulin-binding (Wedekind et al., 1988; Waugh et al., 1989; Fabry et al., 1992).

This Chapter describes my attempt to identify the insulin-binding site(s) on its receptor by using various conventional biochemical approaches. The laboratory of Dr. Yip originally localized the insulin-binding site to the α subunit of IR (Yeung, 1980), and then more specifically to the Cys-rich domain of the α subunit by combining affinity labeling and immunological techniques (Yip et al., 1988,1991). My project was a continuation of these studies. The main objective was to use different insulin photoprobes with high efficiency of cross-linking to label the insulin-binding domain on the IR, followed by proteolysis to obtain smaller cross-linked receptor fragments for peptide mapping and amino acid sequencing, thus to identify the putative insulin-binding domain. This Chapter describes this approach and the results obtained.

2. MATERIAL AND METHODS

2.1. Over-expression of the Extracellular Domain of the HIR

Intact receptor or a truncated receptor with full insulin-binding activity of the intact IR was used in the study. Intact receptor protein has previously been extracted and purified from human tissues or mammalian cell lines (Cautrecasas et al., 1972; Fujita-Yamaguchi et al., 1983; Whittaker, 1987). However, a sufficient quantity of the intact receptor is difficult to obtain from these sources for the identification of the insulin-binding site(s). Since it is well established that the entire extracellular domain of IR is required for the high-affinity binding of insulin (Sweet et al., 1987; Schaefer et al., 1990), I used the baculovirus expression system (BES) to express the entire ectodomain of HIR to obtain substantial quantities of the protein for this study.

Construction of a cDNA Expression Plasmid Encoding the Extracellular Domain of HIR

The cloning strategy of the BES expression vector is shown in Fig. 2-1. To take advantage of the baculovirus expression system, the gene of the HIR must be cloned into a baculovirus transfer vector which is designed to position the HIR gene immediately downstream of the powerful baculovirus polyhedrin gene promotor. All the restriction and modifying enzymes in these experiments were purchased from Pharmacia, Boehringer-Mannheim, or New England Biolab. All adapters and linkers were custom synthesized by the HSC Biotechnology Service Center, Toronto

Preparation of constructs Preparation of the transfer vector consisted of several steps. cDNA encoding the entire ectodomain of HIR (including all of the α

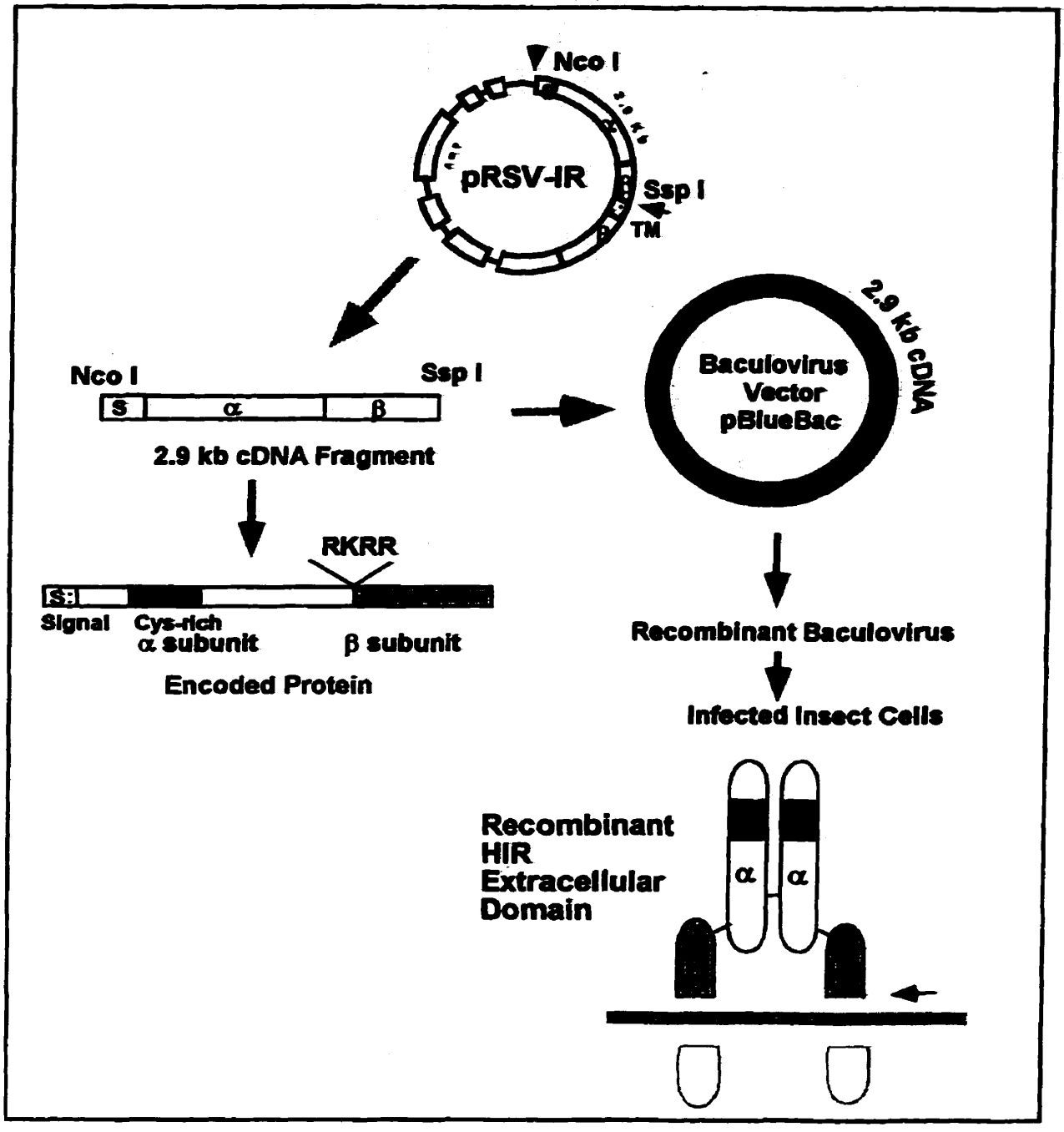

Fig. 2-1. Expression of human insulin receptor extracellular domain with baculovirus expression system. A 2.9 kb cDNA encoding the extracellular domain of hIR was cut from pRSV-IR plasmid and subcloned into a baculovirus expressing vector. Insect cells infected with the recombinant virus were used to express the recombinant receptor protein.

subunit and all of the extracellular portion of the β subunit, except for three amino acids N-terminal to the transmembrane domain) was excised from the 9.7 Kb plasmid pRSVIR (a generous gift from Dr. Ira Goldfine, UCSF). Restriction endonuclease *Ssp* I was used to digest the pRSVIR to remove the cDNA, starting from nucleotide 2999 of the receptor cDNA, which encodes the putative transmembrane domain and the entire cytoplasmic portion of the β subunit of the HIR. To facilitate the expression and the purification later, a stop codon (TAG) in a *Xba*I linker:

5'-CTAGTCTAGACTAG-3'

3'-GATCAGATCTGATC-5'

L V stop

or, alternatively, an adaptor encoding an extra 6-Histidine amino acids prior to the stop codon was introduced at the *Ssp*I site. In the latter case, the adapter and the expected deduced protein sequence at the C-terminus of the protein is therefore:

5'-TCTCATCATCATCATCATCATGT-3'

3'-AGAGTAGTAGTAGTAGTAGTACAGATC-5'

S H H H H H H V stop

The resulting intermediate plasmid, designated as pIRX or pIRXH (H represents poly-His tag), was digested with *Nco*I, which cleaves at a single site at the beginning of the cDNA (nucleotide 137) corresponding to the first methionine of the signal peptide at position -27 of the HIR protein. The digested plasmid was then blunted with the Klenow fragment of DNA polymerase I to fill in the ends. A *Nhe*I linker

5'-ATCGCTAGCGAT-3'

3'-TAGCGATCGCTA-5'

was then introduced at the blunted *Nco*I site to generate the second intermediate plasmid of pIRXN or pIRXNH (~6.0 KB). Digestion of above the plasmids with *Nhe*I and *Xba*I generated a 2.9 Kb restriction fragment of the truncated HIR, nucleotides 138-2998. It encodes the entire extracellular domain of the HIR, except the three amino acid residues, I A Y, prior to the transmembrane domain of the β subunit, with or without a 6-histidine tag on the C-terminal end. The *Nhe*I-*Xba*I fragment was then subcloned into a *Nhe*I cut, calf intestinal phosphotase-treated baculovirus transfer vector pBlueBac2 or pBlueBac4 (Invitrogen). The right orientation of the insert cDNA in the transfer plasmid, designated as pHIRα or pHIRαH, was determined by various restriction endonuclease digestions. These transfer plasmids for co-transfection were prepared by CsCl gradient centrifugation in a Beckman rotor VT80I at 80 K x g, at 22 °C for 4 hours. The purified plasmid constructs were sterilized with 0.22μ filter and saved at 4 °C.

DNA sequencing of the constructs

In order to confirm that the nucleotide sequence was correct for the recombinant protein, the DNA of the 2.9 Kb insert in the transfer construct was subcloned into pBluescript (Stratagene) vector at the *Xba*I site (pBSHIRa, bp 138-2998), or cut with restriction enzymes and subcloned into three sub-constructs in pBluescript vector (pBSHIR1, bp 559-1273; pBSHIR2, bp 1101-1695; pBSHIR3, bp 1695-2606), thus allowing the whole 2.9 Kb cDNA fragment to be sequenced (Fig. 2-2). All constructs were manually (Phamacia DNA sequencing Kit) or automatically (Perkin-Elma-ABI Genetic Analyser) sequenced. All sequenced DNA showed no error in the nucleotide sequences.

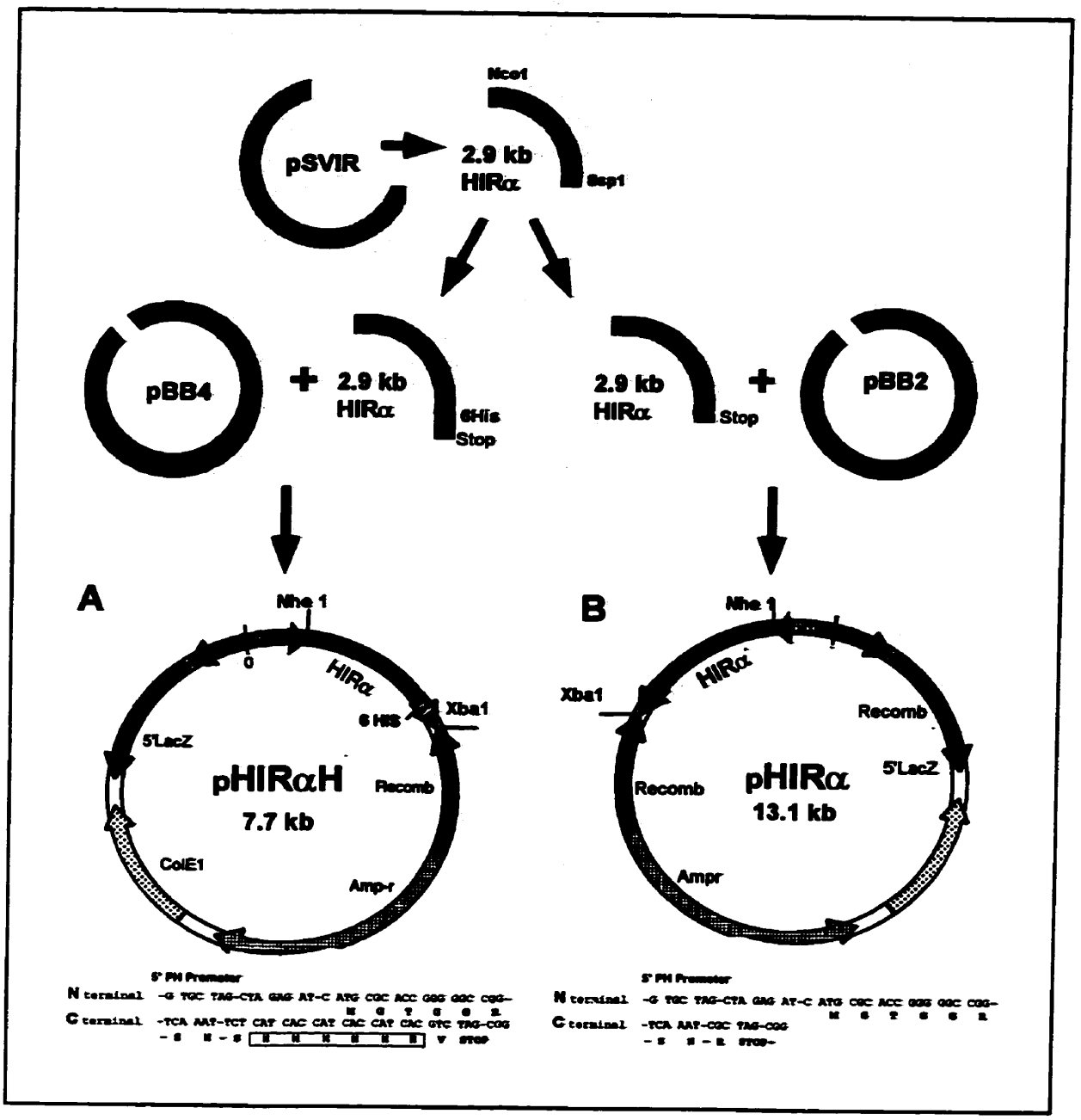

Fig. 2-2. Construction of the BES transfection vectors for the hIR ectodomain with (A) or without (B) 6 His tag. A 2.9 kb cDNA fragment was cut from pSVIR and modified by adding proper adaptors, with or without 6 His residues, and stop codon. The modified cDNA fragments were subcloned into pBlueBac4 (pBB4) or pBlueBac2 (pBB2) baculovirus transfection vector.

Cell culture and Co-Transfection

Log phase insect *Sf*9 (S. frugiperda) cells (Invitrogen) were grown as an adherent culture at 27°C in modified Grace's medium supplemented with 0.33% lactalbumin hydrolysate, 0.33% yeastolate, 10% fetal bovine serum (FBS), 10 μg/ml gentamycin and 250 μg/ml amphotericin B (Life-Technology). In some experiments 0.1% of Pluronic F-68 (Life-Technology) was added to suspension culture of *Sf*9 cells to reduce the sensitivity of the culture to mechanical shearing. Another insect cell line, High-five (Hi5) cells (Trichoplusia nl) (Invitrogen), was cultured in Excell 401 serum free medium (JRH Scientific) containing 10 mg/ml gentamycin and 0.25 mg/ml amphotericin B to yield a higher expression level. All procedures involving cell culturing, including routine subculturing, and protein expression, were performed as described in the Manuals of Methods for Baculovirus Expression from Invitrogen.

Recombinant plasmids were co-transfected into *Sf*9 cells along with the linearized wild-type AcMNPV viral DNA (for pHIRα) or Bac-N-Blue linearized viral DNA (for pHIRαH) by the technique of cationic liposome mediated transfection (Invitrogen). *In vivo* homologous recombination between the polyhedrin sequences in the wild-type viral DNA and the recombinant plasmids resulted in the generation of recombinant viruses coding for the expression of HIR ectodomain. Briefly, 1μg viral DNA, 1μg of recombinant transfer plasmid, and 20 μl of Insectin liposome (Invitrogen) were mixed in 1 ml of Grace's media without FBS and supplements. The mixture added to freshly seeded *Sf*9 cells in plates and incubated for 4 hours on a slowly rocking platform at 27°C. Then, 1 ml of complete Grace's medium was added and incubated at 27° C for 48-72

hours. The medium from successfully co-transfected, cultured cells was screened by a plaque assay for the recombinant virus containing the insulin receptor cDNA.

Plaque Assay and Preparation of High Titer Viral Stock

For the plaque assay, *Sf*9 cells in 60 mm plates were infected with 1 ml of 1 x 10^2, 10^3, 10^4 diluted media containing co-transfected virus for 1 hour at 27°C. The media were then removed and replaced with a 4 ml overlay of 1.5% Sea-Plaque agarose (FMG Bioproducts) containing 0.01% X-Gal. After 4-6 days' incubation at 27° C, well separated, distinct blue plaques were isolated and used to inoculate *Sf*9 cells in multi-well plates for further screening and preliminary virus amplification. Usually, 6-12 plaques for each recombinant protein were selected and 3-4 clones of the final purified virus were saved at 4° C as P-1 viral stock for further characterization and amplification. The P-1 viral stock was then used to infect log-phase *Sf*9 cells in a T-25 flask for 5-10 days at 27° C to generate P-2 viral stock. The amplified P-2 viral stock then was used to infect *Sf*9 cells at a ratio of 1:10 (v/v) or MOI 0.5 - 1 (see details later), either in adherent culture in T-225 flasks (Costar) or in suspension culture in 500 ml spinner flasks (Bellco Glass) at 27° C for 5-8 days. This P-3 high titer viral stock was analyzed in a plaque assay following the same schedule as previously described except the viral inoculate was diluted up to 1 x 10^{-9}, to measure the virus titer. The plaque forming units per ml (pfu/ml) were calculated using the following formula to set the optimal conditions for protein expression:

pfu/ml= 1/dilution x mean number of plaques/plate x plate/ml

To obtain a synchronous infection for expressing the recombinant receptor, a particular multiplicity of infection (MOI) index of 5-10 was used to calculated the volume of the virus stock with the following formula:

[MOI (virons/cell) x number of cells]/titer of virus (virons/ml)=ml of inoculum stock

High-titer viral stock was kept at 4° C in the dark until use. A small aliquot was frozen at -70° C for long-term storage.

Expression and Characterization of the Recombinant IR

MOI optimization for virus infection High titer viral stock was used to infect the Hi5 cells in 2 ml of Excell-401 medium in T-25 flasks at ~90% confluence at varying MOIs (2, 5, 8, 10 and 15) for 1 hour. Three ml of fresh media were then added and the cells were cultured for 4 days at 27° C. Anti-HIR immunoblotting and B_{29}-MAB-[^{125}I]-iodoinsulin photoaffinity labeling (see details later in this chapter) were used to check the levels of protein expression. An MOI of 5-10 was chosen in our expression infection. On the other hand, for generating high-titer viral stock, an MOI of 0.5-1 was used to avoid any unwanted interference in virus production. Western blots with anti-IR α subunit antibody and mono-[^{125}I]A14-insulin binding assays were carried out to confirm the expression of protein and protein function (see details later).

Time course and large scale expression of the recombinant receptor Hi5 cells at ~90% confluence were infected with viral stock at an MOI of 10 in 6 well plates at 27° C for up to 7 days. Media was removed at 0 hour from one well and at every 24 hours from other wells to monitor the infection and expression process. The media from the infected cells, as well as the corresponding cells, washed with pH 7.4 PBS with

protease inhibitors, were collected and frozen at -70° C until analysis. In suspension culture, Hi5 cells were infected at a cell density of 2 x 10^6 cells with viral stock at an MOI of 10 in a 500 ml spinner flask at 110 rpm at 27° C. One ml of suspension was collected at zero time and each day following for 7 days, from the culture. These samples were treated the same as the adherent culture.

In preparative culture for protein expression, Hi5 cells were cultured in Excell-401 medium to ~90% confluence in T-225 flasks at 27° C. After removing 25 ml of media, the cells were infected with viral stock at an MOI of 10 for 1 hour. Fresh medium was replaced to a final 38 ml and the cells were cultured at 27° C for 4 or 5 days. The cultured media were collected for purification of the recombinant protein.

Preparing cell lysates and plasma membranes of the infected insect cells

Cell lysate samples for the time course study were prepared by directly adding SDS-PAGE sample buffer (Laemmli et al., 1970) containing 100 mM DTT to the pre-washed cells for subsequent SDS-PAGE analysis.

The plasma membrane and microsome fractions of the cells were prepared as follows: Hi5 cells in 25 ml of adherent culture were collected at Day 4 after infection and resuspended in 5 ml of pH 7.4 solubilization buffer (Buffer A) containing 50 mM Hepes, 150 mM NaCl, 0.1% Triton X-100, 1.5 mg/ml Bacitricin, 10 mM benzamidine HCl, 2mM pepstatin, 2mM leupeptin, 5 mg/ml aprotinin and 1 mM PMSF. The cells were homogenized with an ice-cooled glass-Teflon tissue grinder (Kontes Glass) for 50 strokes then centrifuged in an SS34 rotor (DuPont) at 1,000 x g, at 4° C for 10 minutes. The pellet containing the nuclei was resuspended in Buffer B (Buffer A without the 0.1% Triton X-100). The supernatant then was centrifuged in an SS34 rotor at 35,000 x g, at 4°

C for 30 min. The pellets were resuspended in Buffer B to yield the sample of plasma membrane. The supernatant was subjected to further ultracentrifugation in a Ti 50 rotor (Beckman) at 250,000 x g at 4° C for 60 min. The pellet was resuspended with buffer B as the microsome sample.

Anti-IR Immunoblotting Samples of cultured media, cell lysates, nuclei, plasma membrane and microsome were solubilized by boiling for 5 min. in Laemmli's sample buffer (Laemmli et al., 1970) containing 100 mM DTT, and then separated by electrophoresis on 7.5% SDS-PAGE, followed by transferred to Immobilon-P PVDF membranes (Millipore). After transfer the membrane was blocked with 5% skim milk powder in pH 8.0 TBST buffer (10 mM Tris-HCl, 150 mM NaCl, 0.1% Tween-20) for 60 min at room temperature and then incubated with rabbit anti-IR α subunit antibody (Santa Cruz) in blocking buffer over night at 4° C. After washing with TBST buffer, the membrane was incubated with goat anti-rabbit alkaline phosphatase conjugated antibody (Sigma) in blocking buffer for 60 min at room temperature. The recombinant proteins were visualized using the AP substrate color kit (Pharmacia).

Insulin Binding Insulin binding was measured by incubating ~ 50 ng of human placenta membrane insulin receptor or recombinant insulin receptor protein, 20-30 fmol of mono-[^{125}I]A14-insulin (final concentration of ~50 pM), and varying concentrations (from 0 - 1 x 10^{-5} M) of unlabeled insulin in 200 ml of buffer, pH 7.6, containing 50 mM Tris-HCl, 150 mM NaCl, 0.1% bovine serum albumin (BSA), 1.5 mg/ml bacitricin (0.1% Triton x-100 in the buffer for placenta membrane receptor) at 4° C over night. The receptor-insulin complex was separated from unbound insulin by adding 50 µl of 0.4% bovine γ-globulin and 250 µl of 20% polyethylene glycol 6000

followed by centrifugation at 1,500 x g for 20 min at 4° C. Radioactivity in the pellets was determined in a Pharmacia-LKB γ-counter. The radioactivity detected in the presence of 10^{-5} M of unlabeled insulin was considered non-specific binding and was always less than 5% of the total activity. All binding experiments were performed in duplicate on three separate occasions. The competition binding curves were compiled from several experiments, and each point was reported as the mean +/- S.D. The Scatchard plot was analyzed with EBDA computer software (Munson and Rodbard, 1980).

For samples of time course and subcellular fractions, insulin binding was measured as follows: 50 µl of harvested media or resuspended fraction samples were dispersed in a total volume of 200 µl of the above binding buffer plus 0.1% Triton X-100, and ~ 20-30 fmol of mono-[^{125}I]A14-insulin, and assayed as described above.

Photoaffinity labeling and autoradiography Purified or crude protein samples, such as harvested media or plasma membrane, were incubated with about 1 x 10^6 cpm of B_{29}-MABI-[^{125}I]-iodoinsulin (Yip et al., 1980) in 200 µl insulin binding buffer with or without an excess (10 mM) unlabeled insulin overnight in the dark at 4° C. Photolysis was carried out for 15 second using a focused light source from a 100 W high-pressure mercury lamp (Yip and Moule, 1983). Photolyzed samples were reduced and solubilized in Laemmli's sample buffer containing 100 mM DTT. Cross-linked receptors were either separated by SDS-PAGE directly or precipitated with anti-insulin receptor antibodies prior to SDS-PAGE. Cross-linked, radiolabeled proteins were identified by autoradiography of the fixed and dried gels. The radioactive bands on the dried gels were cut out and counted in the γ-counter.

Molecular mass determination Samples were analyzed by 3-12% linear gradient SDS-PAGE under reduced (100 mM DTT) or non-reduced conditions. The gels were fixed in 10% acetic acid and 25% isopropanol for 30 min. Proteins were visualized using either a silver stain kit (Bio-Rad) or by Coomassie Brilliant Blue staining. The molecular mass of the detected proteins was estimated by comparing the relative mobility of the receptor bands to molecular mass standards (Bio-Rad, or Novex)

2.2. Purification of the Recombinant IR and Human Placenta Membrane IR

Preparation of insulin affinity column Twenty five ml of Affi-gel 10 (Bio-Rad) were washed with one volume of cold isopropanol, followed by 3 volumes of cold H_2O and were then equilibrated with the coupling buffer, pH 7.4, containing 0.1M phosphate and 6 M urea. Twenty five mg of zinc bovine insulin (a generous gift from Connaught Canada) in 25 ml of coupling buffer was mixed with Affi-gel 10 for 24 hours at 4° C. A trace amount of mono-[^{125}I]A14-insulin was added to monitor the coupling process. The suspended gel then was transferred to a column and washed with 20 volumes of the coupling buffer and further washed extensively with buffer containing 50 mM Tris-HCl, pH 7.4, 1 M NaCl and 0.02% NaN_3. Total radioactivity in the washed buffer and the column was counted to calculate the coupling efficiency.

Preparation of MA51 monoclonal antibody affinity column Mouse anti-insulin receptor monoclonal antibody, MA51 (IgG1 subclass, a generous gift from Dr. Ira Goldfine, UCSF) was prepared from the mouse ascites the mAb MA51 at ~ 1-3 mg/ml. The pH of the ascites was adjusted to 9.0 (with borate buffer) and NaCl was added to a concentration of 3 M. Twenty ml of ascites containing MA51 were mixed with

15 ml of protein A-Sepharose beads (Pharmacia) and incubated for 60 min at room temperature. The beads were washed twice with 10 volumes of 3 M NaCl, 50 mM sodium borate (pH 9.0) by centrifugation and aspiration. The beads were resuspended in 10 volumes of 3 M NaCl, 0.2 M sodium borate (pH 9.0) and mixed with dimethylpimelimidate (DMP) to a final concentration of 20 mM. After a 30 min incubation at room temperature, the coupling was stopped by washing the beads once with 0.2 M ethanolamine (pH 8.0) and incubated with the same buffer at room temperature for 2 hours with gentle mixing. The beads were then extensively washed with a buffer containing 50 mM Tris-HCl, pH 7.6, 150 mM NaCl and 0.02% NaN3 at 4 °C.

Purification of the Recombinant Ectodomain of IR

After 4-5 days infection with viral stock, low-serum-containing medium was harvested and adjusted to pH 7.4 with 1 M Tris-HCl buffer. PMSF and NaN_3 were added to a final concentration of 1 mM and 0.02% respectively. The conditioned medium was centrifuged in a JA14 rotor (Beckman) at 4° C, at 10,000 x g for 25 min to remove any cells or debris. The supernatant was concentrated ~50 fold using a Minitan Ultrafiltration System (Millipore) with a 100 kDa cut-off membrane to remove proteins of lower molecular as the first step of purification. The concentrated medium was then adjusted to 50% ammonium sulfate by drop-wise addition of saturated ammonium sulfate at 4° C. After overnight stirring, the mixture was centrifuged at 10,000 x g for 30 min at 4° C, to obtain a pellet which was resuspended in 20 ml of 50 mM Tris buffer (pH 7.4) and dialyzed exhaustively at 4° C against either the His-binding buffer (20 mM Tris-HCl, pH

8.5, 0.5 M NaCl, 10 mM imidazole, 10% glycerol, 0.02% NaN_3 and 1 mM PMSF for 6-His tagged ectodomain), or the buffer containing 50 mM Tris-HCl, pH 7.6, 150 mM NaCl, 0.02% NaN_3 and 1 mM PMSF for the ectodomain without the 6-His tag. Ammonium sulfate precipitation followed by dialysis further removed low molecular mass molecules and up to 40% of the BSA in the concentrated medium to facilitate subsequent purification.

Purification of the ectodomain of the IR with 6-His tag Ni-NTA resin (Qiagen) was washed and pre-charged with 100 mM NiCl and then equilibrated with His-binding buffer, pH 8.5. Twenty five ml of concentrated, dialyzed was mixed by rotation with 300-500 µl Ni-NTA resin over night at 4° C. The resin was transferred to a 2 ml mini-column (Bio-Rad) and washed with 10 volumes of His-binding buffer, followed by 50 volumes of washing buffer (20 mM Tris-HCl, pH 7.8, 0.5 M NaCl, 20 mM immidazole, 10% glycerol, 0.02% NaN_3 and 1 mM PMSF). All buffers were kept on ice when in use except that the Ni-NTA column was used at room temperature. Recombinant protein was eluted by washing the resin 5 times with 0.5 ml of elution buffer (20 mM Tris-HCl, pH 7.8, 0.15 M NaCl, 250 mM immidazole, 10% glycerol, 0.02% NaN_3 and 1 mM PMSF). The pooled eluted protein was ultrafiltered in Ultramax-50 (Millipore) to concentrate the protein and change the buffer to 50 mM Tris-HCl, pH 7.5, 150 mM NaCl, 1 mM PMSF and 0.02% NaN_3. Purified protein samples were aliquoted into several siliconized microfuge tubes and stored at -70° C.

Purification of the ectodomain of the IR without 6-His tag Twenty five to fifty ml of concentrated and dialyzed medium was mixed with 12 ml of MA51-protein A beads by rotation overnight at 4° C. The mixture was transferred to a column and washed

with 500 ml buffer containing 50 mM Tris-HCl, pH 7.4, 150 mM NaCl and 1 mM PMSF. The bound protein was eluted with an elution buffer containing 2.5 M $MgCl_2$, 0.2 M sodium borate, pH 6.5. The fractions containing the eluted protein were pooled and concentrated in an Amicon ultrafiltration device with a PM-30 membrane. The concentrated protein then was loaded on a Dextran G-25 column to remove the high concentration of salt. The purified protein from the MA51 affinity column was saved in siliconized microfuge tubes at -70° C.

Both Ni-NTA and MA51-protein A column purified proteins were purified further by gel filtration chromatography on a FPLC Superdex-200 HR 16/60 column (Pharmacia) in 20 mM Tris-HCl, pH 7.6, containing 150 mM NaCl, and 0.02% NaN_3 to remove either glycerol or/and the small amount of co-eluted contaminated proteins. The purified ectodomains of IR were analyzed by SDS-PAGE (Laemmli et al., 1970) with or without reducing agent (100 mM DTT) to check the purity, and by ^{125}I-insulin binding for their activity.

Purification of human insulin receptor

The methods of preparing the placenta membrane human insulin receptor were modified from Fujita-Yamaguchi et al.(1982). Briefly, a fresh normal human placenta was obtained within 1 hour after delivery, kept on ice, washed with normal saline (150 mM NaCl) 3 times and 0.25 M sucrose once, and then cut into small pieces. The pieces were transferred to 1 volume of 50 mM Tris-HCl buffer, pH 7.4, containing 0.25 M sucrose and 1 mM PMSF, homogenized for 90 seconds with a Polytron homogenizer (Polytron), and centrifuged at 15,000 x g in a JA14 rotor (Beckman) for 35 min at 4° C.

MgCl and NaCl were added to a final concentration of 0.041 mg/ml and 5.84 mg/ml, respectively. The supernatant was then centrifuged in a SW28 rotor (Beckman) at 100,000 x g for 25 min at 4° C. The pellets obtained were resuspended in homogenization buffer and the spin/resuspend steps were repeated three times at the same speed but with increased times (30, 35 and 45 min). The final pellets were saved at -70° C until analyses or further purification.

Placenta membranes (0.8-1.2 g of protein) from two fresh placentas was used to obtain the purified human insulin receptor. The placenta membrane pellets were solubilized in 25 ml of 50 mM Tris-HCl, pH 7.4, buffer containing 2% Triton X-100, 100 mM EDTA, 1.5 mg/ml bacitracin, 10 mM benzamidine HCl, 2mM pepstatin, 2mM leupeptin, 5 μg/ml aprotinin and 1 mM PMSF. The suspension was centrifuged in a SW28 rotor at 100,000 x g for 90 min at 4° C. The supernatant was then loaded on the insulin column which had been pre-equilibrated with the washing buffer of 50 mM Tris-HCl, pH 7.4, containing 1 M NaCl, 0.1% Triton X-100 and 1 mM PMSF. The column was rotated overnight at 4° C. It was then washed with 400 ml of washing buffer and eluted with 50 mM acetate buffer, pH 5.0, containing 1 M NaCl, 0.1% Triton X-100 and 1 mM PMSF. The neutralized fractions with insulin-binding activity were pooled and further concentrated and desalted by ultrafiltration using Diaflo membrane PM-30 (Amicon). The partially purified receptor was further purified by gel filtration chromatography on a FPLC Supercryl-200 HR 16/60 column (Pharmacia) as previously described, and saved at –70 °C.

The amount of protein was measured by a modified Lowry's method (Bensadoun and Weinston, 1976) or Bradford's method (Bio-Rad), using BSA as a protein standard. Amino acid analysis was performed by the SHC Biotechnology Service Center, Toronto.

2.3. Photoaffinity labeling and Limited Proteolysis

Insulin Photoprobes and Photoaffinity labeling

N-4-(4'-Azido-3'-[^{125}I]iodophenylazo)-3-aminopropyl insulin ([^{125}I]-AZAP-insulin) (Fig.2-3) is a cleavable radioactive insulin photoprobe which allows the insulin moiety to be cleaved from the labeled receptor protein after photoaffinity labeling. N$^{\alpha B29}$-Monoazido-benzoyl-[^{125}I]-iodoinsulin (B29-[^{125}I]-MABI) is insulin derivatized near its putative receptor-binding region, and it retains more than 75% of the bio-activity of insulin (Yip et al., 1980; Ng and Yip, 1985). Both [^{125}I]-AZAP-insulin and B29-[^{125}I]-MABI were synthesized in Dr. Yip's laboratory. [^{125}I]-Iodo-biotin^{B29}-p-benzoylphenylalanine^{B25}-insulin ([^{125}I]-BBpa-insulin) was provided by Dr. Steven Shoelson, Harvard Medical School. It was a new photoprobe with two markers (radioactivity and biotin) for detection, and was reported to have much higher cross-linking efficiency of 60-100% (Shoelson et al., 1993). In preparative photolabeling, the photoprobes used in photolysis were a mixture of trace amounts of radioactive ^{125}I labeled photoprobe and non-iodinated photoprobe.

Photolysis conditions were optimized for high photolabeling efficiency with the least damage to the protein. In preparative photoaffinity labeling, the mixture of non-iodinated and ^{125}I labled photoprobe and receptor protein at a 5:1 molar ratio (for

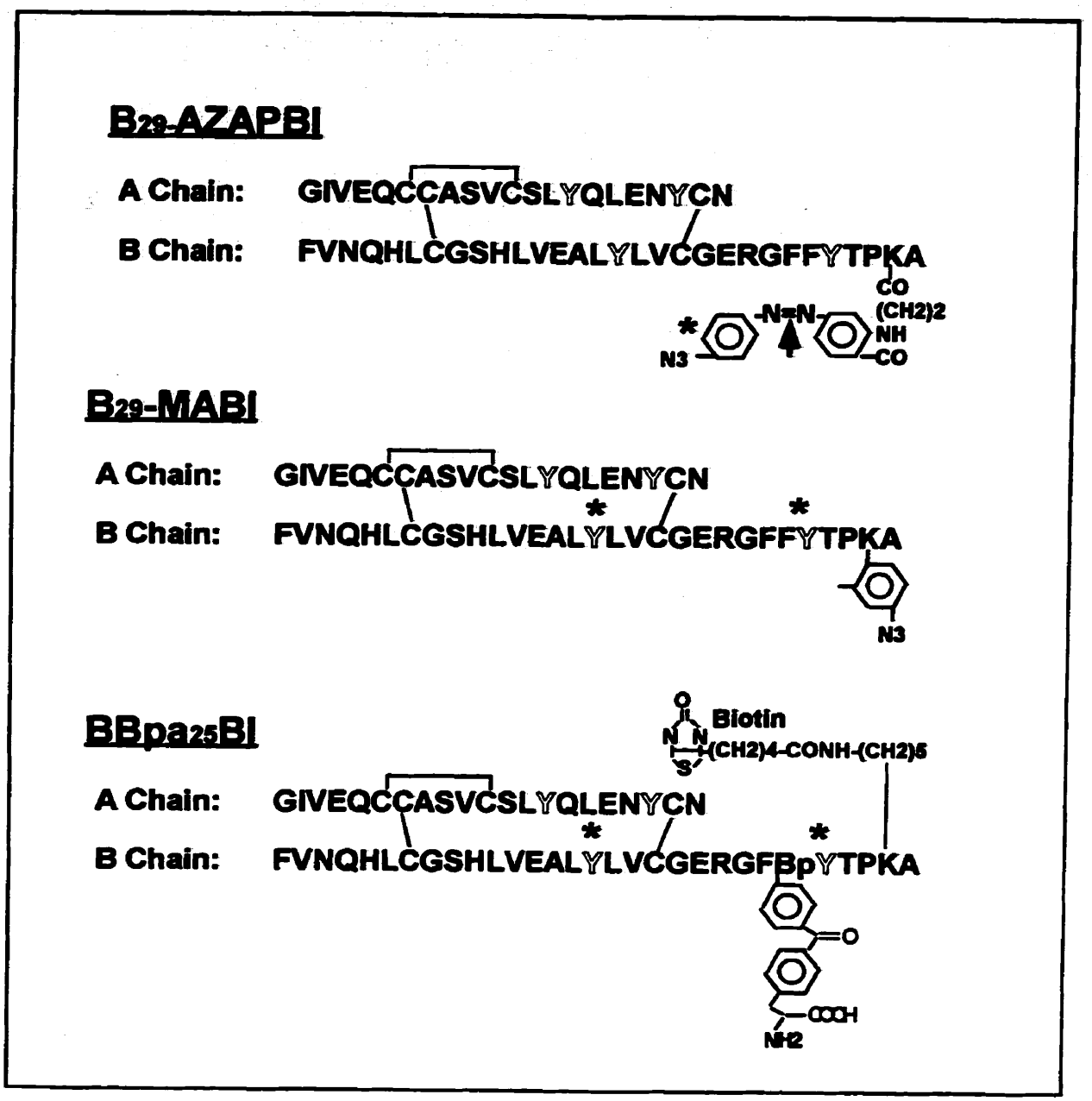

Fig. 2-3. Insulin photoprobes used. AZAPBI is a cleavable photoproble. Arrowhead indicates cleavage site on the probe. BBpa25BI has a biotin marker on the B29 Lysine. * indicates Radiolabeling sites on the B chain (MABI and BBpa25BI) or the cross-linking group (AZAPBI).

example, 18 nmole of insulin photoprobe: 3.6 nmole (~1mg) of purified ectodomain of HIR) were incubated at pH 7.5 Tris/NaCl binding buffer with protease inhibitors at 4°C in the dark for 20 hours. Photolysis in preparative experiments was carried out under UV light with 100 Watts power for 15 seconds or with a 365 nm filter for 45 minutes. During photolysis the protein-photoprobe mixture was kept on ice.

Reduction and Alkylation

The photolyzed IR mixture was adjusted to pH 8.2, 0.1 M Tris, 10 mM EDTA and 8 M urea and kept at 50°C under N_2 and dark for 30 minutes. A 25-fold molar excess dithiothreitol (DTT) then was added and incubated at 37°C under N_2 for 2 hours. Freshly prepared iodoacetamide in 8 M urea, 0.1 M Tris, pH 8.2 buffer was added and the preparation was incubated at room temperature for 30 minutes. The reduction and alkylation were carried out in the dark.

To remove excess free photoprobes, the β subunit portion of the receptor and salts, the reaction mixture was separated by electrophoresis in SDS-PAGE under reducing condition. After electrophoresis, the gel was immediately frozen in dry ice and an autoradiograph of the gel was obtained to locate the photolabeled receptor band on the gel. This gel band was then excised, cut into small pieces and soaked in a pH 7.6, 20 mM NH_4HCO_3 buffer at 4° C overnight. The extract was lyophilized and the gel pieces were then discarded.

Limited Fragmentation

Different proteases or chemical reagents were tried to obtain complete fragmentation of the labeled receptor. Direct digestion of the extracted labeled protein or

the electroblotted protein on PVDF membrane was tried to avoid loss during sample transfer. Before proteolysis, SDS was removed by using the acetone-triethanolamine precipitation method. Typically, the enzyme to protein ratio was kept at 1:50 (w/w) to maintain sufficient digestion while the amount of enzyme was at a minimum. The digestion time for each enzyme or cleavage with CNBr was tested. Control digestion with enzyme only was always carried out at the time of a proteolysis experiment. Protein fragmentation was monitored by 9-26% gradient SDS-PAGE, 40% alkaline PAGE and autoradiography. All enzymes used were of sequence grade purity.

For digestion with trypsin, 10-30 μl of TPCT-treated trypsin, depending on the quantity of protein, was added to the extracted protein dissolved in 250 μl of freshly prepared 2 M urea 0.4 M NH_4HCO_3 buffer (pH 8.0) and incubated at 37 °C for 24 hours. Endoproteinase Glu-E (V8) was used under similar conditions to digest the receptor. Digestion with endoproteinase Lys-C or Achromobacter protease I (Wako Chemicals USA Inc) was carried out by adding a small volume to the protein solution to give a 1:50 to 1:100 (w/w) protease: receptor ratio and the mixture was incubated at 37 °C for 6-8 hours. The reaction was stopped by immediately freezing the solution at –70 °C.

Cyanogen bromide (CNBr) cleavage of the receptor protein was carried out by dissolving the protein in 200 μl of 70% formic acid followed by the addition of CNBr at 100-fold molar excess over the methionine residues of the protein. The mixture was kept in the dark, under nitrogen, at room temperature for 24 hours. The sample was diluted 10-fold with water and lyophilized.

HPLC Peptide Isolation

The enzymatic or chemical digest was acidified with 10 µl of 10% trifluoroacetic acid (TFA) and then injected into a 2.1 mm x 25 cm Vydac C18 narrowbore 300Å reverse phase HPLC column in a Waters 410 HPLC system (Waters) with a detector at a leading wave length of 214 nm. The column was eluted at a flow rate of 0.15 ml/min with a linear gradient from 0-70% acetonitrile/0.065% TFA in 120 minutes. The fractions were frozen immediately after collection.

Identification of Labeled Fragments

Identification by antibody to the B chain of insulin The fragment of the receptor that cross-linked to the insulin photoprobe should contain a fragment of the B chain of insulin after reduction - alkylation and enzyme digestion. To identify this peptide which specifically cross-linked to the B chain of insulin, bovine insulin B chain was used to immunize a rabbit to generate a polyclonal antibody for an enzyme-linked immunosorbant assay (ELISA) experiment to detect HPLC fractions that contain B chain or B chain-receptor fragments.

ELISA was established for detecting peptides containing the B chain of insulin. To increase the reduced antigen absorption to the solid phase of the multiwell plates due to the acetic, organic solvent from HPLC (pH 2.0, up to 70% acetonitrile), a covalent cross-linking plate, Reacti-Plates (Pierce) was used to fix the peptide on the plates. Briefly, 10 µl of the fraction from HPLC was added to the well containing 100 µl of PBS, pH 7.6, and incubated at 4 °C over night. Then the plate was blocked with 3% BSA in PBS for 60 minutes at room temperature. 25 µl of anti-insulin B chain antibody at 1:1000

dilution was added and 100 µl of AP (alkaline phosphatase)-conjugated second antibody at 1:25,000 dilution was used for the color reaction. Varied concentrations of insulin B chain were measured at the same time as the standard curve.

Identification based on biotin-avidin interaction To take advantage of the second marker of biotin on the BBpa-insulin, a sensitive biotin-avidin assay method was established to detect the fraction containing the biotin-B chain signal. Similar sample fixation was done for the ELISA. After blocking, AP-conjugated streptavidin was added to bind the biotin-contained peptide onto the plates. The color reaction with the enzyme then was carried out. Alternatively, to obtain higher sensitivity, extra biotin was added to bind the remaining binding sites of streptavidin, resulting in more streptavidin-enzymes bound, which, in turn, led to an amplified signal.

3. RESULTS

3.1. Recombinant HIR Extracellular Domain

All inserts in the virus constructs were found to have the correct DNA sequences by manual sequencing (data not shown). The titer of purified recombinant viruses was 5 x 10^8 to 1 x 10^9 as obtained by plaque assay. Within 24 hours of infection of Hi5 cells with the recombinant virus, insulin-binding activity was detectable in the culture media and increased with time until Day 4 or 5 after infection. Then the secreted protein in the culture media degraded gradually when the cells started to lyse (Fig. 2-4). While the

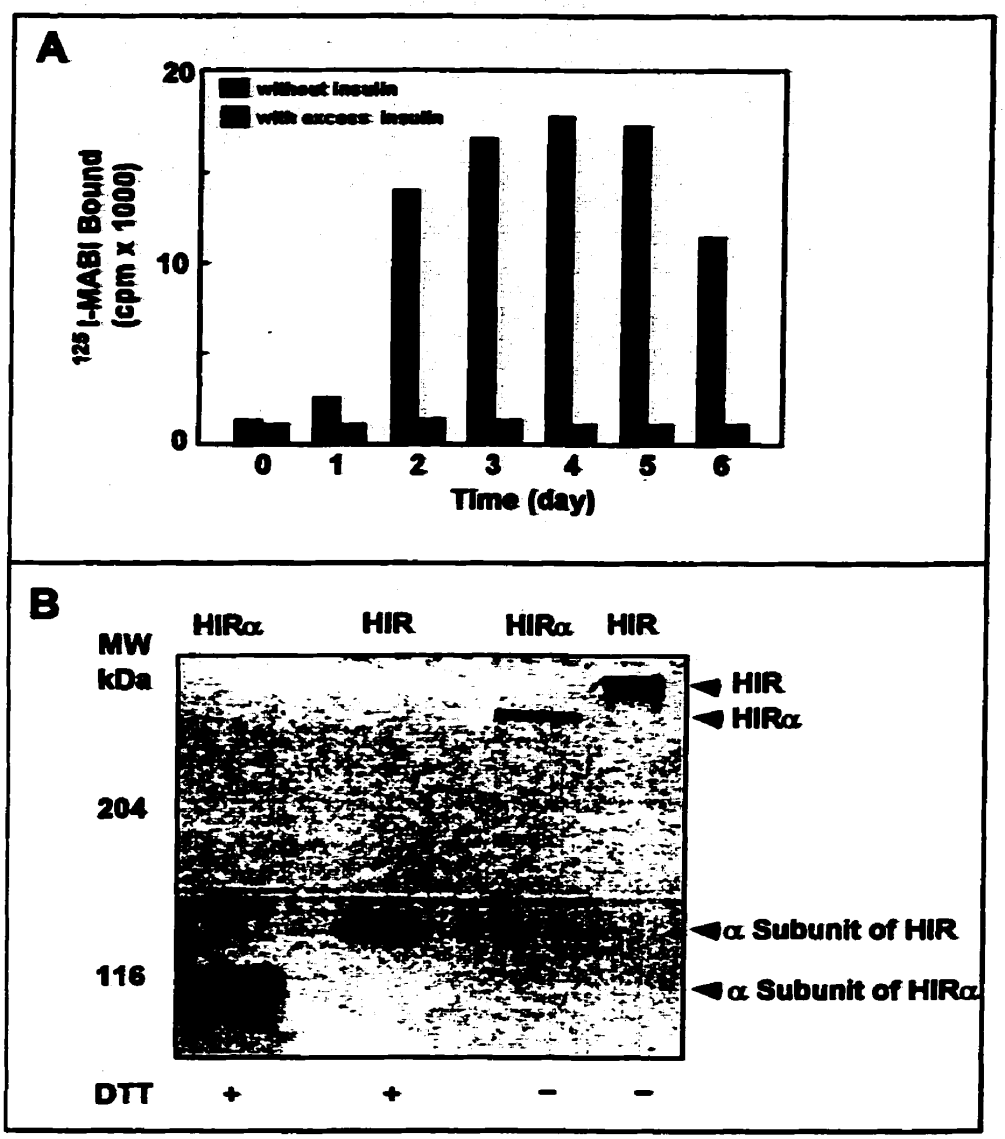

Fig. 2-4. Time course of theexpression of the recombinant extracellular domain of hIR (hIRα) (A), and Western blot (anti-α subunit of hIR) of hIRα and human placental insulin receptor (hIR) (B). The heterotetrameric hIR has a molecular mass of 450 kDa, and a molecular mass of 130 kDa for its α subunit The recombinant hIRα shows a molecular mass of ~280 kDa, and a molecular mass of 110 kDa for its α subunit. A small amount of uncleaved recombinant receptor (~140 kDa) can be seen on the reduced gel, which represents the uncleaved single chain containing the α subunit and the extracellular domain of the β subunit.

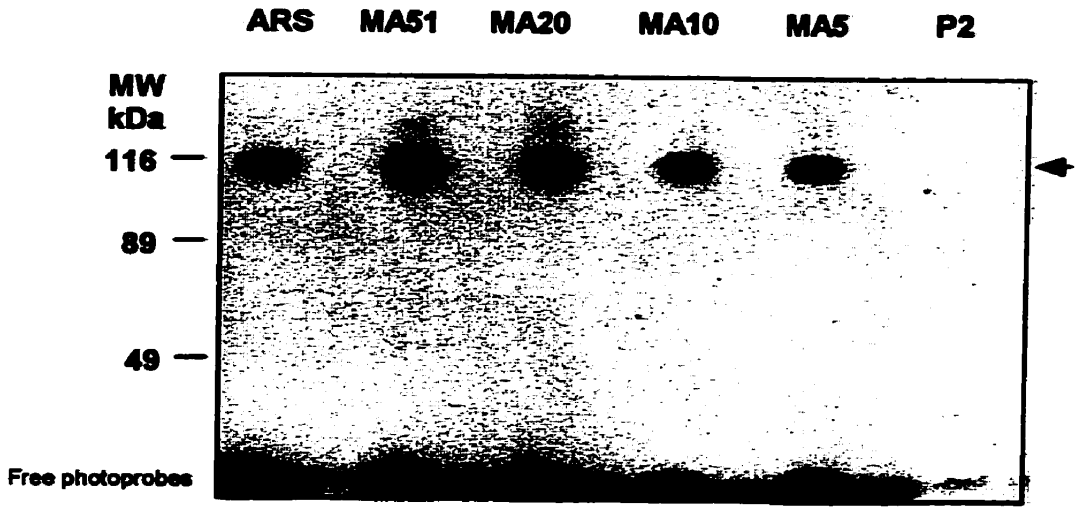

Fig. 2-5. Immunoprecipitation of B29-MABI labeled hIRα. Human anti-hIR antibody (ARS), mouse monoclonal anti-hIR antibodies MA51, MA20, MA10 and MA5, Rabbit anti-fragment P2 of hIR antibody were incubated with B29-MABI photolabeled hIRa and Protein A Sepharose. The washed Protein A Sepharose beads were then analyzed in the reduced SDS-PAGE. All antibodies, except P2, recognized the recombinant hIRα. Arrow indicates labeled hIRα.

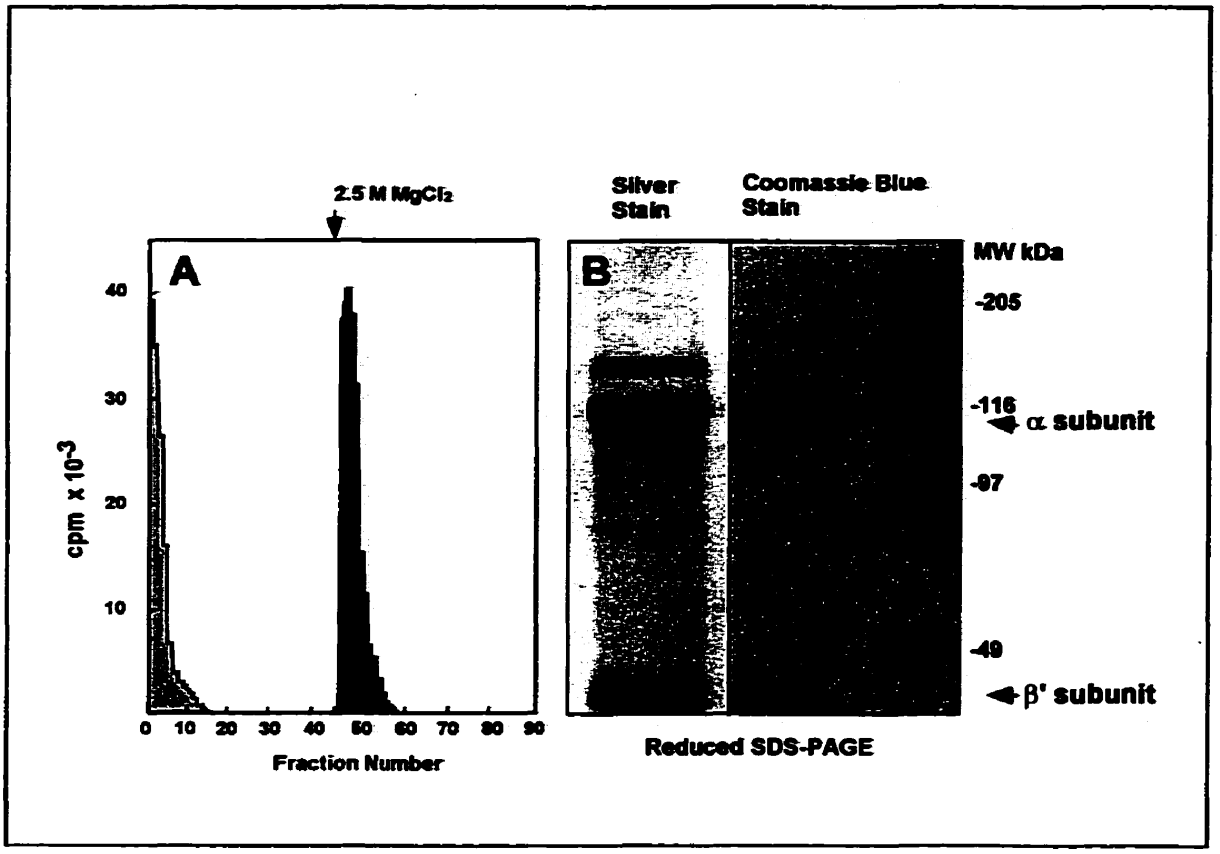

Fig. 2-6. Affinity purification of expressed hIR extracellular domain with anti-hIR monoclonal antibody (MA51) column. A) The purification profile monitored by radioactive tracer of ^{125}I labeled bovine insulin. Expressed insulin receptor extracellular domain was eluted with 2.5 M MgCl2. B) Purified recombinant hIR extracellular domain was analyzed by SDS-PAGE under reducing condition. The gels were stained either with silver or Coomassie blue. Trace amount of uncleaved αβ' single chain receptors and bovine albumin can be seen in silver stained gel.

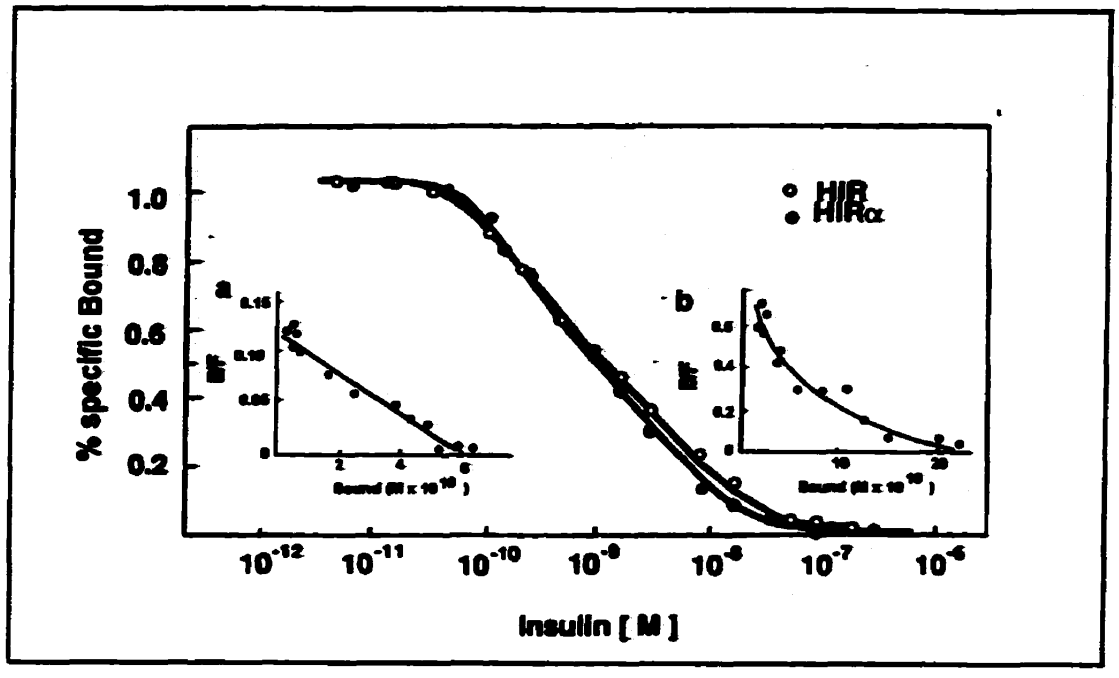

Fig. 2-7. Insulin binding assay of recombinant extracellular domain of hIR (hIRα) compared with human placenta insulin receptor (hIR). Competition binding studies were performed with purified placenta hIR or hIRα as described in the methods. A14-^{125}I-bovine insulin was used as the tracer ligand. Inserts are Scatchard plot of insulin binding to hIR (open circles) or hIRα (closed circles). Insulin binding to the placental hIR shows a typical curvilinear curve (b) with K_{d1}=0.5 x 10^{9} M and K_{d2}=2 x 10^{-7} M, while insulin binding to hIRα shows a linear line (a) with a K_d= 1 x 10^{-9} M.

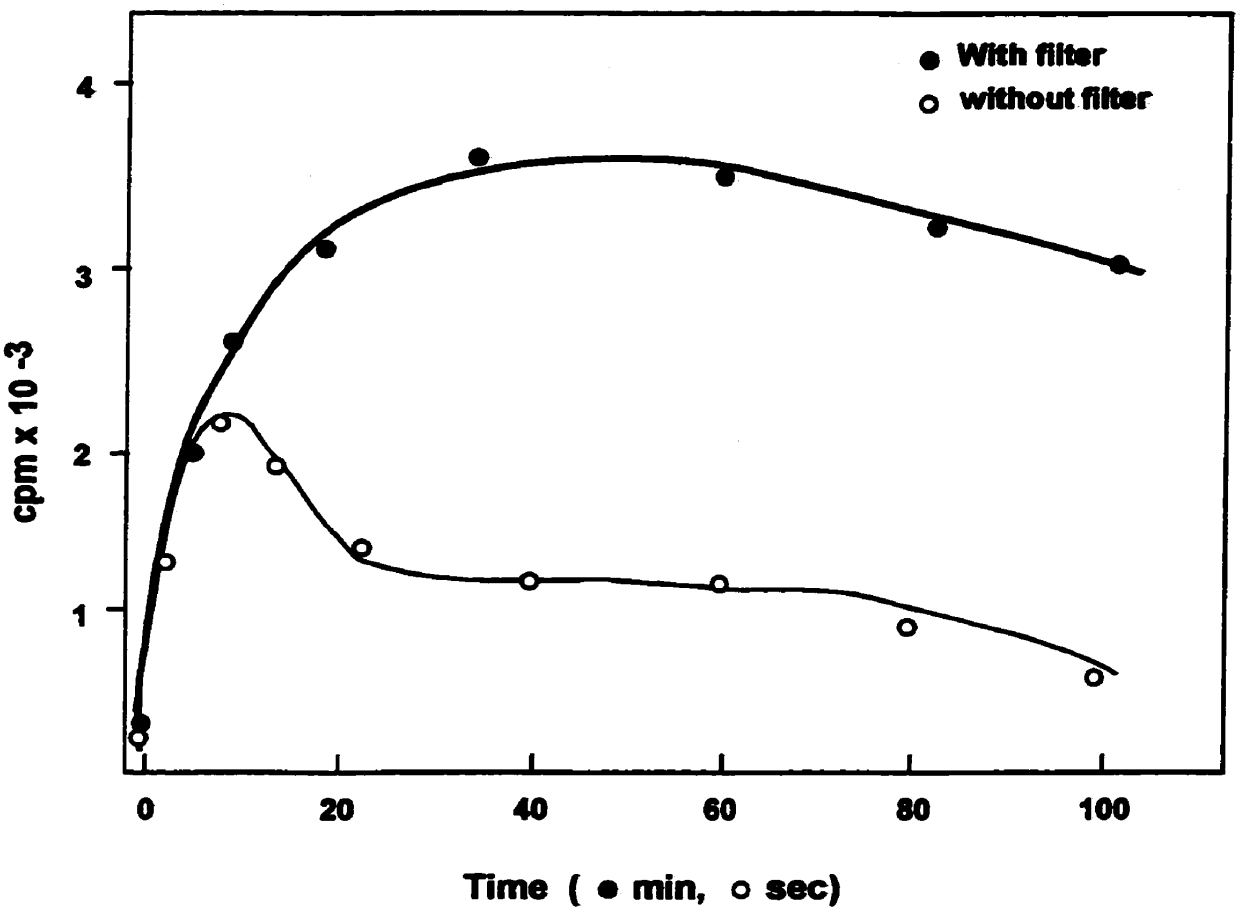

Fig. 2-8. Time course of photolysis. Radioactive labeled insulin photoprobe was incubated with hIR in binding buffer in the dark at 4° C for 20 hours, followed by exposure to UV light (100 Watts) for 5, 10, 15, 20, 40, 60, 80 and 100 seconds, or with a 365 nm filter for 5, 10, 20, 40, 60, 80 and 100 minutes. Higher cross-linking efficiency and less protein damage were observed with 365 nm filter.

secreted fully processed ectodomain of HIR accumulated in the culture media, many unprocessed precursors accumulated in the plasma membrane (data not shown). The secreted recombinant receptor was recognized by human autoimmune anti-HIR antibody and monoclonal anti-HIR antibodies (Fig. 2-5). More than 90% of secreted protein was shown to have a fully processed $\alpha_2\beta'_2$ heterotetramer structure (two ~ 110 kDa α subunits and two ~30 kDa truncated β' subunits). A small amount of protein was secreted as non-cleaved $(\alpha\beta')_2$ dimer (two ~140 kDa $\alpha\beta$' monomers) (Fig. 2-6). The yield of expression was ~ 1 mg/liter of culture media as measured by immunoassay (data not shown). The affinity purified receptor binds insulin with a high affinity (Kd = 1 x 10^{-9} M) which is comparable with that of wild-type human placenta IR (Fig. 2-7). This receptor exhibits a linear Scatchard plot.

3.2. A Small Labeled Peptide Fragment on the Insulin Binding Region

To optimize photolysis I tested different photolabeling conditions. Without the filter, photolysis occurred very fast in seconds. Protein damage could be seen with exposures longer than 20 seconds. With a narrow band optical filter at 365 nm, which eliminates most short-wave UV light, the cross-linking efficiency was increased 2-fold and the protein damage, resulting mostly from short wave UV light, was reduced (Fig. 2-8).

In a preliminary study, both the cleavable ([^{125}I]-AZAP-insulin) and the uncleavable (B29-[^{125}I]-MABI) photoprobes were used to characterize the proteolyzed peptide containing the putative insulin binding site. In the case of the cleavable

photoprobe, insulin B chain should be cleaved after photolysis, and only radioactive iodine left cross-linked to the receptor. A single radioactive band containing no attached insulin B chain appeared after endopeptidase digestion. In the case of the other photoprobes, since insulin B chain has two iodination sites, TyrB16 and TyrB26, two radioactive fragments should be generated in the enzyme digests. A small 1-3 kDa radioactive labeled fragment was generated by either trypsin or V8 treatment of HIR labeled with B29-[^{125}I]-MABI (Fig. 2-9). In the case of HIR labeled with [^{125}I]-AZAP-insulin trypsin digestion generated a single small labeled peptide. Most of the digestion occurred in the first few hours but complete digestion took 20 hours. Similar results were obtained when using endopeptidase Lys-C digestion. CNBr treatment failed to completely cleave the labeled receptor (data not shown).

Antibody against the B chain of insulin was shown to recognize with high affinity the intact insulin B chain or its tryptic digest at pmole levels (Fig. 2-10). However, when the same method was used to detect fragments in HPLC fractions, the sensitivity of detection decreased several thousand fold. To obtain enough sensitivity to recognize the peptide(s) of interest in HPLC fractions, I cross-linked the peptides in the HPLC fractions to ELISA plates instead of using the conventional coating method. The conventional sample preparation method showed a dramatic drop in the sensitivity of ELISA analysis due to the very low pH (~pH 2) and high concentration of organic solvent (~30-70% of acetonitile). The modified method could detect the peptide containing B chain fragments in HPLC fractions (Fig. 2-10) or in digests of receptor labeled with B29-MABI (Fig. 2-11) at the pmole level.

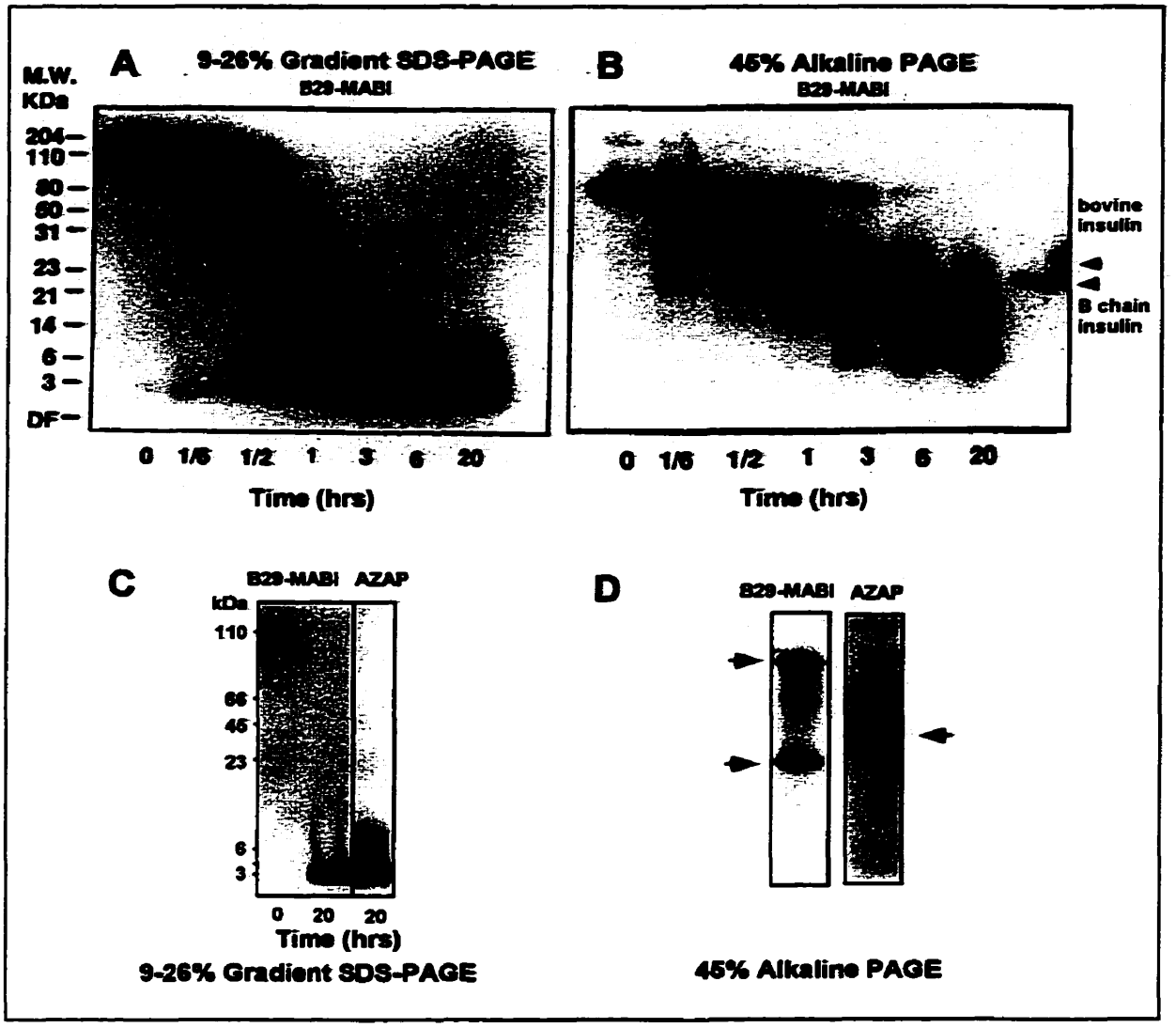

Fig. 2-9. Time course and products of trypsin digestion of B29-MABI or AZAP labeled hIR extracellular domain. Panels A and B show that trypsin digestion starts within an hour and is completed in 20 hours. Complete digestion generates ladeled fragmants smaller than 3 kDa (A and C) with both B29-MABI and AZAP photoprobes. The 45% alkaline gel analysis shows that B29-MABI labeling generates two radiolabeled fragments by trypsin digestion, arising from the presence of two radioactive iodine labeling sites on the insulin B chain. One of the labeled fragments contains the putative insulin-binding site. In the case of AZAP photoprobe labeling, since radioactive iodine labeled on the cross-link group instead of the insulin B chain, which is cleaved after photolabeling, a single radolabeled receptor fragment is seen on the gel (D). Bovine insulin and the insulin B chain insulin were loaded on the right lanes of the gel as a control (B).

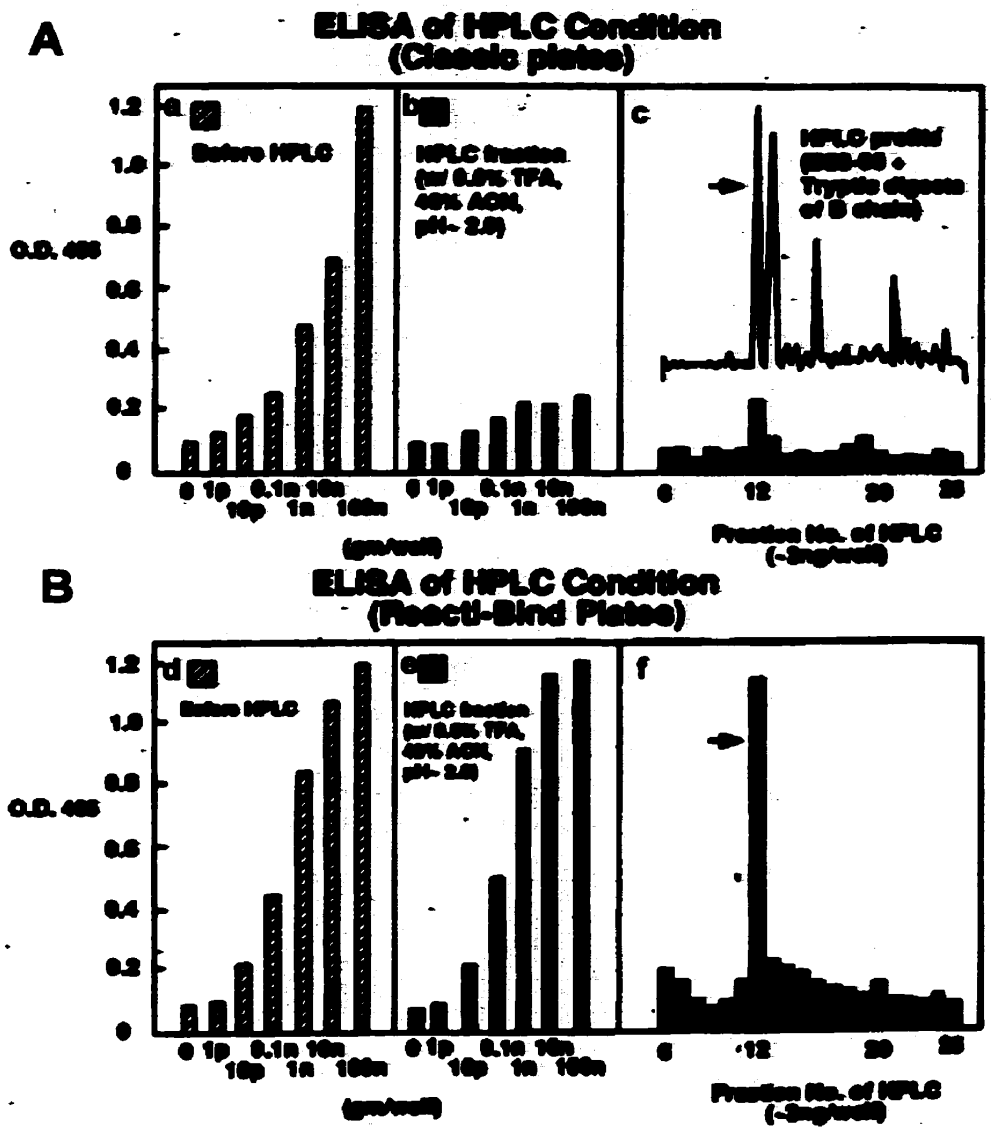

Fig. 2-10. The sensitivity of ELISA in detecting B chain fragment of bovine insulin before (a and d) and after HPLC analysis (b, c, e and f). A dramatically reduced sensitivity (b, c) was observed under the acidic condition in the HPLC fractions when using regular plates. Using Reacti-Bind plates (Pierce) restores the sensitivity of ELISA to pg/well level (e, f). Synthetic B22-30 fragment of the insulin B chain was used as standard in a, b, d and e. Tryptic digests of the insulin B chain containing the fragments of B1-21 and B22-30 (arrowhead) were used as HPLC sample.

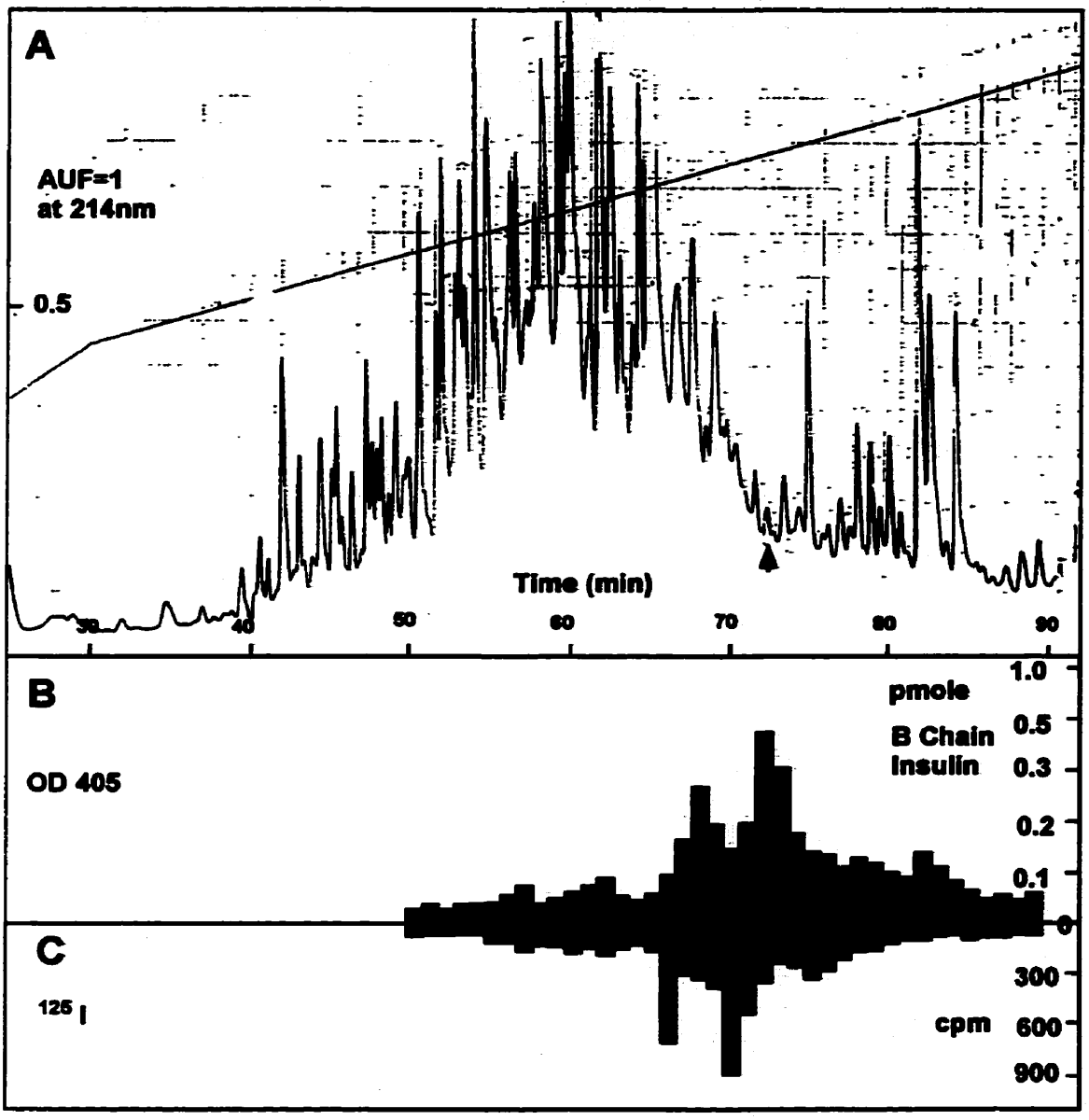

Fig. 2-11. Trypsin digests of ^{125}I-B29-MABI labeled hIRα

A) HPLC profile. B) An aliquot (10 ml) of each fraction was assayed by ELISA using alkaline phosphatase-conjugated anti-B chain insulin antibody. C) Radioactivity of each fraction (0.5 ml) determined. Due to the slight difference in hydrophobicity between the radioactive labeled and unlabeled IR fragments, ELISA signals (B) are slightly shifted when compared to the radioactive signals (C). The two major peaks in panel B and C represent the two fragments of the insulin B chain, generated by enzyme digestion. Only one of the two fragments would be expected to be is cross-linked to the insulin-binding site of the IR. Based on the ELISA results, fractions 73 (arrowhead in A) and 74 were pooled and analyzed again by HPLC.

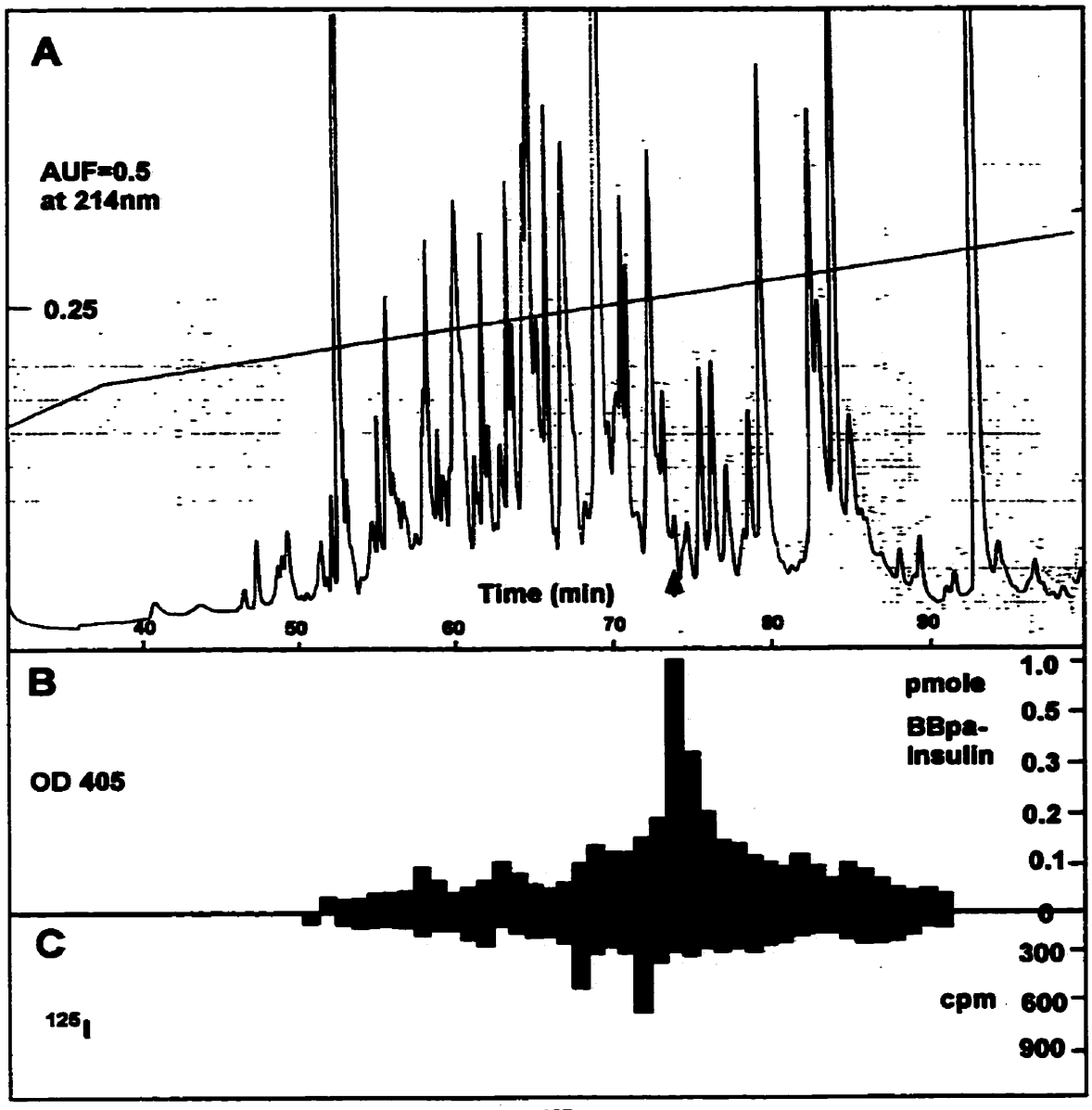

Fig. 2-12. Achromobacter protease I digests of ^{125}I-BBpa-Insulin labeled hIRα. A) HPLC profile. B) An aliquot (10 ml) of each fraction was assayed by ELISA using alkaline phosphatase-conjugated streptavidin. C) Radioactivity of each fraction (0.5 ml) was determined. One streptavidin-positive peak and two radioactive peaks were detected. Based on the ELISA results, fractions 74 (arrowhead in A) and 75 were pooled and analyzed again by HPLC.

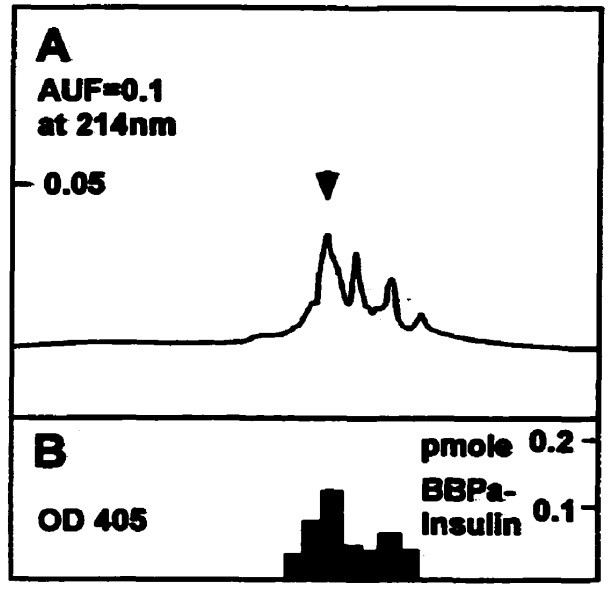

Fig. 2-13. HPLC analysis of pooled fractions as identified in Fig. 2-12 (A).
A) HPLC profile obtained using a mobile phase different from that used to obtain the profile shown in Fig. 2-12. B) An aliquot (10 ml) of each fraction was assayed by ELISA using alkaline phosphatase-conjugated streptavidin. The streptavidin-positive fractions showed very poor recovery.

In the case of HIR labeled with BBpa-insulin, I used both the antibody and the streptavidin method of detection. Radioactivity was also used in the detection when radioactive photoprobes were used. A typical HPLC profile is shown in Fig.2-12. The fraction containing the peptide of interest was further purified by HPLC under different conditions, resulting in a great loss of the peptide (Fig. 2-13). I was unable to collect a sufficient quantity of the peptide for amino acid sequencing.

4. DISCUSSION

The baculovirus expression system (BES) has been successfully used to express many functional proteins (Luckow and Summers, 1986). It is a very powerful eukaryotic protein expression system, and it is superior to bacterial, yeast and mammalian expression systems for many reasons. Most recombinant proteins from BES are soluble and fully functional. Insect cells used in the protein expression utilize many of the protein modification, processing and transport systems present in higher eukaryotic cells that are essential for full biological activity of the recombinant protein. Like other investigators, I was not able to express soluble intact HIR in bacteria or yeast (unpublished data). Mammalian cell systems, on the other hand, usually express limited quantities of recombinant proteins. My preliminary study and the results from other investigators suggest that the extracellular domain of the HIR expressed from BES maintains full binding affinity for its ligand (Paul et al., 1990; Sissom and Ellis, 1989).

In this study, I have successfully used the baculovirus system to overproduce the truncated, soluble, secretory ectodomain of HIR which retains full insulin-binding affinity compared to native placenta insulin receptor (Fig. 2-8). While a satisfactory

quantity (a few mg/liter) was secreted in the media with full function, a significant amount of uncleaved αβ' precursor accumulated inside the cell (Fig. 2-5). Other investigators (Paul et al., 1990; Sissom and Ellis, 1989) have previously reported the expression of similar versions of the ectodomains of HIR in the baculovirus expression system, and mammalian expression system (Cosgrove et al., 1995). The molecular mass of the α subunit expressed in the baculovirus system is smaller (110 kDa versus 130 kDa for the its native counterpart), likely due to different glycosylation during the post-translation process (Paul et al., 1990; Sissom and Ellis, 1989). Nevertheless, the carbohydrate content of the receptor has been demonstrated to have no effect on the ligand-receptor interaction (Caro et al., 1994).

Several investigators have reported that the secreted HIR ectodomain produced by BES exhibits a linear Scatchard plot (one class of high-affinity site only) whereas the native membrane HIR exhibits a curvilinear plot, suggesting one high-affinity and one low-affinity site. Interestingly, the Scatchard plot obtained with the secreted HIR ectodomain expressed in mammalian cells was curvilinear (Whittaker and Okamoto, 1988). This difference in the ligand-binding behavior is not understood. It might result from the different processing of the heterotetramer in the different expression systems. Alternatively, the relative abundance of the uncleaved proreceptor produced by the insect cell may affect the binding of a second insulin molecule. It is known that the αβ half receptor exhibits a linear Scatchard plot, but with low affinity for insulin (Sweet et al., 1997). The fact that only the heterotetramer structure of the HIR can bind insulin with high affinity suggests that high affinity insulin-binding sites require both halves of the receptor to participate. Insulin itself has no obvious intrinsic symmetry but must interact

with two identical αβ-receptor halves for high affinity binding. I believe that there may exist identical but more than one contact site in each α subunit of IR. High affinity insulin binding requires contacting different sites on each half of the receptor. At low physiological insulin concentrations, insulin can contact its binding sites on both α subunits for high-affinity binding. At higher concentrations of insulin, a second insulin molecule can only contact some of the sites required for high affinity binding, leading to low affinity binding. The fact that the IR binds one insulin with high affinity and the second with low affinity suggests that asymmetry may be induced in the receptor by insulin binding. It also suggests that one insulin molecule binding to the receptor with high affinity either leads to a conformational change of the receptor, or simply one insulin occupies the space allowing for high affinity binding making it difficult to bind the second insulin. The different post-translational processes in the baculovirus expression system may lead to some conformational variation in the recombinant receptor to allow either one insulin molecule only to bind or two insulin molecules to bind with similar affinity.

Affinity labeling of the receptor with photoreactive insulin derivatives followed by isolation of receptor-insulin fragments has allowed the identification of regions of the α subunit as potential hormone-receptor contact sites. Several regions have been suggested by various investigators (Wedekind et al., 1989; Waugh et al., 1989; Yip et al., 1988; Fabray et al., 1992). Most of the studies resulted in relatively large fragments (from 14-55 kDa), making it difficult to pinpoint accurately the contacting location. Results obtained in the present study indicate that a very small fragment (~1–3 kDa) contained the insulin binding site, or part of the binding site on the α subunit. Results obtained from

HPLC peptide mapping based on the highly sensitive detecting methods suggested that it may be possible to identify this fragment by its amino acid sequence if sufficient quantities of the peptide could be obtained. On the other hand, smaller peptides are more difficult to isolate and identify. Western blots used by many investigators to detect their larger receptor fragments, would be difficult to use to isolate such a small peptide for sequencing. Reverse-phase HPLC analysis has been successfully used to isolate a small peptide fraction from other peptides. However, the low photolabeling efficiency makes it difficult to load enough protein digests on the column to yield a sufficient quantity in the fraction containing the labeled fragment. The large percentage of non-productive, non-labeled receptor also contributes to the difficulty of purification. It will require a second or third re-purification of the HPLC fractions to obtain a pure fragment for amino acid sequence analysis. The current amino acid sequencing method also requires up to ten times more material to have reasonable results for a smaller peptide compared to larger polypeptides. Since most photoaffinity probes have low cross-linking efficiency (<1-10%), either more starting material or a probe with higher efficiency is required to isolate enough fragment. Alternatively, a higher efficiency purification method or a more sensitive amino acid sequencing method needs to be developed. The new BBPa-insulin photoprobe with higher cross-linking efficiency has shed new light on this project although we failed to achieve the efficiency claimed by the original investigators (Lee et al., 1993). Unfortunately, the new BBPa-insulin photoprobe we obtained was only sufficient for developing the methodology. It is clear that more work would need to be done to overcome the obstacles in this biochemical approach.

CHAPTER 3

QUATERNARY 3D STRUCTURE OF THE INSULIN-INSULIN RECEPTOR COMPLEX DETERMINED BY SCANNING TRANSMISSION ELECTRON MICROSCOPE: STRUCTURAL LOCALIZATION OF INSULIN-BINDING SITE ON THE HIR

1. INTRODUCTION

Protein-protein interactions at the molecular level are largely related to their three-dimensional (3-D) structures. Elucidation of 3-D structures of proteins at high resolution is crucial to the understanding of many fundamental functions of macromolecules and macromolecular complexes. Besides its significance in understanding the chemistry of life, the refined structure of a protein also provides highly valuable information for medical applications, such as new drug design (Giranda et al., 1994).

The most commonly used methods for solving macromolecular structure are x-ray crystallography, nuclear magnetic resonance (NMR) spectroscopy and electron microscopy (EM). While the 3-D structure of a great number of proteins has been determined by x-ray crystallography, if they crystallize, and by NMR spectroscopy, if they are sufficiently small, the vast majority of biological macromolecules have not been crystallized or are too large for these approaches. X-ray crystallography has been successfully employed to determine 3-D structure at a resolution of 1.5 ~ 3 Å. However, due to the difficulty in growing crystals of proteins suitable for x-ray crystallography, most proteins whose 3-D structure have been solved by this technique are smaller than 100 kDa. Using NMR spectroscopy, investigators can solve the structure of a protein at

atomic resolution but the molecule must be even smaller, around 25 ~ 30 kDa, and highly purified. However, electron microscopy, combined with computer processing algorithms, has successfully solved the 3-D structure of macromolecules with molecular weight from several to several thousand kDa at Å to nm level (Ottensmeyer, 1982; Schrag et al., 1989; Chiu and Schmid, 1997; Rosenberg et al., 1997). This technique offers a powerful high-resolution tool in structural biology, and is especially useful for large protein molecules that cannot be studied by either x-ray crystallography or NMR method. The EM-based 3D reconstruction enables investigators to solve the molecular architecture of proteins, and to determine the overall size and shape of their constituent protein subunits with atomic details. In addition, this technique also allows researchers to investigate distinct functional states by monitoring conformational changes or structural reorganizations (Whittaker et al., 1995; Jontes et al., 1995; Unwin N, 1995, 1998). Such studies have provided insight into the structure and function of many proteins, including virus structure and morphology (Shaw et al., 1993; Zhou et al., 1994), localization of individual protein components (Zhou et al., 1995), identification of cellular receptors (Olson et al., 1993) or monoclonal antibody binding sites (Wang et al., 1994; Chiu and Smith, 1994) and protein-protein interactions (Beckmann et al., 1997).

The electron microscope provides much higher magnification than the light microscope by the combination of magnetic lenses and short wavelength electrons at high voltage. However, compared to the case in material science, biological specimens are more difficult to image in the electron microscope because of their low contrast and their sensitivity to radiation. Much effort has been made in the last few decades to make EM more useful to biology. High contrast heavy atoms (osmium, lead, uranium, etc) are

usually required to stain or coat the biological samples in a controlled way to make them become "visible". However, the object being imaged is actually an "artifact" composed of the distribution of heavy atoms surrounding the features of interest.

Scanning Electron Microscope One of the commonly used electron microscopes in biology is the scanning electron microscope (SEM). SEM images are obtained by using a very narrow electron beam to scan over the surface of the specimens and by mapping the signal of emitted secondary electrons (or of back-scattered electrons) into the corresponding pixel of the recording/display image (Fig. 3-1). Although SEM provides much higher resolution and a much greater depth of field than the light microscope, biological specimens usually need to be coated with a conducting layer of heavy atoms to avoid charging under the scanning electron beam. This approach limits the detailed interpretation of small structures and provides only the surface feature of the specimen. In addition, although improvements are being made, the resolution commonly at about 20 nm is also not high enough to reveal detail in individual protein structures, which usually requires resolution at nm or sub-nm level. SEM has been mostly used in the studies of organ or tissue structure in biomedical research.

Transmission Electron Microscope and Scanning Transmission Electron Microscope Compared with the SEM, the transmission electron microscope (TEM) is a more powerful tool available for the investigation of the microstructure of bio-macromolecules (Fig. 3-1). The TEM is somewhat similar to the SEM in that both use a high-energy beam of electrons and a series of magnetic lenses to control the beam. However, the electron beam voltage is much higher (100 KeV or greater; shorter wavelength) in the TEM, and the high energy beam passing through the specimen is used

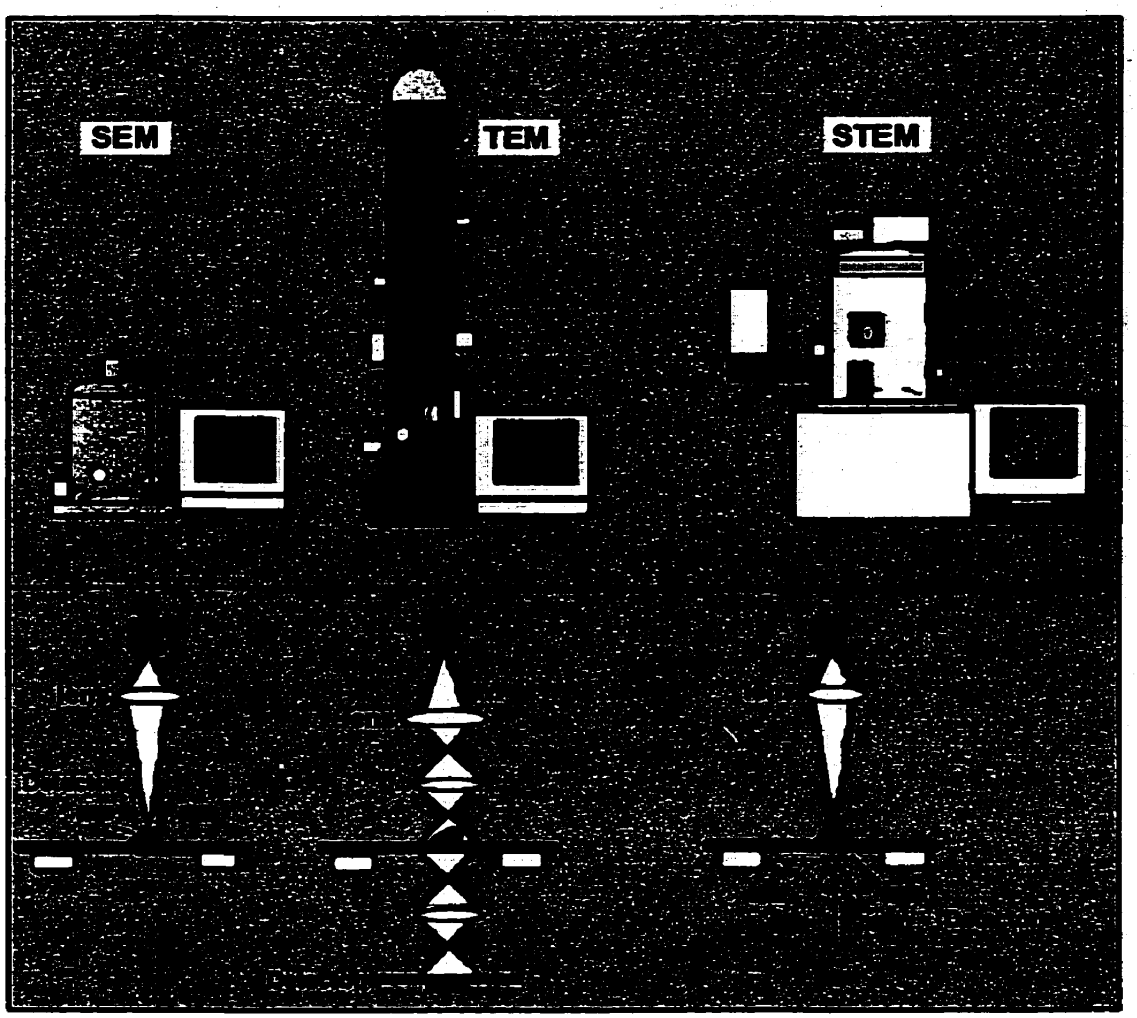

Fig. 3-1. Different electron microscopes used in biomedical studies. The scanning electron microscope (SEM) is mainly used to study the structure of organ or tissue at relatively low resolution. The transmission electron microscope (TEM) is used to investigate the microstructure of biomolecules. The scanning transmission electron microscope (STEM) combines the advantages of both SEM and TEM and is more efficient in the use of scattered electrons, and consequently can reduce specimen damage. STEM has been used for high resolution 3D reconstruction of protein molecules.

to form a direct image. A magnification of about 500,000 x is typical and the resolution can approach 1 nm or better.

Within the last few years, tremendous progress in EM technology and computer image processing have been made. The introduction of low-dose and cryo-preservation techniques into electron microscopy has opened a new era for 3-D structure determination of biomacromolecules. Cryo-fixation, ice-embedding or freeze-drying the protein sample in its physiological buffer, permit direct imaging of the protein itself in a near-physiological state. It has been widely accepted that these methods reduce adsorption artifacts and reproduce structural details more accurately and faithfully. Most importantly, in addition to mapping out the overall size and shape of biomacromolecules, cryo-transmission electron microscopy, and cryo-scanning transmission electron microscopy (STEM) enables investigators to look "inside" biomacromolecules and is beginning to image their secondary structural elements, or even their atomic details. The 3-D EM structural information can, under some conditions, be obtained at a resolution of as good as several Ångstroms, similar to the resolution in X-ray crystallography, to directly reveal the α-helix structural details of some proteins (Kühlbrandt et al., 1994; Cheng et al., 1997; Walz et al., 1997). Consequently, more researchers are beginning to use electron cryo-microscopy for structural and functional studies of biomacromolecules. The 3-D image reconstruction of EM has become a new tool and a very powerful approach in biomedical research.

The uniqueness of the STEM is its ability to visualize individual biological molecules directly without staining, fixing or shadowing. In the STEM, image acquisition is digitized as a small electron probe (3 Å beam size in the HB601UX STEM), produced

by a cold-field emission gun, a condenser and objective lens, scans in raster fashion across the specimen. The microscope operates in a dark-field mode with high efficiency annular detectors collecting virtually all the scattered electrons. The high efficiency of STEM permits dark-field images to be obtained using lower radiation doses (ten to hundreds times less than by dark-field imaging in TEM, resulting in less damage to protein structures). The number of scattered electrons received by the detector is directly proportional to the mass thickness of the scanned molecules. Thus the molecular mass of the individual molecule can be calculated by subtracting the background and using a scattering cross-section or calibration standard. Another unique feature of STEM is that individual heavy atoms can be visualized and thus specific sites on biological molecules can be mapped (Hainfeld, 1992). Recently, a monofunctional reactive gold cluster (1.4 nm in size), Nanogold, has been successfully used to localize specific functional sites with STEM in several proteins (Boisset et al., 1992; Wilkinson et al., 1994). With low-dose electron beam scanning, high contrast dark-field imaging and digitally recording features, STEM can collect high-resolution images from a specimen as small as a single heavy atom to proteins larger than a thousand kDa. Combined with novel computer processing techniques developed for the microscope, STEM has been successfully used to reconstruct 3-D structures of several proteins, such as SRP54 and Klenow fragment of DNA polymerase I (Farrow and Ottensmeyer, 1992; 1993; Czarnota et al., 1994) at a resolution of 12 - 20 Å.

1.1. Electron Microscopic 3-D Reconstruction Techniques

3-D electron cryomicroscopy of biological macromolecule consists of several

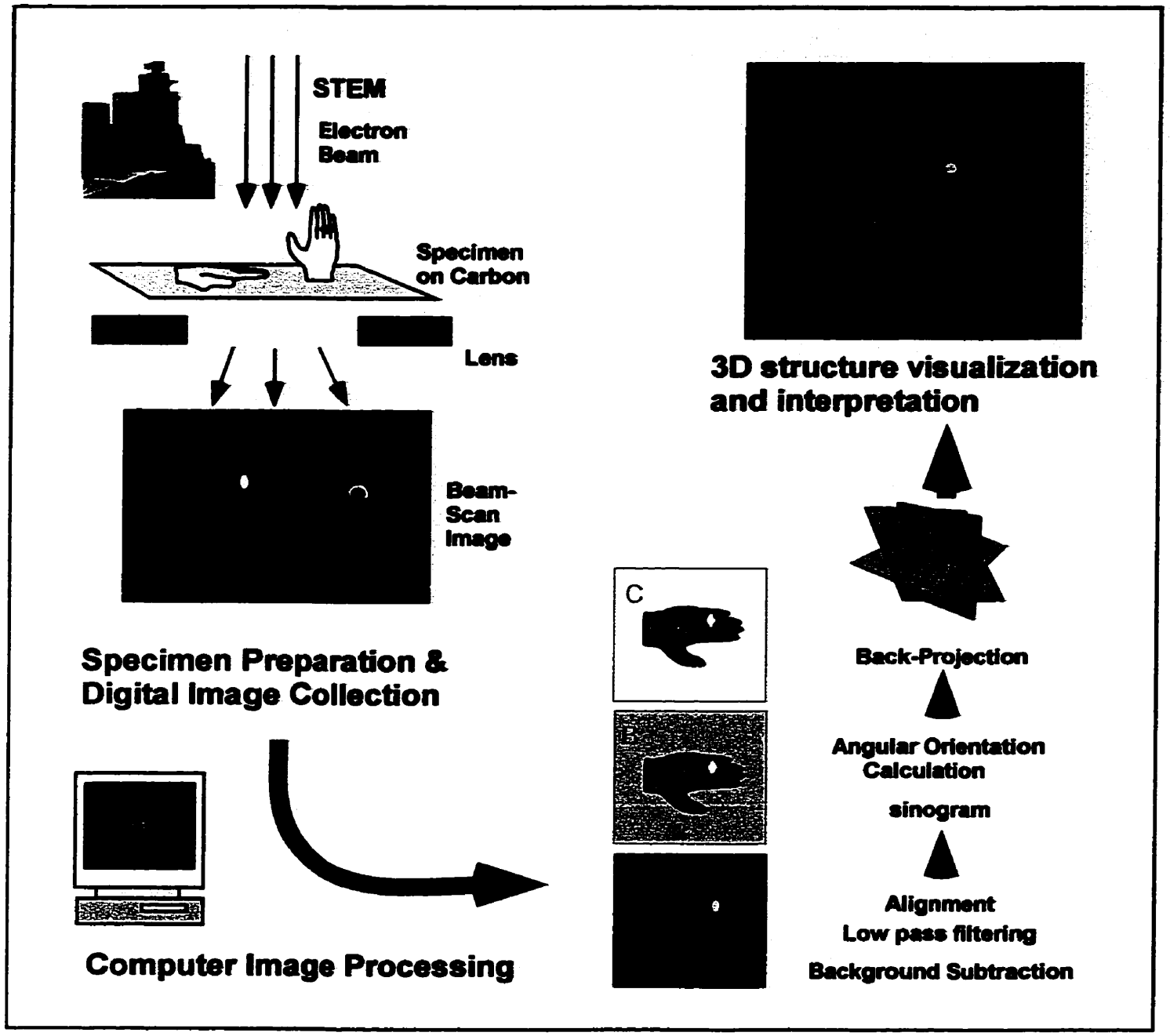

Fig. 3-2. An overview of STEM 3D reconstruction. Single particles of the insulin/insulin receptor complex, represented as a hand, were subjected to STEM. Images were collected and analyzed and processed by computer involving (A) background subtraction, (B) low pass filtering, and (C) alignment. Further processed images were back-projected and displayed as a 3D structure.

major steps: specimen preparation; image collection, normalization and processing; and 3-D reconstruction and interpretation (Fig. 3-2.). Briefly, many large images of digitized single molecules are collected and placed in a computer file with hundreds or thousands of individual particles. The individual images then undergo two-dimensional (2D) image analysis, including variance normalization, background subtraction, low band pass filtering, as well as statistical analysis. The processed 2D images then are ready for 3D image processing. The background has been completely removed during this process. A sinogram, a stack of one-dimensional projections of the 2-D image rotated 360° around its Y axis, of each single particle is calculated and is used to relate the orientation of one image to any other. After the relative angular orientation of each image is calculated, all images are back-projected to produce the final 3-D reconstruction.

A number of recent developments in computational techniques and experimental approaches have greatly improved this process and for special cases, increased the resolution of the electron microscopy reconstruction from the early 30 Å (Dryden et al., 1993) to a few Ångstroms (Bottcher et al., 1997; Trus et al., 1997). One of the approaches, which greatly increases the structure resolution in 3-D reconstruction, is the use of 2-D electron crystallography. In this method each image contains thousands of identical units in identical orientations, which can be accurately and easily averaged. As a consequence, structural analysis by electron cryomicroscopy of 2-D crystals can extend the resolution to the atomic level. For example, by using this technique, the structural resolution of bacteriorhodopsin with a resolution approaching 3.5 Å permits visualization of α-helical bundles in this membrane protein (Henderson et al., 1990). Another technique, known as the random conical tilt method, is able to use samples in which

molecules assume one, or a few, preferred orientations so that a higher resolution can be attained (Radermacher et al., 1992; Serysheva et al., 1995). However, this technique is limited by the requirement that the specimen adopt recognizable preferred orientations with respect to the support film.

Novel methods which do not require crystallization, structural symmetry or preferred orientations have been developed and implemented as well, and used in our work (van Heel, 1987; Ottensmeyer and Farrow, 1992; Farrow and Ottensmeyer, 1993; Ottensmeyer et al., 1994). This approach was designed for random orientations of non-symmetric molecules, and makes use of quaternion mathematics to solve the structure of biomacromolecules even from noisy images of single particles. An advantage of this method is that it permits structural determinations of macromolecules under many different conditions including different ionic environments, molecule size or post-translational modifications, which overcome many limits in crystallization or pre-requirement in sample preparation. Recently, a signal sequence binding protein has been successfully resolved to its 3-D structure at 12 Å resolution with this technique (Czarnota et al., 1994).

1.2. Structural Determination of IR and Localization of Insulin Binding Site

Insulin binding to the cell surface IR activates its intrinsic cytoplasmic tyrosine kinase through the autophosphorylation of specific tyrosine residues, initiating the intracellular signal transduction cascade, which is essential to insulin actions such as glucose homeostasis, protein synthesis, growth and development (Taylor, 1991). However, IR has not been crystallized, probably due in part to its molecular mass of 450

kDa, being a membrane protein, and being highly glycosylated. After more than 25 years of intensive studies by many investigators, the quaternary structure of IR and the structural basis for the mechanism of IR activation by insulin binding remains unknown. It is known that insulin binds to the extracellular α subunit of the whole receptor, and also with unaltered affinity to the isolated ectodomain (Schaefer et al., 1990). Several large regions of the ectodomain have been implicated in binding insulin, but a more detailed description of the binding site is not yet available because the crystal structure of neither IR nor its ectodomain is known. On the other hand, for an analogous receptor, IGF-IR, the crystal structure of a fragment containing the first three domains (L1-Cys-rich-L2) involved in ligand binding has been solved (Garrett et al., 1998). IGF-IR and IR are closely related members of the tyrosine kinase superfamily and highly homologous in their primary structure (Ullrich et al., 1986). The structure of the fragment, which lacks ligand-binding activity, shows that the three domains form a central notch sufficient for ligand binding. In addition, the structure of the fragment of the intracellular tyrosine kinase domain of IR has been determined by x-ray crystallography, both in the unphosphorylated and phosphorylated state (Hubbard et al., 1994; Hubbard, 1997).

Since the IR is a model protein in signal transduction system, and is involved in basic metabolism, in development and in many human diseases, solving its structure is very important. Since determining IR by x-ray crystallography or by NMR analysis has proven difficult, electron cryomicroscopy seems to be a possible alternative approach to solve this problem. As mentioned before, the large molecular size and the high degree of glycosylation of IR should not present a problem in STEM analysis. Another advantage of STEM is the visualization of heavy metal atoms, such as the 70 atom gold cluster,

Nanogold. This heavy metal marker can be used to map specific functional sites on protein molecules since it will appear microscopically as single "spots" of about 1.4 nm in diameter (Hainfeld and Furuya, 1992). If insulin is labeled with Nanogold, this insulin derivative can then be used to locate the insulin-binding site on the IR with electron cryomicroscopy. In addition, available structural information on the TK domain of IR and the L1-CR-L2 domain of IGF I receptor (Habbard et al., 1994; Garrett et al., 1997; Baron et al., 1992) could be helpful in analyzing the results obtained from STEM study of the whole receptor.

In this Chapter, I describe the result from experiments carried out to determine the 3-D quaternary structure of the human insulin receptor by 3-D reconstruction from STEM images of single molecules. Nanogold-bovine insulin as an EM marker was prepared and used to localize the insulin-binding site in the structure of the intact insulin-insulin receptor complex. Results described in this Chapter have been published in abbreviated form in *Science* (Luo et al., 1999).

2. MATERIALS AND METHODS

2.1. Biological Materials

Preparation of Nanogold Bovine Insulin (NGBI)

Nanogold (Nanoprobes, Stony Brook, NY) is a newly developed gold cluster label, prepared by using a discrete gold compound rather than the traditional colloid. Nanogold is an extremely uniform 1.4 nm diameter gold cluster particle containing approximately 70 gold atoms with a molecular mass of 15 kDa. This heavy metal particle

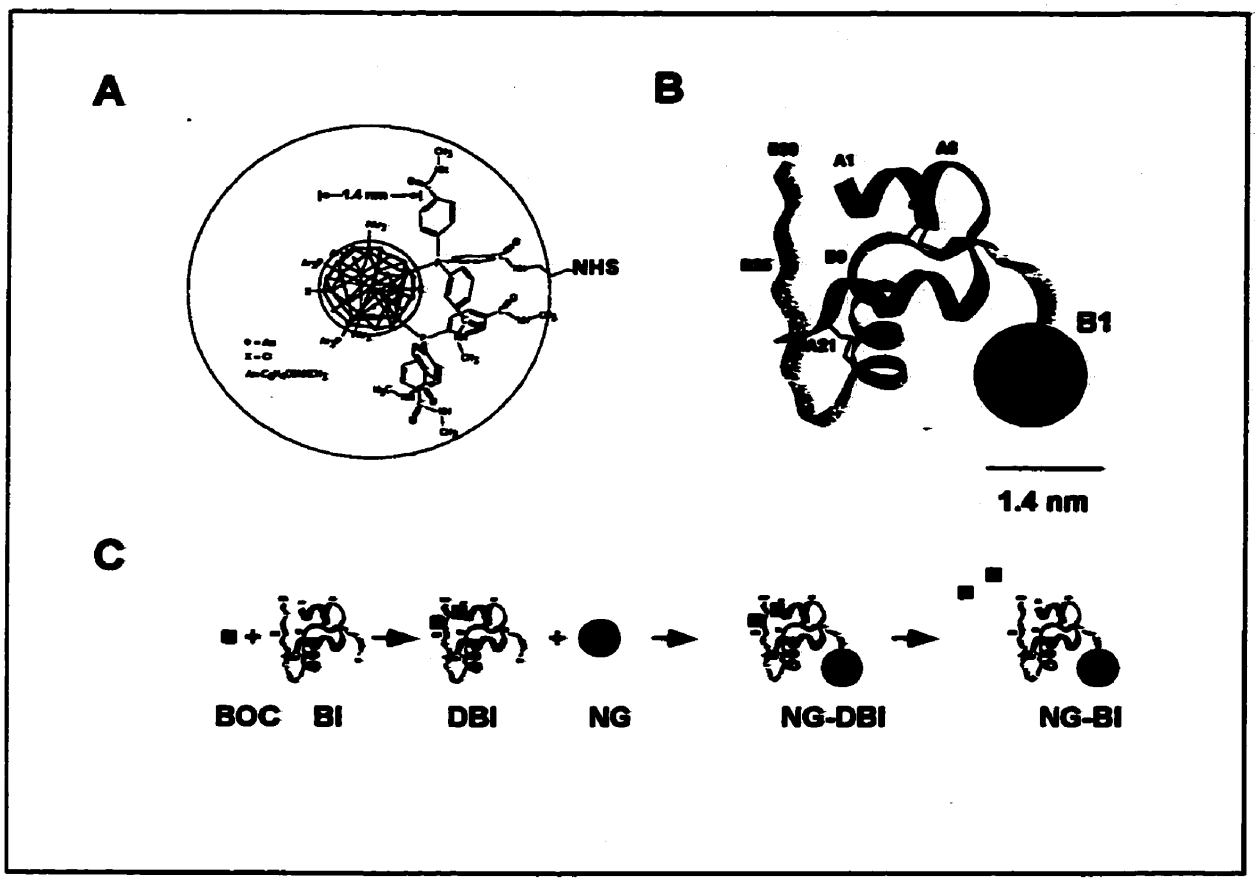

Fig. 3-3. Outline of the preparing NanoGold-Bovine-Insulin. A) Mono-Sulfo-NHS-Nanogold is a 1.4 nm gold compound with a single organic reactive group, N-hydroxysuccinimide ester sulfo (NHS) that reacts with primary amines. C) Two (A1 and B29) of the three amino groups of bovine insulin were blocked with tBOC and the only free amino group of B1 was then cross-linked to Nanogold (NG-DBI. B) NG-DBI was then de-blocked to yield Nanogold-bovine insulin (NGBI).

can be easily seen as a bright ball shape spot under the electron microscope at a magnification factor higher than 200,000 x. The sulfo-N-hydroxy-succinimido (NHS) Nanogold (Fig.3-3a) used to label bovine insulin has a mono-reactive group which is able to cross-link to an accessible reactive amine group on a protein.

An insulin molecule contains three reactive amine groups, one each at residue, A1, B1 and B29. Since the amino terminal of the B chain (B1) is known not to be involved in binding to the receptor (Nakagawa and Tager, 1986, 1987, 1993; Schaffer, 1994) the amino group of Phe1 was derivatized with a gold cluster. This was done using bis-(t-Boc)-bovine insulin (DBI) in which the amino group of A1 and B29 are protected. DBI was prepared in Dr. Yip's laboratory (Yeung et al., 1980). One mg of DBI (~150 nmole) and 30 nmole of mono-NHS-Nanogold were dissolved in 200 µl of N'N-dimethylacetamide (DMA) containing 2 µl di-iso-propylethylamine (DIPEA), pH 7.6. The mixture was vigorously mixed at room temperature for 60 minutes then dried in a SpeedVac (Savant Instruments). The pellet obtained was dissolved in 20 µl of trifluoroacetic acid, kept at room temperature for 5 minutes, and then dried in the SpeedVac. The pellet was washed twice with 100 µl of 1 M acetic acid, resuspended in 120 µl of 1 M acetic acid and chromatographed on a Bio-Gel P-10 column (1.7 x 25 cm) in 1 M acetic acid. Fractions of 0.5 ml were collected, and their absorbency at 280 nm was measured. An aliquot of each fraction was subjected to electrophoresis in 10-20% SDS-tricine gel in tricine/glycine buffer (pH 8.8). The fractions containing NGBI (Fig. 3-3b) were pooled and re-chromatographed on the Bio-Gel P-10 column. The purified NGBI was stored at a concentration of 0.5 pmol/ml at -70° C.

Preparation of Nanogold-insulin/insulin receptor complex

Insulin receptor protein (HIR) was solubilized from human placenta membranes and purified by affinity chromatography on an insulin column followed by further FPLC purification on a Sephacryl S-200 HR column (1.6 x 60 cm, Pharmacia FPLC set and column) as described in Chapter 2. The purified HIR was immediately quick frozen in liquid nitrogen in aliquots of 20 μl at a protein concentration of 20 μg/μl and kept at -70°C until needed. For gold labeling, HIR was incubated at 4°C overnight in 20 mM HEPES buffer (pH 7.5) with NGBI (final concentration of ~ 0.5 x 10^{-6} M) at a molar ratio of insulin:HIR of ~ 10:1. Free NGBI was removed from the mixture by ultrafiltration through a microfilter with a cut-off of 300 kDa (Sigma) after incubation. The NGBI-hIR complex was then diluted to 7.5 μg of receptor protein/ml with 20 mM HEPES buffer, pH 7.5, prior to loading on the microscope grid support. The presence of one NGBI per one hIR in the majority of the complex particles was confirmed by preliminary TEM and STEM imaging before loading the specimen for the final STEM analysis.

2.2. Electron Microscopy and Image Analysis

Preparation of specimen for STEM

Copper grids (300 mesh) coated with a holey plastic film (pore size 5-10 μm) overlaid with a carbon film 23 Å thick were used to support the protein in both TEM and STEM analysis. The thin carbon film was prepared by high vacuum electron gun evaporation of carbon onto freshly cleaved mica. The thin carbon film was then floated on a dish of double distilled, de-ionized water that had been passed through a 0.2 μm

millipore filter. The thin carbon film was picked up with the plastic coated grid and the grid was air-dried.

To determine the optimal concentration of protein for STEM analysis, 20, 10, 7.5, 5, and 2.5 ng/μl of HIR diluted with 20 mM HEPES, pH 7.5 buffer, were tested in a Zeiss 902 TEM using electron energy loss dark-field condition at the magnification factor of 20,000 x. The specimen (5 μl) was injected into 5 μl of dilution buffer preloaded on the carbon film of the grid. The specimen was washed with 3 drops of 20 mM, pH 7.5 HEPES buffer and 1 drop of 10 mM ammonia acetate buffer (pH7.5). For purposes of concentration optimization, the grid was left to air dry. The concentration of 7.5 ng/ μl of HIR was then chosen for the specimen concentration for STEM study.

For STEM analysis, the same sample preparation was performed, except that after washing, the grid was drained by wicking with Whatmam No. 1 filter paper to leave a very thin layer of solution, as observed with an optical microscope. The sample grid was immediately quick-frozen by plunging the grid into liquid ethane at -150° C. Quick-freezing to liquid nitrogen temperature assured immobilization of the molecules in a solid glass-like environment similar to the aqueous state. The frozen specimen was transferred at liquid nitrogen temperature into the STEM (Vacuum Generators, Model HB601UX). The specimen was freeze-dried within the cold-stage holder of the STEM at –140 °C. Freeze-drying at this temperature resulted in a contrast-rich specimen that has not been distorted structurally by phase boundary forces during dehydration.

Image acquisition and analysis

Images in a 480 x 480 pixel format were acquired in the STEM with the specimen at -150°C, using cold-field emission at an accelerating voltage of 100 kV, a

dose of 6e/Å^2, and a magnification of 252,000 x, corresponding to a pixel size of 6.5 Å. The beam size was 3 Å per pixel. Both inelastic and elastic annular dark field signals were detected and digitally recorded simultaneously. The sharp Nanogold signal was used to adjust the stigmatism and focus on the images.

The paired electron images acquired from the elastic and inelastic detectors were combined to increase the signal-to-noise ratio two-fold compared to the elastic signal alone. To process molecular images, single particles were interactively selected in 64 x 64 pixel windows using the program WEB (Wadsworth Laboratories, Albany, NY). In preparation for orientation determination the selected images were low-pass filtered to 11 Å using a Gaussian filter in the program SPIDER (Wadsworth Laboratories). The molecular mass was calculated from the selected particle images in relation to the mass of the 23 Å thick carbon support with a carbon density of 2.0 g/cm^3. The particles had a Gaussian mass distribution with a modal mass of 570 kDa, which included the mass of 480 kDa for HIR and NGBI plus the weight of an estimated 150 Triton X-100 molecules. To determine the molecule boundary, particle images were "grown" from a center high density point in expanding contiguous contour levels until a global cut-off was reached that corresponded to contiguous structures with the average mass. 704 Particles with apparent structural integrity, appropriate relative molecular mass and showing the presence of the high-density Nanogold spots were selected for further processing.

2.3. Three Dimensional Reconstruction

Iterative Quaternary-assisted Angular determination

Three-dimensional reconstructions were computed from the images of randomly oriented HIR/NGBI complex particles using Iterative Quaternary-assisted Angular Determination (IQAD) method (Farrow and Ottensmeyer, 1992; 1993a; 1993b; Czarnota et al., 1994; 1997) based on sinogram correlation and the common axis theorem (van Heel, 1987; Crowther et al., 1970; Crowther, 1971).

The IQAD approach to determining macromolecular structure permits the determination of the three-dimensional structure of a biological macromolecule by calculating *a posteriori* the angular relationship of a biological macromolecule in a particular image with respect to many other images of an identical macromolecule at different random orientations. Briefly, in Fourier space any 2D Fourier transforms (frequency space representations) of corresponding 2D projections of a 3D density distribution will be central sections of the 3D Fourier transform of the 3D density distribution, and thus will share a common line of intersection in 3D Fourier space. By calculating the relative position of common lines to one another in a 3D coordinate system, the relative orientations of the images can be determined. The addition of IQAD processing, sinograms, sinogram correlation functions and quaternion mathematics to optimize the fitting together makes it possible to use even sets of noisy image to obtain the optimal orientation among them of any individual image (Farrow and Ottensmeyer, 1992, 1993). 3D reconstructions then are performed by filtered back-projection using an angular distribution-dependent filter. Calculations were carried out on an SGI Indigo work station (Silicon Graphics Inc.).

Resolution measurements and results display

Measurements of resolution for reconstructions were calculated by computing 3D Fourier transforms for two independent reconstructions and from a set of half of the images. From these 3D transforms the average differences in phase between them is calculated in radial shells from the center of each transform outwards. This phase differences related to the correlation of structural detail at each shell. Since the radius of the shell corresponds to a resolution level (larger radius, better resolution) the loss of correlation at a given radius indicates the resolution limit.

The program IRIS EXPLORER 2.0 (Silicon Graphics Inc) was used to display the 3D reconstructions at a chosen intensity-based contour level, a threshold which corresponds to the calculated volume of a 450 kDa protein, assuming a protein density of $1.3g/cm^3$. To show domain relationships and structural links, the constructions were displayed with intermediate densities 5% to 10% higher than the average density of the full volume.

Crystallographic model or co-ordinates of L1-Cys-rich-L2 domains of the IGF-1R (Garrett, et al., 1998), the tyrosine kinase domain of IR (Hubbard, et al., 1994, Hubbard, 1997; PDB: 1IRK, 1IRp) and human fibronectin III repeats domain (Baron et al., 1992; PDB: 1fmn) were fitted into the reconstruction volume of the insulin-HIR complex by modeling the electron density of the x-ray crystallographic structures into the volume of the assigned domains of the 3D recontruction using program INSIGHT II (Molecular Simultations Inc.). Since the co-ordinates of the first three domains of the IGF-1R were not available, a computer drawn 3D model of approximate cylinders based on the x-ray structure information in the publication of Garrett et al. (1998) was used instead.

3. RESULTS

3.1. Specimen Preparation for Electron Microscopy

The purity of the receptor protein (HIR) was found to be better than 95% as determined by sodium dodecyl sulfate polyacrylamide gel electrophoresis (Fig. 3-4). The purified HIR showed the same binding affinity as placental membrane IR for insulin. (Fig. 3-4). In the preparation of nanogold-bovine insulin, we carried out the reaction in organic solvent instead of aqueous solvent as suggested by the manufacturer. Our method significantly increased the efficiency of derivatization to greater than 70% as compared to about 15% in aqueous condition (data not shown). The derivatization and purification processes were monitored by SDS-PAGE and acid-urea gel electrophoresis (Fig. 3-5). The purified NG-BI was found to be more than 95% pure and to have a molecular mass of 19796 Da by matrix-assisted laser desorption/ionization time-of-flight (MALDI-TOF) mass spectrometry (Fig. 3-5), a mass consistent with one insulin molecule having been derivatized with one Nanogold cluster. Compared with native bovine insulin, NG-BI showed only a slight decrease in binding affinity to human placental membrane insulin receptor (Fig. 3-5). As a compact particle containing about 70 gold atoms surrounded by an organic matrix, Nanogold was visible as a bright ball shape spot in the STEM at a magnification higher than 200,000 x. The purified NGBI showed no visible damage in the STEM at 2,000,000 x (Fig. 3-6). The insulin signal was too weak to display when compared to Nanogold at the same time.

3.2. Image Processing of NGBI-HIR Complex

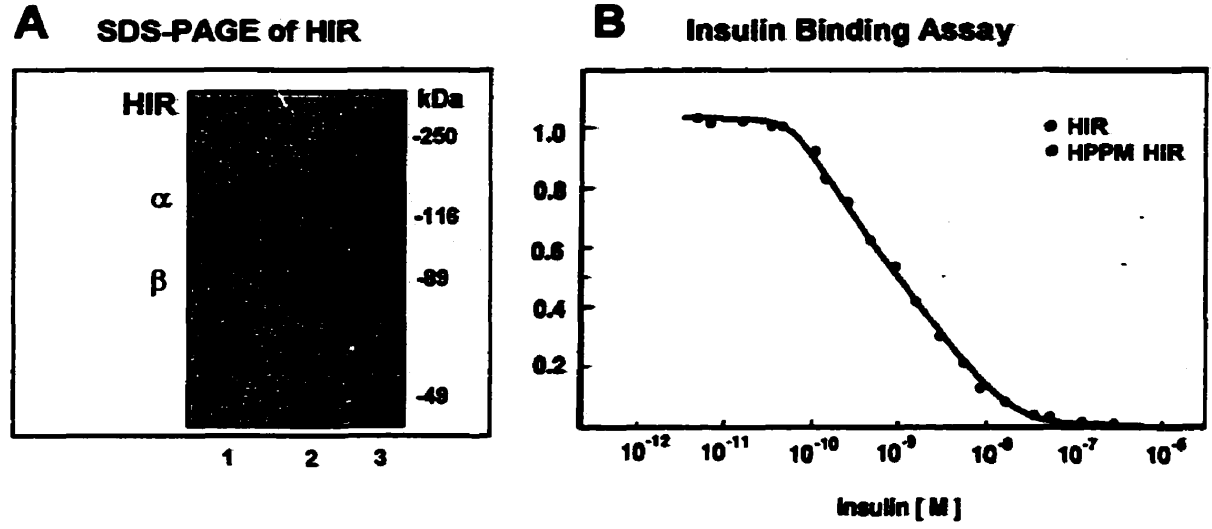

Fig. 3-4. Purification of human placentaol insulin receptor (hIR). hIR protein was purified by affinity chromatography using an insulin-Affi-gel column, followed by gel filtration. A) SDS-PAGE of the purified hIR, stained with Coomassie blue. Lane 1 shows a band corresponding to the unredused hIR of 450 kDa. Lane2 shows two stained bands corresponding respectively to the 130-kDa α subunit and 95-kDa β subunit of the hIR after reduction. B) Insulin binding to purified hIR and to placental membrane hIR. The competition curves obtained show that there was is no detectable difference in the binding affinity for bovine insulin between the purified hIR and the hIR in placenta membrane (HPPM hIR).

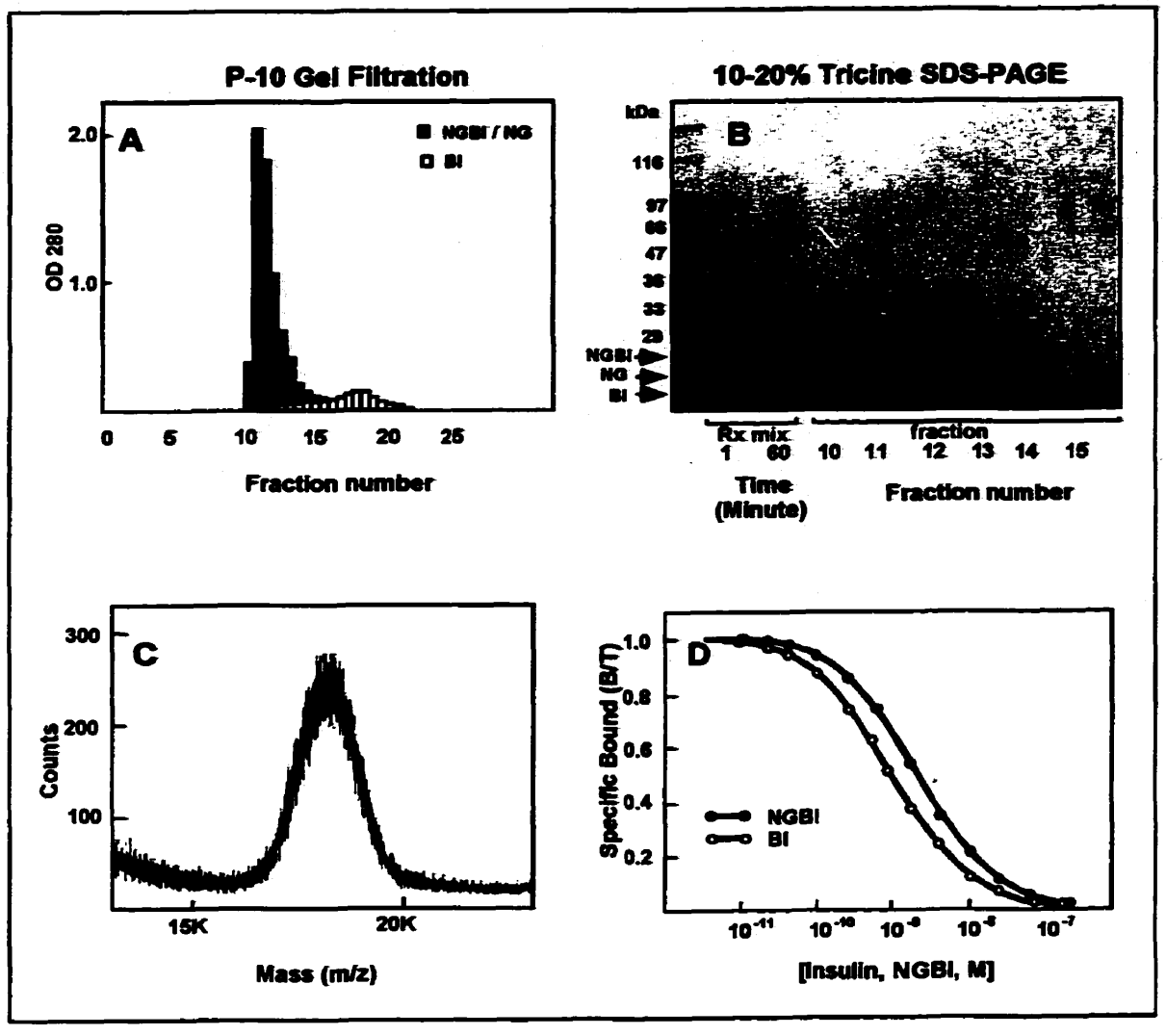

Fig. 3-5 Purification and characterization of nanogold insulin (NGBI). A) Gel-filtration separation of the reaction mixture. Solid bars represent the O.D. of NGBI and free NG, and open bars represent the O.D. of free insulin. B) SDS-PAGE in 10-20% tricine gradient gel of the reaction mixture and fractions obtained in (A). The gel was stained with Coomassie Blue. The stained band seen in fraction 11 shows that NGBI can be partially purified from the reaction mixture. C) MALDI-TOFF analysis established that the NGBI obtained from repeat gel filtration was more than 90% pure, and that the mass of the NGBI was consistent with a stoichiometry of one Nanogold per one insulin molecule. D) Receptor-binding assay showed that NGBI binds to hIR with a slightly reduced affinity compared to nonderivatized insulin.

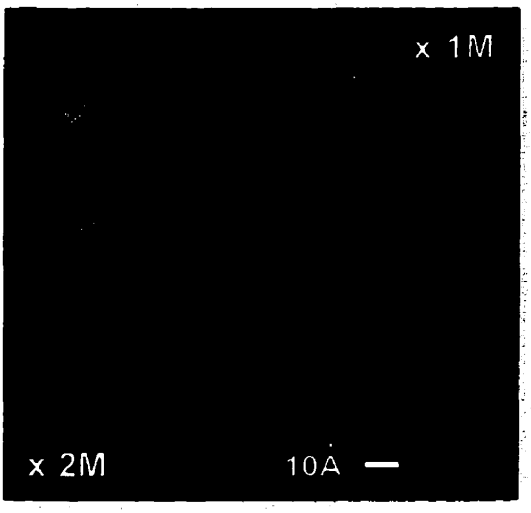

Fig. 3-6 STEM images of purified NGBI at a magnification of 2,000,000 X (insert). The bright round images seen are signals from Nanogold. Signals from insulin would be very weak compared with Nanogold. There is no obvious damage of Nanogold particles as evident from their well-round spherical shape.

To increase the signal to noise ratio for a given dose, the simultaneously recorded elastic and inelastic detector signals of the STEM were combined. A representative unprocessed STEM dark-field image containing a few NGBI-HIR complexes is shown in Fig. 3-7A. As indicated by arrows, obvious intense signals can be seen from the Nanogold marker. Randomly orientated complex particles have an average size of about 15 nm. Most of the complexes exhibit one bright spot (or two in less than 10% of the complexes) on the particles, that can be seen directly or can be visualized by varying the threshold on the displayed intensity. Figures 3-7B and 3-7C show that bright NGBI locations are even more striking in the high-density threshold representations of the extracted particles after low pass filtering. When two NGBI particles are detected, they are in close proximity to each other (Fig. 3-7B, lower two images).

Figure 3-8 shows a group of selected complexes extracted into a circular mask from the raw images. Figures 3-9 and 3-10 show two further processing steps for the same group of particles: low pass filtering to 11 Å using a Gaussian filter, and molecular boundary determination. The latter images are ready for 3D image processing such as orientation determination.

The relative molecular weights for approximately 1,600 particles, using the 23 Å carbon support film as a mass standard, are shown in the histogram in Fig. 3-11. Only the particles having a calculated molecular weight no greater than a difference of 18 % from the average were chosen for reconstruction. The calculated average model mass is about 570 kDa, which includes the mass of 480 kDa for HIR and NGBI plus the weight for an estimated 150 Triton X-100 molecules.

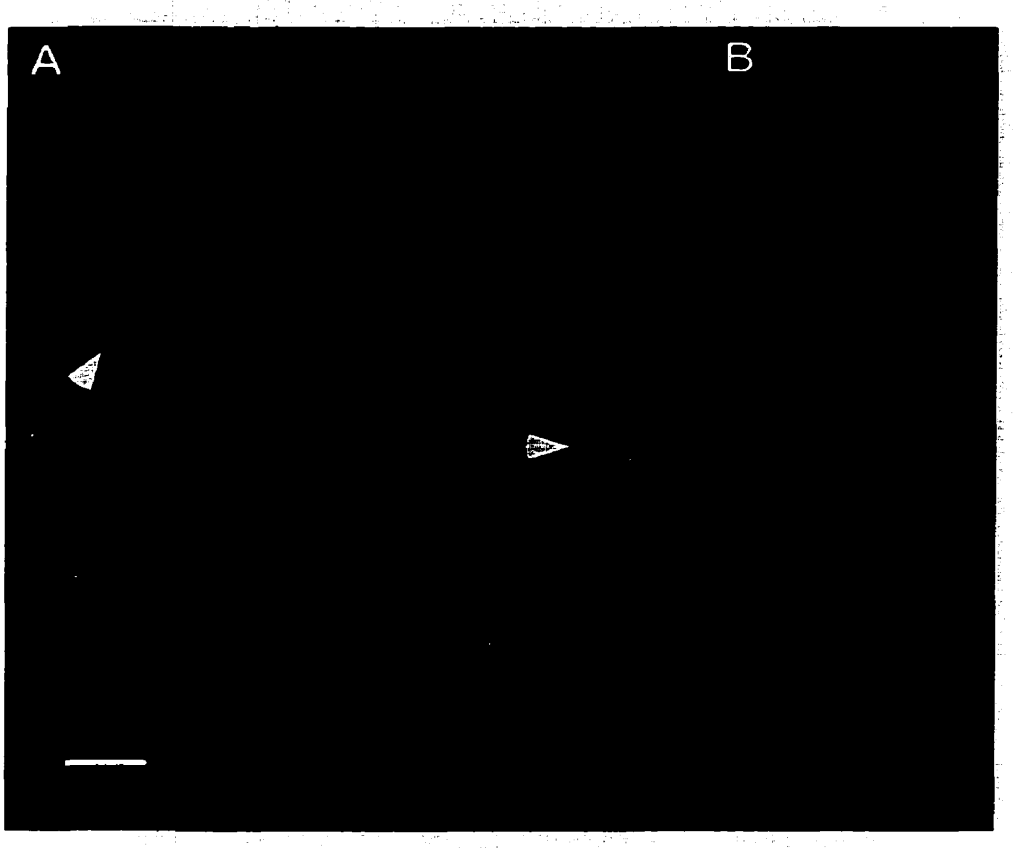

Fig. 3-7. STEM darkfield images of human insulin receptor bound to Nanogold insulin (IR/NGBI). A) A field of view showing several complexes. Arrowheads point to the Nanogold markers. Scale bar = 20 nm. B) IR/NGBI images extracted from image fields, low-pass filtered to 1.0 nm (left column), and obtained at high density threshold (right column) showing one or two Nanogold markers indicating the binding of one or two Nanogold-insulin (Luo et al. Science 285:1077, 1999).

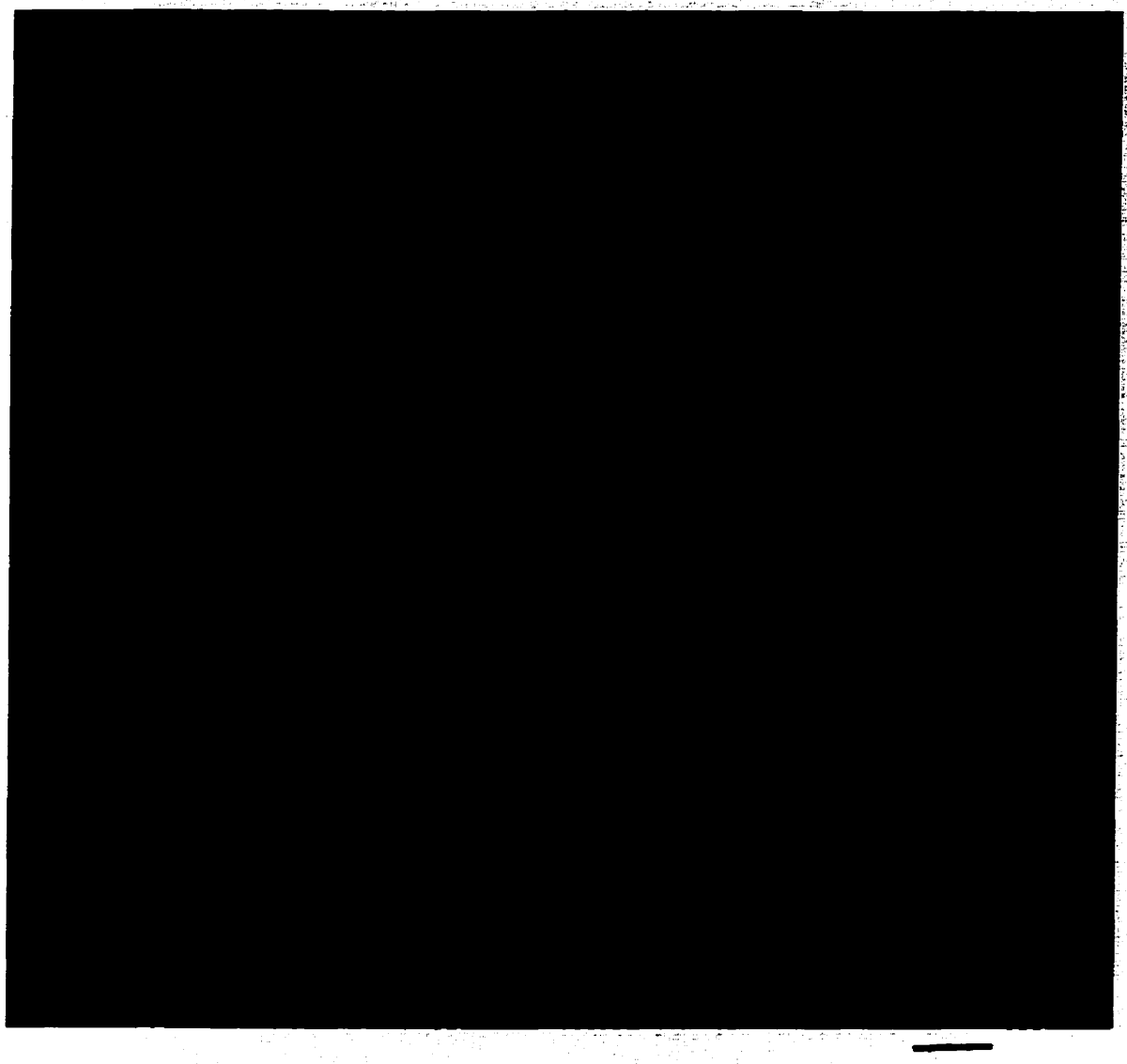

Fig. 3-8. Composite raw images of NGBI-hIR molecules. 100 images of the molecules are shown here. Each is a combined image from the paired electron images acquired from the elastic and the inelectic detectors in order to increase the signal-to-noise ratio. Scale bar = 20 nm.

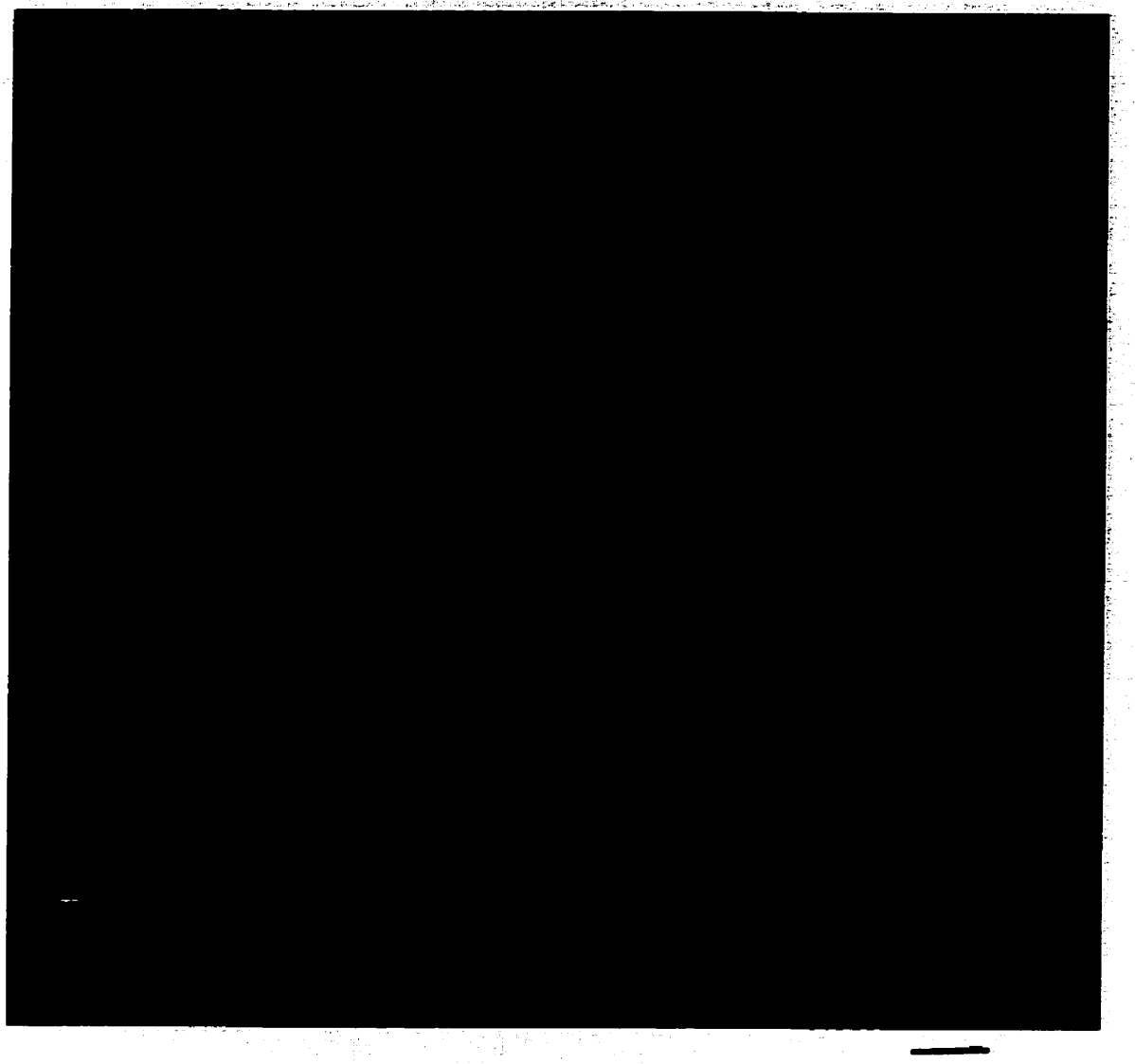

Fig. 3-9. Low band-pass filtered images. The same images as in Fig. 3-8 were low-pass filtered to 11 Å using a Gaussian filter and background was substracted to increase the signal-to-noise ratio. Scale bar = 20 nm.

Fig. 3-10. Final images used for 3D reconstruction. To further refine the images for 3D reconstruction, the same images as in Fig. 3-9 were processed using "grown" software to determine the molecule mass center and boundary. Various shapes of the images were obtained which represent the same molecule being viewed in different orientations. The location of NGBI is seen as a brighter spot on the image. After this refinement, images were ready for 3D image processing. Scale bar = 20 nm.

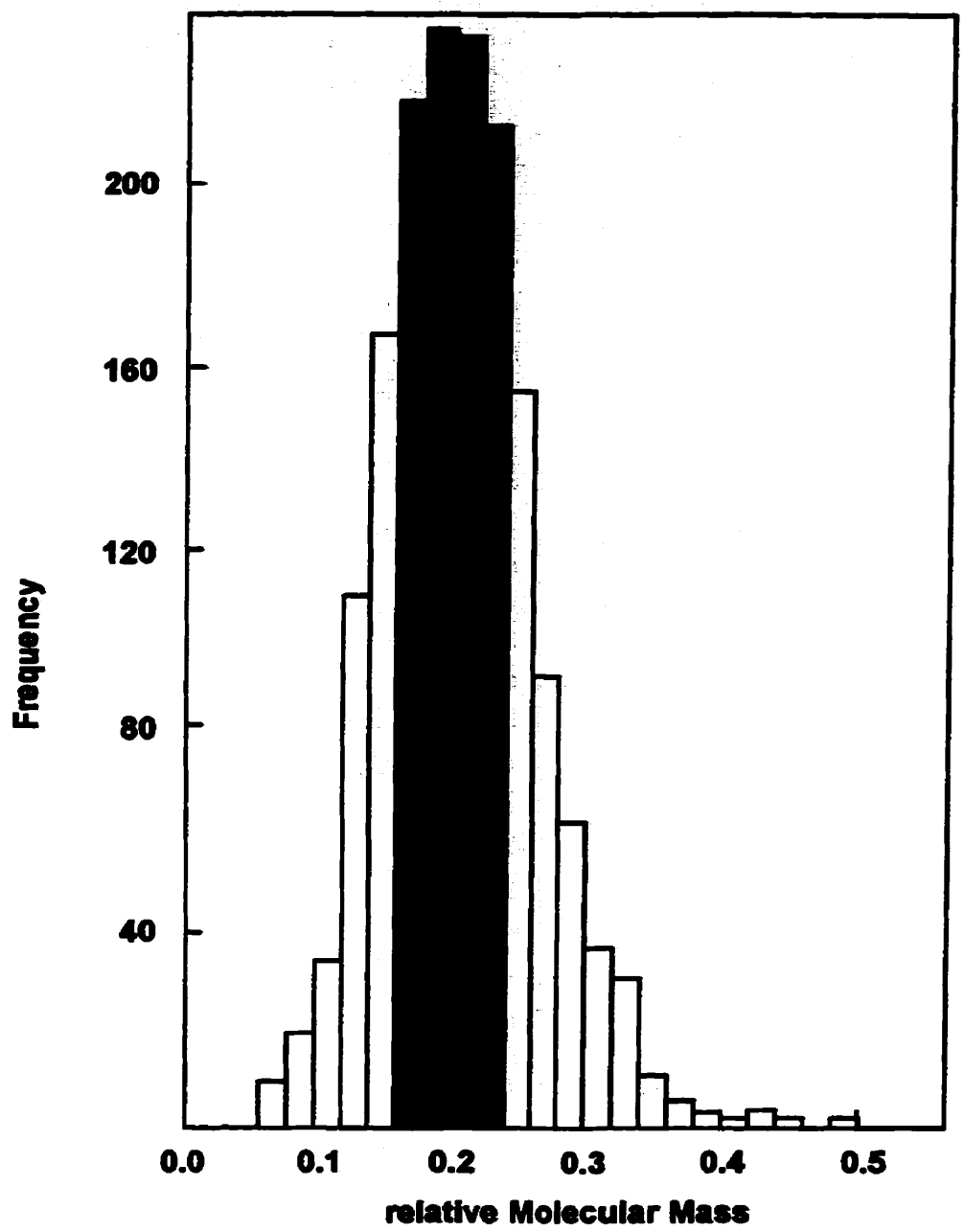

Fig. 3-11. Histogram of calculated mass for 1,625 collected images. The relative molecular weights were calculated using the carbon supporting film as a mass standard. The particles in the shaded area represent the ones having a calculated molecular weight within 18% of the average. 704 IR/NGBI particles from the shaded area were chosen for reconstruction.

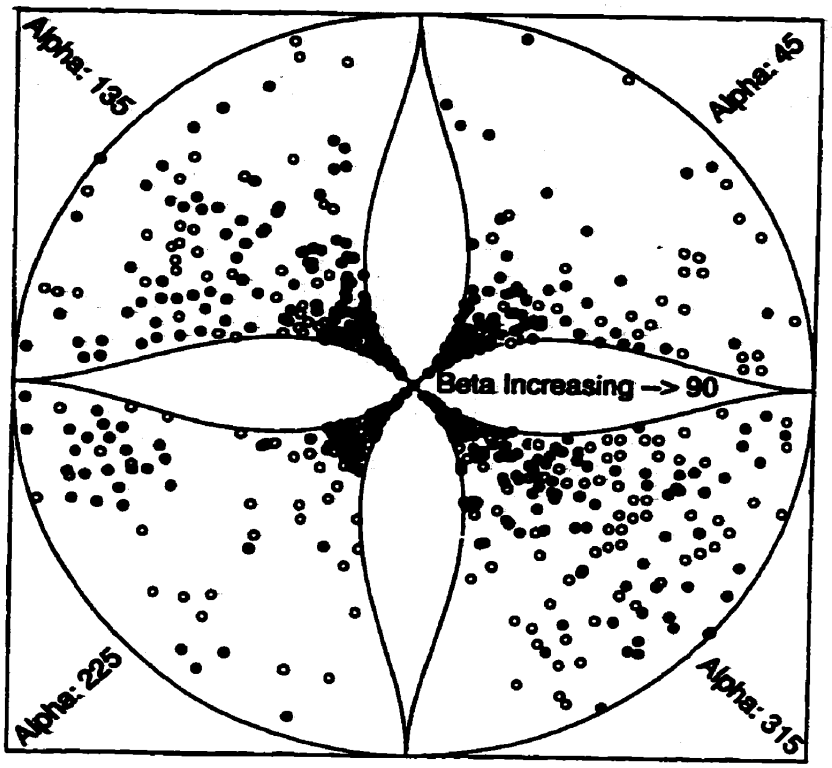

Flr. 3-12. Calculated relative angular orientations for individular molecular images in terms of their first two Euler angles (α,β) for the IR/NGBI 3D reconstruction. The first two Euler angles for each image are shown in a cartographic representation of points on the surface of a sphere (Farrow and Ottensmeyer, 1993). Open circles represent orientations on the top half of the sphere (Euler angle β less than or equal to 90°), circles with crosses represent orientations on the bottom half (Euler angle β greater than 90°).

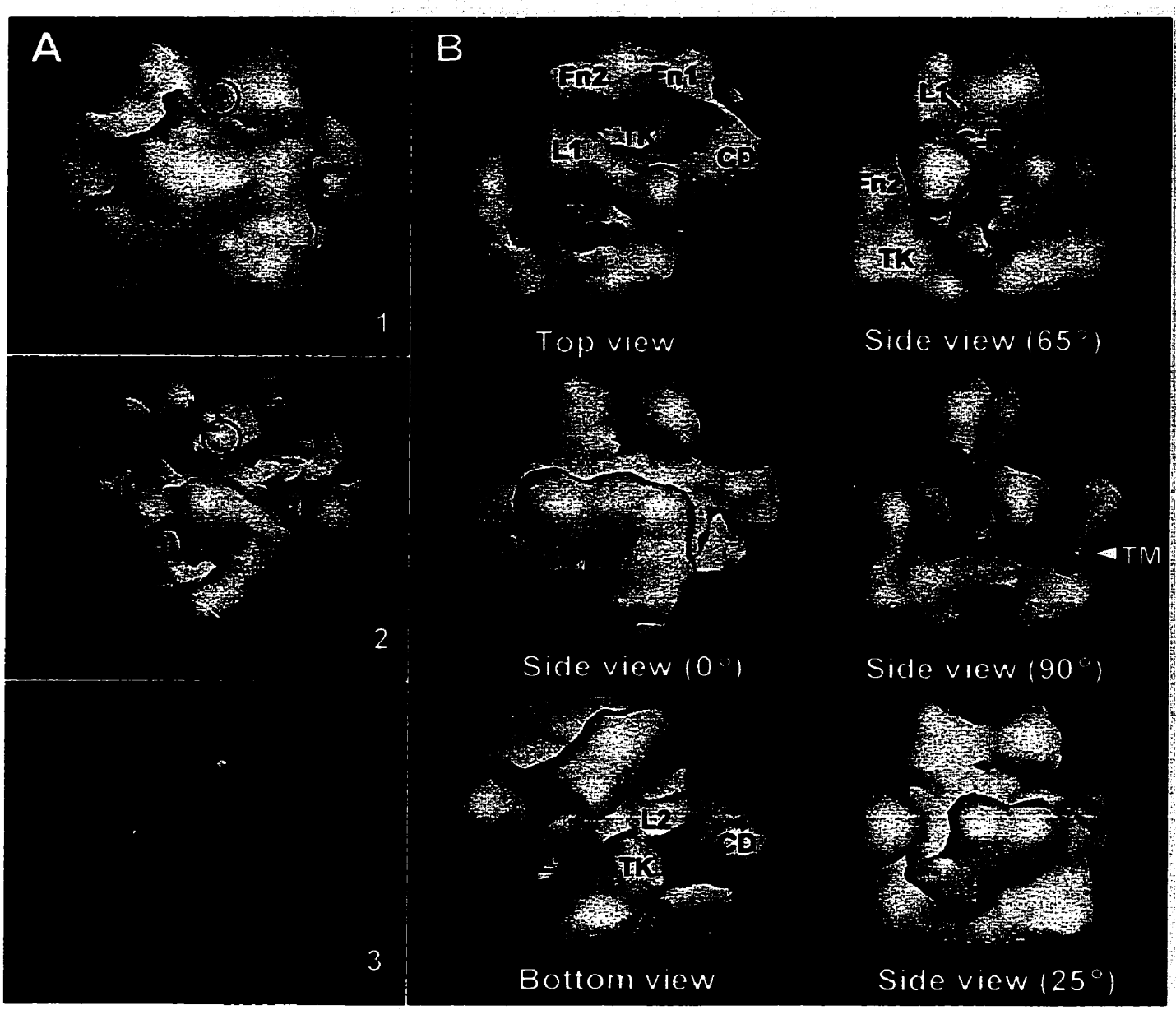

Fig. 3-13. **3D reconstruction of the IR/NGBI complex (surface representation).** A) Density threshold representing the total expected volume for the complex (A1); intermediate density threshold, unsymmetrized (A2); high density threshold of (A2) showing only the Nanogold label (A3). Circles indicate location of the gold marker within the reconstructions. Resolution was 20 Å by phase residual analysis. B) Reconstruction with two-fold symmetry shown at ~70% of full volume, indicating relationships and connectivity of structural domains. Labels, for only one αβ monomer, refer to biochemical domains. Arrowhead indicates proposed plane of cell membrane. L1, C-R, L2 = L1-Cysteine-rich-L2 domains; CD = connecting domain; Fn1, Fn2 = fibronectin III repeats 1 and 2; TK = tyrosine kinase; TM = transmembrane domain (Luo, et al. Science 285:1077, 1999).

The relative orientations of the selected molecule images of NGBI/HIR were determined using sinogram correlation functions and geometric approaches (Farrow and Ottensmeyer, 1993). They are plotted in Fig. 3-12, indicating a fairly random distribution of angles for these images with some tendency towards a preferred orientation. Such tendencies away from randomness in orientation are compensated prior to 3D reconstruction by orientation dependent weighting of the images.

The 3D reconstruction of the NGBI/HIR complex is shown in Figure 3-13A. The structure at the fully expected volume, shown in Figure 3-13A (top panel), is compact and globular in overall shape. The domain-like features of the structure are shown in Figure 3-13B at intermediate density thresholds.

3.3. Location of the Insulin-Binding Region

The location of NGBI on the reconstruction was determined by increasing the density threshold without imposing symmetry (Fig. 3-13A, panel 2 and 3) to pinpoint the site of highest density (panel 3). Based on the results of biochemical evidence, insulin binds to the ectodomain of the receptor, particularly in the region of L1-Cys-rich-L2, the first three contiguous domains of the IR (Fabry et al., 1992; Murray-Rust et al., 1992). The highest density in the 3-D volume indicates the location of the NG cluster and, with it, the location of insulin binding (Fig. 3-13A, panel 3). It identifies this region of the structure as the receptor ectodomain and, more specifically, part of the L1-Cys-rich-L2 domains.

When we fit a NGBI molecule into the tentative region (see details in Chapter 3.3. and 3.4), the best fit is obtained with a molecule of insulin being in contact with the L1-

Cys-rich domains of one α subunit and with the L2 domain of the other α subunit. This is consistent with the previously proposed model involving both α subunits in the high-affinity binding of insulin (Yip 1992; Schaffer 1993; DeMeytes et al., 1993).

3.4. Domain Structures of the HIR

The domain-like features of the structure become evident when the structure is viewed at intermediate density thresholds (Fig. 3-13A, panel 2), and, except for the NG-BI region, indicate a strong 2-fold vertical rotational symmetry as would be expected from the oligotetrameric primary structure of IR. This symmetry was used to reduce noise in the reconstructions and render the structures shown in panel 1 and in Figure 3-13B. This Figure shows the top, bottom and side views of the structure, putatively as being viewed in the plane of the membrane, and in the extracellular (top) and intracellular (bottom) perspectives.

In the side views, the top part of the structure, where NG is located, is identified as the ectodomain of the α subunit. The dog-bone-shaped substructure of the 3D reconstruction (Fig. 3-13B, top view), and the equivalent top-most, bow-tie-shaped structure (Fig. 3-13B, 0°), are designated as the two L1 domains of the dimeric receptor on the basis of the x-ray structure of the L1-Cys-rich-L2 domains. The side view at 65° shows the putative L1-Cys-rich-L2 domains as contiguous substructures across the upper central region of the molecule, with enough additional volume in this region to account for most of the remaining mass of the two α subunits, primarily the fibronectin-like connecting domains (CD) (O'Bryan et al., 1991) and the smaller insert domain (ID) where the second disulfide bond forms between the two α subunits.

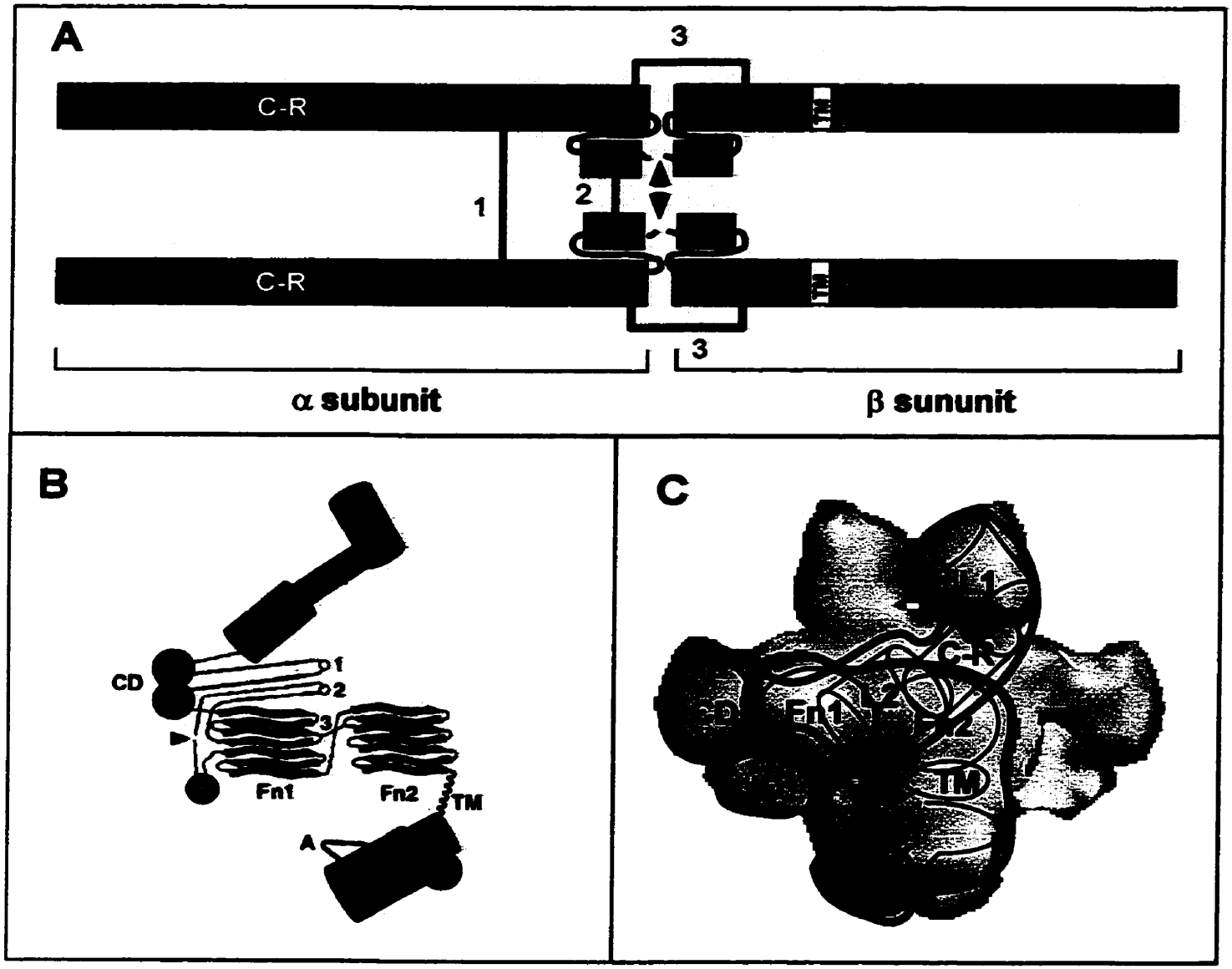

Fig. 3-14. The secondary domain structure of hIR (A) and the domain location in 3D structure. A) Linear locations of domains in the dimeric hIR. B) Schematic representation of the domain structure of one αβ monomer based on the connectivity in 3D reconstruction, the primary domain sequence, the symmetry requirement for two disulfides on two-fold axis, the fit of known domain structures, and on the principle of keeping unknown domains compact. Distances between modeled locations of CD, Fn1, and symmetrical disulfides commensurate with numbers of intervening amino acids (structures not to scale; alpha subunit: red; beta subunit: blue and green; unknown structures: spheres or lines): Labels: A = TK activation loop; 1 = Cys524; 2 = Cys682, 683, 685; 3 = disulfide bond between Cys647 and Cys872; arrowhead = cleavage site of precursor receptor protein (A and B); other labels as described in Fig. 3-13). C) Approximate locations of the domains on the 3D structure of hIR/NGBI complex.

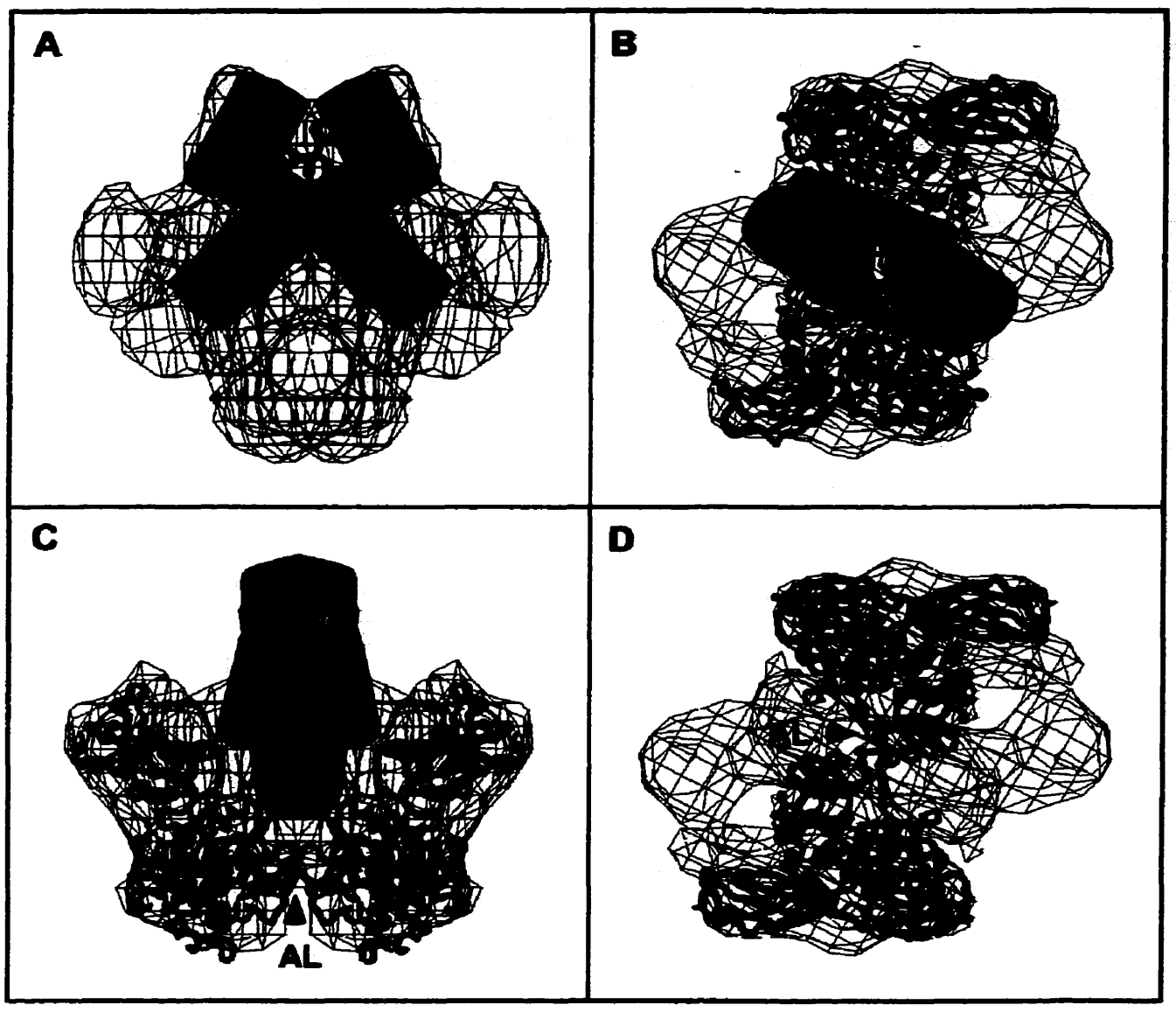

Fig. 3-15. **Fitting of biochemical domains and their known x-ray structures to the 3D reconstruction** (alpha subunit: red; beta subunit: blue and green). A) Fitting of the L1-Cys-rich-L2 (LCL) domains as approximate cylinders to ectodomain of IR (wiremesh representation). One insulin molecule (purple ribbon) inserted with its receptor-binding domains contacting the L1-Cys-rich domains of one a subunit (fuchsia) and the L2 domain of the other (red). Nanogold marker (yellow) on insulin B chain coincides with high-density site. C) Image of right angle view of (A) with LCL domains (insulin partly hidden), fitted TK structure (green), two dimeric FnIII structures (blue and red), A-loop (black) of left TK domain in crystallographic position, and A-loop (dark blue) of symmetric TK extended to overlap peptide substrate of opposite TK. B) and D) Image of right angle top view of (A) with (B) or without (D) LCL domains showing FnIII domains (blue/red), TK domains (green), and crystallographic (black) and extended (dark blue) A-loops. The two α subunits are shown in red, β subunits in blue and green. One wire mesh square is 6.5 Å. Accession numbers: insulin (PDB: 1BEN), TK structure (PDB: 1IRK), and FnIII (PDB: 1mFn). AL = TK activation loop (Luo et al. Science 285:1077, 1999).

The contiguity of the domain structure (Fig. 3-13B, top and side view 90°), along with the primary domain sequence (Fig. 3-14A, B), suggests that the two β subunits occupy the lower half of the structure, distal from L1, reaching up and out as a contiguous mass. The intracellular TK domain of IR would then occupy the bottom portion of this structure with two IR fibronectin type III (FnIII) repeats in each receptor half (O'Bryan et al., 1991; Pasquale, 1991) being in the top portion of the crescent-shaped spiral of the β subunit at the same level as the L2 domain in the α subunit. One of the FnIII repeats, composed of residues from both the α and β subunit, is assigned to the upper left end of the crescent (side view, 0°) where it is contiguous with the CD portion of the α subunit (top view). It has been suggested recently that the CD has a fibronectin-like structure (Mulhern et al., 1998). Fig. 3-15C and 3-15D (cf. Fig. 3-13B, 90°, top view, respectively) show the fitting of the crystal structure of the TK domain (green) of the β subunit and of the two FnIII repeats (blue/red) modeled as the canonical fibronectin type III structures (O'Bryan et al., 1991; Pasquale, 1991).

The spatial relationship between the domains of the α and β subunits (e.g. side view, 90°) suggests the location of the cell membrane lipid bilayer as the space below the α subunits and above the bridge linking the two assigned TK domains. Instead of a flat open region, this space in the 3D reconstruction forms a thick dome-like slab above the bridge with a thickness variation of 2.2 to 2.7 nm.

Starting from the putative transmembrane domain, the β subunits become slightly twisted toward each other. Here the intracellular TK domains of IR would then occupy this portion of the structure (side view, 65°, bottom view). There is a separation of several nanometers between the faces of the masses of the two putative kinase domains. Around the

center of the TK domains there is a small slender horizontal bridge connecting the two TKs, which suggests an interaction between the two TK domains.

4. DISCUSSION

By blocking two of the three free amine group on insulin molecule, we derivatized the B1 phenylalanine of bovine insulin with Nanogold. The amino terminal region of the B chain of insulin is believed to be minimally involved in receptor binding. Binding experiments showed that the receptor-binding affinity of NG-BI after de-blocking was decreased only slightly compared to native bovine insulin. The conditions of derivatization were gentle enough for Nanogold since the product showed no structural damage of the gold cluster afterward. The high purity of NG-BI, with no contaminating free insulin or Nanogold molecules, ensured the specificity of NG-BI binding to HIR. Although we incubated both NGBI and the hIR at relatively higher concentration (10^{-6} to $^{-7}$ M) to ensure maximal binding of NGBI to the IR, the subsequent removal of free ligand and the dilution of the bound complex established a new equilibrium condition. The new equilibrium would result in the binding of one NGBI to one hIR. STEM imaging confirmed the presence of one NGBI bound to one hIR in the majority of the complex particles. There was also very few free NGBI particles seen in the background (Fig. 3-7A).

To achieve high-resolution reconstruction of the NGBI-HIR complex, we applied the recent advances in electron cryo-microscopy to our study, including the instrument, sample preparation and image processing. To prepare the specimen, we carried out the ligand-receptor binding in physiological buffer, followed by quick freezing, and freeze-drying inside the STEM at –130 to -140° C. This maintained the protein in the near

physiological hydrated condition during image acquisition. At a very low dose (~6e/Å^2), imaging at –150° C markedly reduced the radiation damage. The use of both elastic and inelastic detectors to capture more signals in the STEM further increased signal-noise ratio. A sharp Nanogold signal was used to maintain all the images in sharp focus. These improvements are fundamental for the successful 3D reconstruction. As a result, for the first time, the 20 Å resolution obtained in this study revealed clear domain structures of the HIR/NG-BI complex. A strong two-fold vertical rotational symmetry as anticipated from the dimeric configuration of the oligotetrameric $(\alpha\beta)_2$ structure of IR can be seen in Figure 3-13B. A clear Nanogold-insulin signal can be distinguished on the 3D complex structure and localized on the assigned L1-Cys-rich-L2 domain.

The overall 3D structure of the insulin-insulin receptor complex

In this study, we have shown that the overall shape of the 3D reconstruction of the insulin-IR complex by STEM is compact and globular (Fig. 3-13A-1,). In studies by others, the HIR images obtained by electron microscopy have been shown as X-, T- or Y-shaped particles (Christiansen et al., 1991; Schaefer et al., 1992). Following the publication of our present study (Luo et al., 1999) Woldin et al. (Woldin et al., 1999) reported their TEM imaging of vesicle-reconstituted HIR cross-linked to a biotinyl derivatized insulin photoprobe (BBpa insulin) whose localization was visualized by binding to Nanogold streptavidin. The TEM images were rather fuzzy and not clearly discernable from the background. Nonetheless, they showed the image of the receptor as Y or T shape with very thin "rod-like" structures of only 1.5 nm in width for the arms, the putative extracellular domains of the receptor. This is significantly smaller than that reported (about 3 nm) for the

crystal structure of the three N-terminal domains of IGF-I receptor (Garrett et al., 1998) or what we have observed in this study. The images obtained by Woldin et al. were therefore apparently different from ours. Nevertheless, when viewing the domain-like structures in some orientations at intermediate density thresholds (Fig. 3-13B), we do find images with shapes reminiscent of X- or Y-shaped particles. Although Woldin et al. used about 7 times larger dose in obtaining their TEM images, the difference between our observations made in this study and observations by others using TEM may be the result of sample preparation. For example, the negative-stain method, which was used in TEM studies may introduce artifacts by highlighting the boundaries or filling in small spaces, or altering the shape of molecules by introducing a non-physiological ionic environment. Furthermore, staining also limits the potential resolution by the large size of the staining ions.

Superimposing known crystal structures of smaller domains of the receptor on substructures of the reconstruction has made it possible to deduce the spatial relationship among the domains in the overall complex. There is no crystal structure available for a protein with such a big molecular size. However, crystal substructures of several domains of the human insulin receptor are available. They are either from the insulin receptor or its closely homologous family members. These include the TK domain of the insulin receptor (Hubbard et al., 1974; Hubbard 1977), L1-Cys-rich-L2 domain of IGF-1 receptor (Garrett et al., 1998) and fibrectin III repeats domains (O'Bryan et al., 1991; Pasquale et al., 1991). All these domains can be properly fitted into the corresponding domain volume of our 3D reconstruction. Taken together, the overall structure shows the division of the complex into the extracellular and the cytoplasmic segments along a plane, the putative cell membrane, on which the fibronectin type III repeats lie. These repeats appear pontoon-like to support the

centrally located insulin-binding segment of the ectodomain. Underneath the putative transmembrane region, TK domains occupy the major volume of the intracellular portions of the β subunits (Fig. 3-13B).

Structural correlation with the primary structure of HIR

As a complex heterotetramer membrane protein, the HIR contains several functional domains. It has been proposed that the specific functional properties of the IR reside in its separate domains. Based on its primary structure (Fig. 3-14A), the structural relationship of the various domains in one αβ monomer is schematically shown in Figure 3-14B. Beginning at the N-terminal, the L1-Cys-rich-L2 domain (each contains about 150 amino acid residues) leads into a connecting domain (as a structure of Fibronectin III repeat (see Ward, 1999), assigned Fn0) of about 140 amino acid residues, followed by part of one FnIII repeat (Fn1) and the insert domain. The connecting and insert domains contain Cys524, 682, 683 and 685 that form at least two disulfide bonds between two α subunits (Sparrow et al., 1997). The FnIII repeat in general is a β structure of seven strands (Baron et al., 1992; Leahy et al., 1992). The second FnIII repeat is constituted by amino acid sequences from both α and β subunits, and is interrupted by the cleavage site between the two subunits. The N-terminal of the β subunit contains about three of the seven β strands of the second repeat (Fn1) and the entire third repeat (Fn2). From symmetry consideration, the disulfides are located at the center portion of the 3D structure. The two αβ dimers are linked by the disulfide bonds between Fn0 and insert domains and the α and β subunits are connected by a disulfide bond between Fn1 and Fn2 repeat domains. The third repeat is linked to the TK domain by a sequence of 70 amino acids, including the 23-residue transmembrane sequence.

Distal to a short juxtamembrane domain, the tyrosine kinase domain (more than 300 amino acid residues) occupies the major volume of the intracellular portion of the β subunit.

Structural correlation with related crystal structures

Superimposition of known crystal structures of smaller domains of the receptor on substructures of the 3D reconstruction would confirm the domain assignment as discussed above and thus helps to deduce the spatial relationship among the domains in the complex. Available x-ray coordinates were fitted to the respective substructure by modeling the electron density of the x-ray crystallographic structures into the volume of the assigned domains of the 3D recontruction. Figures 3-15C and 3-15D (cf. Fig. 3-13B, 90°, and top view, respectively) show the fitting of the crystal structure of the TK domain (green) of the β subunit and of the FnIII repeats (blue/red) to the reconstruction. When fitted into the top of the two crescent-shaped αβ monomers, the type III repeats lie on a horizontal plane flanking on two sides, pontoon-like, the remaining structure of the α subunits.

Two symmetrical TK crystal structures (Fig. 3-15C and D) can be fitted into the putative intracellular space of the receptor structure. The masses of the putative kinase domains are connected via a slender horizontal bridge (Fig. 3-13B, side view 90°) that was not observed in the x-ray structures of the TKs. The presence of this bridge can be explained in terms of the reconstruction being in a transition between free IR and its ligand-activated form. In this situation, the TK domains of the IR have undergone a conformational change such that the A loop of one TK domain would be reaching out to the catalytic loop of the opposing TK domain. However, since there was no ATP in the binding buffer in the preparation of the NGBI-IR complex for STEM, the activation of the IR stopped in this

stage and no *trans*-phosphorylation occurred. The catalytic loops in the two fitted TK domains are separated by 4 nm. Interestingly, this distance is just sufficient to permit the tyrosine triplet (Tyr1158, 1162 and 1163) in a fully extended flexible activation loop of one TK, to reach the catalytic loop of the opposite TK as modelled from the x-ray coordinates (PDB 1IRp). The extension of the activation loops could account for the linking density observed between the lower portions of the β subunits in the structure assignments.

Our 3D structure showed a limited space for the transmembrane region of the putative plasma membrane. This spacing is a change in shape, and a decrease in the thickness from that expected for a membrane bilayer that would accommodate an alpha-helical transmembrane domain (TM) of 23-26 hydrophobic amino acids. However, since the purified IR in the absence of its native membrane was fully active, the relative positions of the extracellular and intracellular domains must still represent a close to native arrangement.

The crossing L1-Cys-rich-L2 domains of the dimeric α subunits are presented in the reconstruction only in their general shape (Fig. 3-15A, B and C), since the known x-ray coordinates were not available (Garrett et al., 1998). An approximate model composed of cylinders for the L1-Cys-rich-L2 domains was generated instead. This approximate structure was fitted into the extracellular portion of the 3D structure. Based on the location of the Nanogold signal in the complex structure, one, or two if the condition allowed, molecule(s) of insulin should be fitted into this region as discussed below.

Structural localization of the insulin-binding site on the insulin receptor

By labeling the receptor with NGBI, we clearly demonstrated the stoichiometric relation of insulin to its receptor and showed the structural location of insulin on the receptor in the process of interaction. As mentioned above, the crossing L1-Cys-rich-L2 domains of the dimeric α subunits are presented in the reconstruction only in their general shape (Fig. 3-15A, B and C). Nonetheless, using this structure, the localization of the gold cluster, and the known receptor-binding domain of insulin (Murry-Rust et al., 1992), a NGBI molecule is tentatively fitted into this region. The fitted insulin molecule is in contact with the L1-Cys-rich domains of one α subunit and with the L2 domain of the other α subunit. A model involving both α subunits in the high-affinity binding of insulin has previously been proposed based on studies of insulin analogues binding to the IR and IR/IGF-I R chimeras (Yip 1992; Schaffer 1993; De Meyts et al., 1993). The 3D reconstruction provides the structural evidence for this involvement. Although two molecules of insulin can be fitted to this configuration, two molecules of Nanogold-labeled insulin were observed only rarely in the STEM images. The high-affinity binding of the first insulin molecule to the IR has likely induced a conformational change in the binding domain so that the second insulin molecule would bind only at low affinity. Likewise the binding of a second molecule of insulin could effect a conformational change that enhances the dissociation of the bound insulin. Thus the curvilinear Scatchard plot and the negative cooperativity of insulin binding (De Meyts et al., 1976) can be explained on the basis of the 3D reconstruction. The reconstruction also explains why only low-affinity binding is obtained with purified αβ monomer (Boni-Scnetzler et al., 1987; Sweet et al., 1987).

Evidence of insulin activation of the HIR

The 3D structure reveals that a slender horizontal bridge (Fig. 3-13B, side view 90°) connects the masses of the putative kinase domains. It was not observed in the x-ray structures of the TKs, but, as stated above, can be explained in terms of the reconstruction being in a transition between the free IR and its ligand-activated form. In the two symmetrically fitted TK crystal structures (Fig. 3-14C and D) the catalytic loops are separated by 4 nm. This distance is just sufficient to permit the tyrosine triplet (Tyr1158, 1162 and 1163) in a fully extended flexible activation loop of one TK to reach the catalytic loop of the opposite TK as modeled from the x-ray coordinates (PDB 1IRp). The extension of the activation loops, equivalent in cross-section to four extended polypeptide chains, easily accounts for the linking density observed between the lower portions of the β subunits (Fig. 13B, 90°). This is an important difference from the x-ray structures of the inactive and activated TKs as discussed below.

Monomeric inactive receptor TKs such as EGFR are brought together by ligand binding and become activated as dimers resulting in TK autophosphorylation (Cannals, 1992; Schlessinger and Ullrich,1992). In the intrinsically dimeric IR-family receptors, the distance between the two cytoplasmic β-subunit TKs within the dimer must be too great without ligand binding for the activation of the kinase. Hubbard and his colleagues (Hubbard et al., 1974; Hubbard 1997) suggested that insulin binding to IR decreased this distance by disengaging Tyr1162 from the catalytic loop to enable *trans* phosphorylation in the presence of ATP. In the reconstruction a good fit to the ligand-receptor complex is obtained when the two TK domains are oriented with their catalytic loops juxtaposed. In this orientation the extended flexible activation loop of each TK, which moves 30 Å

between the inactive and activated states in the crystal structures (Hubbard et al., 1974; Hubbard 1997), can just reach the catalytic loop of the opposing TK to be activated. These two loops can easily form the linking mass density between the TKs seen in the 3D reconstruction in the absence of ATP.

The 3D structure obtained from images of the HIR-complex contains only a single NGBI. This suggests that one molecule of insulin is sufficient to bring the two αβ monomers to an activating configuration. In light of this supposition, it is significant to note that the dimeric receptor with a Ser323Leu mutation in the L2 domain of both α subunits showed a severe impairment in insulin binding (Roach et al., 1994), whereas a hybrid receptor with only one of the two α subunits mutated was found to bind insulin with high affinity and was fully active as a tyrosine kinase (Taouis et al., 1994). Based on the 3D reconstruction we would suggest that insulin is bound to the L1 domain of the mutant α subunit and the wild-type L2 domain of the hybrid IR and that the binding of only a single molecule of insulin is sufficient for TK activation.

In this study the 3D quaternary structure of the IR-insulin complex formed in the absence of ATP was obtained. Thus the structure was expected to be an intermediate between the insulin-free IR and the fully activated, phosphorylated IR. The reconstruction is readily interpreted as a receptor poised for activation by *trans*-phosphorylation. The full extent of conformational changes induced by insulin binding remains conjectural, without similar reconstructions of the initial state of insulin-free IR and of the final activated state for comparison. Nonetheless, in the absence of a crystallographic structure of the insulin receptor, the 3D reconstruction presented here provides concrete structural information towards the full understanding of transmembrane signal transmission in insulin action.

Furthermore, the approach used in this study can be applied to obtain the quaternary structure of other membrane proteins or receptors that are refractory to crystallization.

CHAPTER 4

CONCLUSION AND FUTURE RESEARCH

The first step in the pathway of insulin action is the binding of insulin to its cell surface receptor, an integral transmembrane glycoprotein, leading to the activation of the cytoplasmic domain of the receptor tyrosine kinase. Much is known about the interaction of the activated receptor with its substrates leading to down-stream signal transduction. On the other hand, how binding of insulin to the extracellular domain of the receptor can lead to receptor activation remains unknown. Understanding where insulin binds to the extracellular domain would provide the foundation to answer this question.

Many approaches, biochemical and biophysical, have been applied to elucidate the site(s) of insulin-insulin receptor interaction. Different results were reported, and various regions in the α subunit of the IR have been suggested to be involved in the insulin-IR interaction. These regions include almost every major domain, such as N-terminal, cysteine-rich domain and C-terminal of the α subunit. An accurate location of the insulin-binding site on the receptor has not been forthcoming.

The specific goal of this study was to localize the insulin-binding site in the IR, and, if possible, to elucidate the molecular details of insulin-IR interaction and the relationship of the structure and function of the insulin receptor. To achieve this goal by the biochemical approach, I have expressed the human insulin receptor extracellular domain in a large scale in the baculovirus expression system and used various specific photoaffinity probes to identify the insulin contact sites. The photolabeled receptor protein was digested with proteases, and high-sensitivity identification methods were developed to detect the labeled IR fragment containing the putative insulin-binding site

by HPLC peptide-mapping analysis. I have focused on a fragment of 1-3 kDa that might contain the putative insulin-binding or contacting site on the receptor α subunit. However, I failed to obtain sufficient quantities of the fragment for amino acid sequencing, partly due to the lack of a high efficiency photoprobe of insulin and a high efficiency peptide mapping method. Availability of insulin photoprobes with higher efficiency is a key in future studies using this approach. The benzoylphenylalanine photoreactive group in a new insulin photoprobe has shown a much higher cross-linking efficiency than the traditional phenylazido photoreactive group. A cross-linking efficiency of more than 50% has been reported for this photoprobe compared to less than 10 % reported for other insulin photoprobes (Shoelson et al., 1993). The use of this high efficiency photoprobe should lead to a higher yield of the cross-linking products. In addition, methods for the purification of the cross-linked fragment and for higher sensitivity in amino acid sequencing need to be developed. The use of MALDI-TOF to determine amino acid sequence of small peptides is clearly a practical alternative.

My next approach to the goal was cryoelectron microscopy, specifically STEM. By using insulin labeled with an electron-dense gold cluster to bind to purified human placenta membrane insulin receptor, I successfully determined the 3D structure of insulin-insulin receptor complex at a resolution of 20 Å and localized the site of insulin binding on the complex. The structure was fitted with available known high resolution crystal domain substructures to obtain a detailed contiguous model of the heterotetrameric $(\alpha\beta)_2$ transmembrane receptor. The 3D reconstruction shows that the two α subunits jointly participate in insulin binding and that the two β subunit kinases in this receptor-ligand complex are in a juxtaposition that permits trans-autophosphorylation

of key tyrosine residues in the first step of insulin receptor activation. In addition, based on finding only one molecule of insulin (as visualized by the gold-labeled insulin), and only rarely two, the reconstruction provides structural evidence for the involvement of only a single insulin molecule in receptor activation.

The quaternary structure of human insulin receptor complex determined by this study provides the structural explanation for many of the known characteristics of insulin binding to its receptor. Fitting the crystal structure of insulin into the reconstruction model shows that the L1, CR and L2 domains of both α subunits contribute multiple contacting sites for high-affinity insulin-IR interaction. The structure also shows that extracellular domains of the β subunits play role in stabilizing the high-affinity insulin-binding site. Moreover the structure provides a mechanistic basis for the mechanism of receptor activation by insulin.

The structure also explains many biochemical findings in the studies of the insulin receptor. A recent study indicated that insulin receptor isoform A in which exon 11 is not expressed, besides its high affinity to insulin, binds to IGF II with an affinity close to that of insulin. It appears to serve as a high-affinity IGF II receptor affecting the growth of fetal and cancer cells (Frasca et al., 1999; Sciacca et al., 1999). This finding suggests that the small variation in the C-terminal of the α subunit of the insulin receptor plays an important role in the conformation for high-affinity ligand binding. Interestingly, binding sites of receptors for many growth factors, such as growth hormone, erythropoietin or prolactin, are composed of the two fibronectin repeats of each monomer that forms the dimeric receptor (Wells, 1996; Bole-Feysot et al., 1998). The structure we have obtained for the complex shows that the C-terminal of the α subunit and the adjacent N-terminal of

the β subunit contains a similar structure of fibronectin repeats dimer. How the presence or the absence of these 12 residues coded by the exon 11, in the C-terminal region could change the IR's affinity to IGF-II is still unknown. However, the structural similarity between the IR C-terminus and growth factor receptors does provide a structural basis for a suggestion that the C terminal region of the insulin receptor isoform A could serve as another ligand binding site in addition to the L1-CR-L2 region for insulin. This hypothesis could be confirmed by STEM similar to the present study, but using Nanogold-IGF-II.

Insulin and impaired insulin action play a key role in the pathogenesis of diabetes, especially in type II diabetes which account for more than 85% of the diabetic population. While a combination of genetic and environmental factors contributes to the development of type II diabetes, defects in the insulin signal transduction pathway beginning with the interaction of insulin with its receptor play a major role in the manifestation of the disease. The 3-D reconstruction of the insulin-IR complex described here presents the first model to explain signaling process from ligand binding to tyrosine kinase activation. The structural localization of the insulin binding sites in the IR provides evidence of how and where insulin interacts with its receptor. Combining with information from crystal structure of the isolated receptor domains, such as L1-CR-L2 of the IGFI-R, it would be possible to obtain more details of the insulin-IR interaction. This would eventually help to develop ~~the~~ new anti-diabetic medicine.

Recently, a non-peptidyl fungal compound L-783,281, was reported to have anti-diabetic activity in mice (Zhang et al., 1999). Rather than interacting with the insulin-binding sites on the α subuints, this compound appears to interact with the catalytic

domain of the tyrosine kinase of the IR. This finding introduces the new concept that substances which can bind to IR at sites different from the ligand-binding domain can still mimic the effects of the ligand of the receptor. Our reconstruction model may provide a structural basis for studying the potential mechanism by which this fungal compound actives tyrosine kinase of the IR. Other oral (or non-oral) anti-diabetic agents have also been reported to have insulin mimic effect, such as vanadates, PTP inhibitors and phosphoinositolglycans (Frick et al., 1998; Shalev, 1999; Chen et al., 1999; Iversen et al., 2000). Some of them directly interact with the IR. It is still not very clear how these compounds mimic insulin action at the molecular level. Nevertheless, more detailed structure and function studies and the subsequent structure-based design for new drugs would help to develop rational therapies for treating insulin resistance.

Besides the principal IRS substrates, other substrates, such as Shc, might also exist in the insulin-signaling pathway. Alternative pathways of the IR may be responsible for the multiple actions of insulin. Shc is a substrate protein rapidly tyr-phosphorylated by insulin stimulation. Shc contains an N-terminal PTB domain which binds to the phosphorylated $NPXY^{972}$ sequence in the insulin receptor and can also bind Grb-2 to link these signals to Ras activation (Skolnik et al., 1993; Pronk et al. 1994; Gustaffson et al., 1995). It has been suggested that Shc, rather than IRS-1, may be the main mediator of the mitogenic actions of insulin and IGF- II (Yamaguchi and Pessin, 1994).

Although our observation represents a significant advance in elucidating the structure of the insulin receptor, and provides a structural basis for the mechanism of receptor activation, additional studies remain to be done. First, the present study was carried out on detergent-solubilized membrane protein in the absence of a bilayer

membrane. Although the solubilized protein has been shown to be fully active in ligand binding and autophosphorylation when compared to placenta membrane receptor, the structure of the complex obtained did show a compressed transmembrane domain in the 3D reconstruction. A receptor in a bilayer support would provide a more natural reconstruction. Studies on 2D crystal of the protein supported by a lipid monolayer or bilayer would greatly increase the final resolution of the 3D reconstruction. Several 3D reconstructions obtained by electron cryomicroscopy based on 2D crystal images have resolved the structure of a number of proteins at resolutions below 7 Å (Cheng et al., 1997; Walz et al., 1997), very close to the resolution obtained by x-ray crystallography. Since the insulin receptor has so far not been crystallized the 3D reconstruction of this protein at a higher resolution is especially important to elucidate the molecular details of the function related structure, such as the insulin-binding site. Understanding the molecular mechanism of the insulin-IR interaction would help in designing new drug for treatment of diabetes mellitus.

Insulin binding to the receptor leads to conformation change of the receptor. This conformation change is the key step to receptor activation. A reconstruction of the free receptor without bound insulin would provide very useful information. Comparison of the activated and the pre-activated conformation of the receptor will provide the information required for understanding the mechanism of receptor activation. In this study we obtained the structure of a receptor bound to insulin at the pre-phosphorylation stage in the absence of ATP. Addition of ATP to the insulin-binding buffer could reveal the conformation of fully phosphorylated receptor kinase. Combining information obtained from different activation states should help us to understand the mechanism of insulin

receptor activation. Furthermore, in addition to monitoring the conformation change during the receptor activation, electron cryomicroscopy would also be an excellent tool for visualizing the conformation change of the receptor resulting from mutagenesis. This visualization would provide the direct explanation of the changed relationship in structure and function. Visualization of down-stream interaction with signal transduction elements, such as IRS proteins is also very important for understanding the mechanism of insulin receptor activation and the insulin signaling system. IRS proteins are another group of proteins that play important roles in signal transduction but are difficult to crystallize structure for studying their structure and function. We can imagine that the combination of molecular genetics in sample preparation, state-of–the-art electron cryomicroscopy for data acquisition, and powerful image processing will open a new era of structure and function studies for the insulin receptor at close to the atomic resolution level.

REFERENCES

Abbott AM, Bueno R, Pedrini MT, Murray JM, Smith RJ. (1992) Insulin-like growth factor I receptor gene structure. J Biol Chem 267(15):10759-63

Adham IM, Blundell TL, Dodsen EJ, Dodson GG, Vijayan M, Baker EN, Hodgkin DC, Rimmer B and Sheat S. (1969) Structure of rhombohedral 2 zinc insulin crystals. Nature 224:491-5

Andersen AS, Kjeldsen T, Wiberg FC, Christensen PM, Rasmussen JS, Norris K, Moller KB, Moller NP. (1990) Changing the insulin receptor to possess insulin-like growth factor I ligand specificity. Biochemistry 29(32):7363-6

Bajaj M, Waterfield MD, Schlessinger J, Taylor WR, Blundell T. (1987) On the tertiary structure of the extracellular domains of the epidermal growth factor and insulin receptors. Biochim Biophys Acta 916(2):220-6

Baker EN, Blundell TL, Cutfield JF, Cutfield SM, Dodson EJ, Dodson GG, Hodgkin DM, Hubbard RE, Isaacs NW, Reynolds CD, Sakabe K and Vijayan M. (1988) The structure of 2Zn pig insulin crystals at 1.5 A resolution. Philos Trans R Soc Lond B Biol Sci 319(1195):369-456

Baron M, Main AL, Driscoll PC, Mardon HJ, Boyd J, Campbell ID. (1992) 1H NMR assignment and secondary structure of the cell adhesion type III module of fibronectin. Biochemistry 31(7):2068-73

Baulieu EE (1990) Hormones: a complex communication network. In: Hormones: from molecules to disease. Baulieu EE Kelly PA (eds), Chapman and Hall, New York, pp1-169.

Beckmann R, Bubeck D, Grassucci R, Penczek P, Verschoor A, Blobel G, Frank J. (1997) Alignment of conduits for the nascent polypeptide chain in the ribosome-Sec61 complex. Science 278(5346):2123-6

Bilan PJ and Yip CC. (1994) Unusual insulin binding to cells expressing an insulin receptor mutated

Blundell TL, Cutfield JF, Dodson GG, Dodson E, Hodgkin DC, Mercola D. (1971) The structure and biology of insulin. Biochem J 125(3):50-1.

Blundell TL, Wood SP. (1975) Is the evolution of insulin Darwinian or due to selectively neutral mutation? Nature 257(5523):197-203

Boisset N, Grassucci R, Penczek P, Delain E, Pochon F, Frank J, Lamy JN. (1992) Three-dimensional reconstruction of a complex of human alpha 2-macroglobulin with monomaleimido Nanogold (Au1.4nm) embedded in ice. J Struct Biol 109(1):39-45

Bole-Feysot C, Goffin V, Edery M, Binart N, Kelly PA. (1998) Prolactin (PRL) and its receptor: actions, signal transduction pathways and phenotypes observed in PRL receptor knockout mice. Endocr Rev 19(3):225-68

Boni-Schnetzler M, Scott W, Waugh SM, DiBella E, Pilch PF. (1987) The insulin receptor. Structural basis for high affinity ligand binding. J Biol Chem 262(17):8395-401

Bottcher B, Kiselev NA, Stel'Mashchuk VY, Perevozchikova NA, Borisov AV, Crowther RA. (1997) Three-dimensional structure of infectious bursal disease virus determined by electron cryomicroscopy. J Virol 71(1):325-30

Boni-Schnetzler M, Rubin JB, Pilch PF. (1986) Structural requirements for the transmembrane activation of the insulin receptor kinase. J Biol Chem 261(32):15281-7.

Brandenburg D, Diaconescu C, Saunders D, Thamm P. (1980) Covalent linking of photoreactive insulin to adipocytes produces a prolonged signal. Nature 286(5775):821-2

Brange J, Ribel U, Hansen JF, Dodson G, Hansen MT, Havelund S, Melberg SG, Norris F, Norris K, Snel L, et al. (1988) Monomeric insulins obtained by protein engineering and their medical implications. Nature 333(6174):679-82

Brissenden JE, Ullrich A, Francke U. (1984) Human chromosomal mapping of genes for insulin-like growth factors I and II and epidermal growth factor. Nature 310(5980):781-4

Brown H, Sanger F and Kitai R. (1955) The structure of sheep and pig insulin. Biochem J 60:556-65.

Brown VI and Greene MI. (1991) Molecular and cellular mechanisms of receptor-mediated endocytosis. DNA Cell Biol 10(6):399-409

Canals F. (1992) Signal transmission by epidermal growth factor receptor: coincidence of activation and dimerization. Biochemistry 31(18):4493-501

Caro LH, Ohali A, Gorden P, Collier E. (1994) Mutational analysis of the NH2-terminal glycosylation sites of the insulin receptor alpha-subunit. Diabetes 43(2):240-6

Cheng A, van Hoek AN, Yeager M, Verkman AS, Mitra AK. (1997) Three-dimensional organization of a human water channel. Nature 387:627-30

Cheatham B and Kahn CR. (1992) Cysteine 647 in the insulin receptor is required for normal covalent interaction between alpha- and beta-subunits and signal transduction. J Biol Chem 267(10):7108-15

Cheatham B and Kahn CR. (1995) Insulin action and the insulin signaling network. Endocr Rev 16(2):117-42

Cheatham B, Vlahos CJ, Cheatham L, Wang L, Blenis J, Kahn CR. (1994) Phosphatidylinositol 3-kinase activation is required for insulin stimulation of pp70 S6 kinase, DNA synthesis, and glucose transporter translocation. Mol Cell Biol 14(7):4902-11

Chen H, Cong LN, Li Y, Yao ZJ, Wu L, Zhang ZY, Burke TR Jr, Quon MJ. (1999) A phosphotyrosyl mimetic peptide reverses impairment of insulin-stimulated translocation of GLUT4 caused by overexpression of PTP1B in rat adipose cells. Biochemistry 38(1):384-9

Chiu W, and Schmid MF. (1997) Pushing back the limits of electron cryomicroscopy. Nat Struct Biol 4(5):331-3

Christiansen K, Tranum-Jensen J, Carlsen J, Vinten J. (1991) A model for the quaternary structure of human placental insulin receptor deduced from electron microscopy. Proc Natl Acad Sci U S A 88(1):249-52

Clapham DE and Neer EJ. (1993) New roles for G-protein beta gamma-dimers in transmembrane signalling. Nature 365(6445):403-6

Conway JF, Cheng N, Zlotnick A, Wingfield PT, Stahl SJ, Steven AC. (1997) Visualization of a 4-helix bundle in the hepatitis B virus capsid by cryo-electron microscopy. Nature 386(6620):91-4

Cuatrecasas P. (1971) Insulin--receptor interactions in adipose tissue cells: direct measurement and properties. Proc Natl Acad Sci U S A 68(6):1264-8

Cosgrove L, Lovrecz GO, Verkuylen A, Cavaleri L, Black LA, Bentley JD, Howlett GJ, Gray PP, Ward CW, McKern NM. (1995) Purification and properties of insulin receptor ectodomain from large-scale mammalian cell culture. Protein Expr Purif 6(6):789-98

Crowther RA, Amos LA, Finch JT, De Rosier DJ, Klug A. (1970) Three dimensional reconstructions of spherical viruses by fourier synthesis from electron micrographs. Nature 226(244):421-5

Crowther RA. (1971) Three-dimensional reconstruction and the architecture of spherical viruses. Endeavour 30(111):124-9

Czarnota GJ, Andrews DW, Farrow NA, Ottensmeyer FP. (1994) A structure for the signal sequence binding protein SRP54: 3D reconstruction from STEM images of single molecules. J Struct Biol 113(1):35-46

Czarnota GJ, Bazett-Jones DP, Mendez E, Allfrey VG, Ottensmeyer FP. (1997) High resolution microanalysis and three-dimensional nucleosome structure associated with transcribing chromatin. Micron 28(6):419-31

Czech MP. (1982) Structural and functional homologies in the receptors for insulin and the insulin-like growth factors. Cell 31(1):8-10

Czech MP. (1989) Signal transmission by the insulin-like growth factors. Cell 59(2):235-8

Takata Y, Webster NJ, Olefsky JM. (1992) Intracellular signaling by a mutant human insulin receptor lacking the carboxyl-terminal tyrosine autophosphorylation sites. J Biol Chem 267(13):9065-70

DeFronzo RA. (1992) Pathogenesis of type 2 (non-insulin dependent) diabetes mellitus: a balanced overview. Diabetologia 35(4):389-97

Derosier RA and Klug A. (1968). Nature 217:130-4.

De Meyts P. (1976) Cooperative properties of hormone receptors in cell membranes. J Supramol Struct 4(2):241-58

De Meyts P. (1993) The diabetogenes concept of NIDDM. Adv Exp Med Biol 334:89-100

De Meyts P. (1994) The structural basis of insulin and insulin-like growth factor-I receptor binding and negative co-operativity, and its relevance to mitogenic versus metabolic signalling. Diabetologia 37 Suppl 2:S135-48

De Meyts P de, Roth J, Neville DM Jr, Gavin JR 3d, Lesniak MA. (1973) Insulin interactions with its receptors: experimental evidence for negative cooperativity. Biochem Biophys Res Commun 55(1):154-61

De Meyts P, Van Obberghen E, Roth J. (1978) Mapping of the residues responsible for the negative cooperativity of the receptor-binding region of insulin. Nature 273(5663):504-9

De Meyts P, Gu JL, Shymko RM, Kaplan BE, Bell GI, Whittaker J. (1990) Identification of a ligand-binding region of the human insulin receptor encoded by the second exon of the gene. Mol Endocrinol 4(3):409-16

Drake PG, Posner BI. (1998) Insulin receptor-associated protein tyrosine phosphatase(s): role in insulin action. Mol Cell Biochem 182(1-2):79-89

Dryden KA, Wang G, Yeager M, Nibert ML, Coombs KM, Furlong DB, Fields BN, Baker TS. (1993) Early steps in reovirus infection are associated with dramatic changes in supramolecular structure and protein conformation: analysis of virions and subviral particles by cryoelectron microscopy and image reconstruction. J Cell Biol 122(5):1023-41

Ebina Y, Ellis L, Jarnagin K, Edery M, Graf L, Clauser E, Ou JH, Masiarz F, Kan YW, Goldfine ID, Roth RA and Rutter WJ. (1985) The human insulin receptor cDNA: the structural basis for hormone-activated transmembrane signalling. Cell 40(4):747-58

Edge AS, Kahn CR, Spiro RG. (1990) Insulin receptor carbohydrate units contain poly-N-acetyllactosamine chains. Endocrinology 127(4):1887-95

Elchebly M, Payette P, Michaliszyn E, Cromlish W, Collins S, Loy AL, Normandin D, Cheng A, Himms-Hagen J, Chan CC, Ramachandran C, Gresser MJ, Tremblay ML, Kennedy BP. (1999) Increased insulin sensitivity and obesity resistance in mice lacking the protein tyrosine phosphatase-1B gene. Science 283(5407):1544-8.

Engl J, Moule M, Yip CC. (1994) Dithiothreitol stimulates insulin receptor autophosphorylation at the juxtamembrane domain. Biochem Biophys Res Commun 201(3):1439-44

Fantl WJ, Johnson DE, Williams LT. (1993) Signalling by receptor tyrosine kinases. Annu Rev Biochem 62:453-81

Fabry M, Brandenburg D. (1992) Analysis of the human insulin receptor. Biol Chem Hoppe Seyler 373(9):915-23

Fabry M, Schaefer E, Ellis L, Kojro E, Fahrenholz F, Brandenburg D. (1992) Detection of a new hormone contact site within the insulin receptor ectodomain by the use of a novel photoreactive insulin. J Biol Chem 267(13):8950-6

Farrow NA and Ottensmeyer FP. (1993) Automatic 3D alignment of projection images of randomly oriented objects. Ultramicroscopy 52, 141-56,

Farrow NA and Ottensmeyer FP. (1992) A posterioi determination of relative projection directions of arbitarily oriented macromolecules. L. Opt. Soc. Am. A9, 1749-60

Feener EP, Backer JM, King GL, Wilden PA, Sun XJ, Kahn CR, White MF. (1993) Insulin stimulates serine and tyrosine phosphorylation in the juxtamembrane region of the insulin receptor. J Biol Chem 268(15):11256-64

Finn FM, Ridge KD, Hofmann K. (1990) Labile disulfide bonds in human placental insulin receptor. Proc Natl Acad Sci U S A 87(1):419-23

Frasca F, Pandini G, Scalia P, Sciacca L, Mineo R, Costantino A, Goldfine ID, Belfiore A, Vigneri R. (1999) Insulin receptor isoform A, a newly recognized, high-affinity insulin-like growth factor II receptor in fetal and cancer cells. Mol Cell Biol 19(5):3278-88

Frattali AL, Treadway JL, Pessin JE. (1991) Evidence supporting a passive role for the insulin receptor transmembrane domain in insulin-dependent signal transduction. J Biol Chem 266(15):9829-34

Frick W, Bauer A, Bauer J, Wied S, Muller G. (1998) Structure-activity relationship of synthetic phosphoinositolglycans mimicking metabolic insulin action. Biochemistry 37(38):13421-36

Froesch ER and Zapf J. (1985) Insulin-like growth factors and insulin: comparative aspects. Diabetologia 28(8):485-93

Fuller PJ. (1991) The steroid receptor superfamily: mechanisms of diversity. FASEB J 5(15):3092-9

Fujita-Yamaguchi Y, Choi S, Sakamoto Y, Itakura K. (1983) Purification of insulin receptor with full binding activity. J Biol Chem 258(8):5045-9

Fujita-Yamaguchi Y, Kathuria S. (1985) The monomeric alpha beta form of the insulin receptor exhibits much higher insulin-dependent tyrosine-specific protein kinase activity than the intact alpha 2 beta 2 form of the receptor. Proc Natl Acad Sci U S A 82(18):6095-9

Garbers DL and Lowe DG. (1994) Guanylyl cyclase receptors. J Biol Chem 269(49):30741-4

Garrett TP, McKern NM, Lou M, Frenkel MJ, Bentley JD, Lovrecz GO, Elleman TC, Cosgrove LJ, Ward CW. (1998) Crystal structure of the first three domains of the type-1 insulin-like growth factor receptor. Nature 394(6691):395-9

Gherzi R, Russell DS, Taylor SI, Rosen OM. (1987) Reevaluation of the evidence that an antibody to the insulin receptor is insulinmimetic without activating the protein tyrosine kinase activity of the receptor. J Biol Chem 262(35):16900-5

Giranda VL. (1994) Structure-based drug design of antirhinoviral compounds. Structure 2(8):695-8

Goldfine ID. (1987) The insulin receptor: molecular biology and transmembrane signaling. Endocr Rev 8(3):235-55

Goldstein JL and Brown MS. (1985) The LDL receptor and the regulation of cellular cholesterol metabolism. J Cell Sci Suppl 3:131-7

Gustafson TA, He W, Craparo A, Schaub CD, O'Neill TJ. (1995) Phosphotyrosine-dependent interaction of SHC and insulin receptor substrate 1 with the NPEY motif of the insulin receptor via a novel non-SH2 domain. Mol Cell Biol 15(5):2500-8

Gustafson TA and Rutter WJ. (1990) The cysteine-rich domains of the insulin and insulin-like growth factor I receptors are primary determinants of hormone binding specificity. Evidence from receptor chimeras. J Biol Chem 265(30):18663-7

Hanks SK, Quinn AM, Hunter T. (1988) The protein kinase family: conserved features and deduced phylogeny of the catalytic domains. Science 241(4861):42-52

Hainfeld JF, Furuya FR. (1992) A 1.4-nm gold cluster covalently attached to antibodies improves immunolabeling. J Histochem Cytochem 40(2):177-84

Haring HU. (1991) The insulin receptor: signalling mechanism and contribution to the pathogenesis of insulin resistance. Diabetologia 34(12):848-61

Haynes FJ, Helmerhorst E, Yip CC. (1986) The structure of the hepatic insulin receptor and insulin binding. Biochem J 239(1):127-33

Henderson R, Baldwin JM, Ceska TA, Zemlin F, Beckmann E, Downing KH. (1990) Model for the structure of bacteriorhodopsin based on high-resolution electron cryo-microscopy. J Mol Biol 213(4):899-929

Hotamisligil GS, Shargill NS, Spiegelman BM. (1993) Adipose expression of tumor necrosis factor-alpha: direct role in obesity-linked insulin resistance. Science 259(5091):87-91

Hubbard SR. (1997) Crystal structure of the activated insulin receptor tyrosine kinase in complex with peptide substrate and ATP analog. EMBO J 16(18):5572-81

Hubbard SR, Wei L, Ellis L, Hendrickson WA. (1994) Crystal structure of the tyrosine kinase domain of the human insulin receptor. Nature 372(6508):746-54

Humbel RE. (1990) Insulin-like growth factors I and II. Eur J Biochem 190(3):445-62

Hunter T. (1991) Protein kinase classification. Methods Enzymol 200:3-37

Hunter T, Cooper JA. (1985) Protein-tyrosine kinases. Annu Rev Biochem 54:897-930

Hotamisligil GS, Peraldi P, Budavari A, Ellis R, White MF, Spiegelman BM. (1996) IRS-1-mediated inhibition of insulin receptor tyrosine kinase activity in TNF-alpha- and obesity-induced insulin resistance. Science 271(5249):665-8

Iversen LF, Andersen HS, Branner S, Mortensen SB, Peters GH, Norris K, Olsen OH, Jeppesen CB, Lundt BF, Ripka W, Moller KB, Moller NP. (2000) Structure-based design of a low molecular weight, nonphosphorus, nonpeptide, and highly selective inhibitor of protein-tyrosine phosphatase 1B. J Biol Chem 275(14):10300-7

Jontes JD, Wilson-Kubalek EM, Milligan RA. (1995) A 32 degree tail swing in brush border myosin I on ADP release. Nature 378(6558):751-3

Kaburagi Y, Momomura K, Yamamoto-Honda R, Tobe K, Tamori Y, Sakura H, Akanuma Y, Yazaki Y, Kadowaki T. (1993) Site-directed mutagenesis of the juxtamembrane domain of the human insulin receptor. J Biol Chem 268(22):16610-22

Kasuga M, Zick Y, Blithe DL, Crettaz M, Kahn CR. (1982) Insulin stimulates tyrosine phosphorylation of the insulin receptor in a cell-free system. Nature 298(5875):667-9

Keegan AD, Nelms K, White M, Wang LM, Pierce JH, Paul WE. (1994) An IL-4 receptor region containing an insulin receptor motif is important for IL-4-mediated IRS-1 phosphorylation and cell growth. Cell 76(5):811-20

Kahn CR. (1978) Insulin resistance, insulin insensitivity, and insulin unresponsiveness: a necessary distinction. Metabolism 27(12 Suppl 2):1893-902

Kahn CR. (1994) Banting Lecture. Insulin action, diabetogenes, and the cause of type II diabetes. Diabetes 43(8):1066-84

Kahn CR, White MF. (1988) The insulin receptor and the molecular mechanism of insulin action. J Clin Invest 82(4):1151-6

Kjeldsen T, Andersen AS, Wiberg FC, Rasmussen JS, Schaffer L, Balschmidt P, Moller KB, Moller NP. (1991) The ligand specificities of the insulin receptor and the insulin-like growth factor I receptor reside in different regions of a common binding site. Proc Natl Acad Sci U S A 88(10):4404-8

Kjeldsen T, Wiberg FC, Andersen AS. (1994) Chimeric receptors indicate that phenylalanine 39 is a major contributor to insulin specificity of the insulin receptor. J Biol Chem 269(52):32942-6

Kobilka B. (1992) Adrenergic receptors as models for G protein-coupled receptors. Annu Rev Neurosci 15:87-114

Kohanski RA. (1993) Insulin receptor autophosphorylation. II. Determination of autophosphorylation sites by chemical sequence analysis and identification of the juxtamembrane sites. Biochemistry 32(22):5773-80

Kruger P, Gilge G, Cabuk Y, Wollmer A. (1990) Cooperativity and intermediate states in the T----R-structural transformation of insulin. Biol Chem Hoppe Seyler 371(8):669-73

Kuhlbrandt W, Wang DN, Fujiyoshi Y. (1994) Atomic model of plant light-harvesting complex by electron crystallography. Nature 367(6464):614-21

Kurose T, Pashmforoush M, Yoshimasa Y, Carroll R, Schwartz GP, Burke GT, Katsoyannis PG, Steiner DF. (1994) Cross-linking of a B25 azidophenylalanine insulin derivative to the carboxyl-terminal region of the alpha-subunit of the insulin receptor. Identification of a new insulin-binding domain in the insulin receptor. J Biol Chem 269(46):29190-7

Laemmli UK. (1970) Cleavage of structural proteins during the assembly of the head of bacteriophage T4. Nature 227(259):680-5

Lammers R, Van Obberghen E, Ballotti R, Schlessinger J, Ullrich A. (1990) Transphosphorylation as a possible mechanism for insulin and epidermal growth factor receptor activation. J Biol Chem 265(28):16886-90

Leahy DJ, Hendrickson WA, Aukhil I, Erickson HP. (1992) Structure of a fibronectin type III domain from tenascin phased by MAD analysis of the selenomethionyl protein. Science 258(5084):987-91

Lee J and Pilch PF. (1994) The insulin receptor: structure, function, and signaling. Am J Physiol 266(2 Pt 1):C319-34

Lee J, O'Hare T, Pilch PF, Shoelson SE. (1993) Insulin receptor autophosphorylation occurs asymmetrically. J Biol Chem 268(6):4092-8

Lemmon MA, Bu Z, Ladbury JE, Zhou M, Pinchasi D, Lax I, Engelman DM, Schlessinger J. (1997) Two EGF molecules contribute additively to stabilization of the EGFR dimer. EMBO J 16(2):281-94

LeRoith D, Werner H, Burguera B, Roberts CT Jr, Mulroney S, Haramati A. (1992) The insulin-like growth factor family of peptides, binding proteins and receptors: their potential role in tissue regeneration. Adv Exp Med Biol 321:21-8; discussion 29-30

LeRoith D, Sampson PC, Roberts CT Jr. (1994) How does the mitogenic insulin-like growth factor I receptor differ from the metabolic insulin receptor? Horm Res 41 Suppl 2:74-8

Luo RZ, Beniac DR, Fernandes A, Yip CC, Ottensmeyer FP. 1999 Quaternary structure of the insulin-insulin receptor complex. Science 285(5430):1077-80

Macaulay SL, Polites M, Hewish DR, Ward CW. (1994) Cysteine-524 is not the only residue involved in the formation of disulphide-bonded dimers of the insulin receptor. Biochem J 303 (Pt 2):575-81

Maddux BA, Goldfine ID. (1991) Evidence that insulin plus ATP may induce a conformational change in the beta subunit of the insulin receptor without inducing receptor autophosphorylation. J Biol Chem 266(11):6731-6

Marino-Buslje C, Mizuguchi K, Siddle K, Blundell TL. (1998) A third fibronectin type III domain in the extracellular region of the insulin receptor family. FEBS Lett 441(2):331-6

Massague J, Pilch PF, Czech MP. (1980) Electrophoretic resolution of three major insulin receptor structures with unique subunit stoichiometries. Proc Natl Acad Sci U S A 77(12):7137-41

Massague J and Czech MP. (1982) The subunit structures of two distinct receptors for insulin-like growth factors I and II and their relationship to the insulin receptor. J Biol Chem 257(9):5038-45

McKeon C and Pham T. (1991) Transactivation of the human insulin receptor gene by the CAAT/enhancer binding protein. Biochem Biophys Res Commun 174(2):721-8

Mirmira RG, Nakagawa SH, Tager HS. (1991) Importance of the character and configuration of residues B24, B25, and B26 in insulin-receptor interactions. J Biol Chem 266(3):1428-36

Mirmira RG and Tager HS. (1989) Role of the phenylalanine B24 side chain in directing insulin interaction with its receptor. Importance of main chain conformation. J Biol Chem 264(29):17613

Mosthaf L, Vogt B, Haring HU, Ullrich A. (1991) Altered expression of insulin receptor types A and B in the skeletal muscle of non-insulin-dependent diabetes mellitus patients. Proc Natl Acad Sci U S A88(11):4728-30

Mulhern TD, Booker GW. (1998) A third fibronectin-type-III domain in the insulin-family receptors. Trends Biochem Sci 23(12):465-6

Muller-Wieland D, Taub R, Tewari DS, Kriauciunas KM, Sethu S, Reddy K, Kahn CR. (1989) Insulin-receptor gene and its expression in patients with insulin resistance. Diabetes 38(1):31-8

Munson PJ, Rodbard D. (1980) Ligand: a versatile computerized approach for characterization of ligand-binding systems. Anal Biochem 107(1):220-39

Murray-Rust J, McLeod AN, Blundell TL, Wood SP. (1992) Structure and evolution of insulins: implications for receptor binding. Bioessays 14(5):325-31

Myers MG, Backer JM, Siddle K, White MF. (1991) The insulin receptor functions normally in Chinese hamster ovary cells after truncation of the C terminus. J Biol Chem 266(16):10616-23

Myers MG Jr, Sun XJ, Cheatham B, Jachna BR, Glasheen EM, Backer JM, White MF. (1993) IRS-1 is a common element in insulin and insulin-like growth factor-I signaling to the phosphatidylinositol 3'-kinase. Endocrinology 132(4):1421-30

Myers MG Jr, Sun XJ, White MF. (1994) The IRS-1 signaling system. Trends Biochem Sci 19(7):289-93

Mynarcik DC, Yu GQ, Whittaker J. (1996) Alanine-scanning mutagenesis of a C-terminal ligand binding domain of the insulin receptor alpha subunit. J Biol Chem 271(5):2439-42

Mynarcik DC, Williams PF, Schaffer L, Yu GQ, Whittaker J. (1997) Identification of common ligand binding determinants of the insulin and insulin-like growth factor 1 receptors. Insights into mechanisms of ligand binding. J Biol Chem 272(30):18650-5

Nakagawa SH and Tager HS. (1986) Role of the phenylalanine B25 side chain in directing insulin interaction with its receptor. Steric and conformational effects. J Biol Chem 261(16):7332-41

Nakagawa SH and Tager HS. (1987) Role of the COOH-terminal B-chain domain in insulin receptor interactions. Identification of perturbations involving the insulin mainchain. J Biol Chem 262(25):12054-8

Nakagawa SH and Tager HS. (1993) Importance of main-chain flexibility and the insulin fold in insulin-receptor interactions. Biochemistry 32(28):7237-43

Ng DS, Yip CC. (1985) Peptide mapping of the insulin-binding site of the 130-kDa subunit of the insulin receptor by means of a novel cleavable radioactive photoprobe. Biochem Biophys Res Commun 133(1):154-60

Nishida E, Gotoh Y. (1993) The MAP kinase cascade is essential for diverse signal transduction pathways. Trends Biochem Sci 18(4):128-31

O'Bryan JP, Frye RA, Cogswell PC, Neubauer A, Kitch B, Prokop C, Espinosa R 3d, Le Beau MM, Earp HS, Liu ET. (1991) axl, a transforming gene isolated from primary human myeloid leukemia cells, encodes a novel receptor tyrosine kinase. Mol Cell Biol 11(10):5016-31

Olefsky JM. (1981) LIlly lecture 1980. Insulin resistance and insulin action. An in vitro and in vivo perspective. Diabetes 30(2):148-62

O'Neill TJ, Craparo A, Gustafson TA. (1994) Characterization of an interaction between insulin receptor substrate 1 and the insulin receptor by using the two-hybrid system. Mol Cell Biol 14(10):6433-42

Olson TS, Bamberger MJ, Lane MD. (1988) Post-translational changes in tertiary and quaternary structure of the insulin proreceptor. Correlation with acquisition of function. J Biol Chem 263(15):7342-51

Olson NH, Kolatkar PR, Oliveira MA, Cheng RH, Greve JM, McClelland A, Baker TS, Rossmann MG. (1993) Structure of a human rhinovirus complexed with its receptor molecule. Proc Natl Acad Sci U S A 90(2):507-11

Ottensmeyer FP. (1982) Scattered electrons in microscopy and microanalysis. Science 215(4532):461-6

Ottensmeyer FP, Czarnota, GL, Andrews DW and Farrow NA. (1994) Proceedings 13th Int. Congress on Electron Microscopy. 509-510

Pasquale EB. (1991) Identification of chicken embryo kinase 5, a developmentally regulated receptor-type tyrosine kinase of the Eph family. Cell Regul 2(7):523-34

Paul JI, Tavare J, Denton RM, Steiner DF. (1990) Baculovirus-directed expression of the human insulin receptor and an insulin-binding ectodomain. J Biol Chem 265(22):13074-83

Paredes AM, Heidner H, Thuman-Commike P, Prasad BV, Johnston RE, Chiu W. (1998) Structural localization of the E3 glycoprotein in attenuated Sindbis virus mutants. J Virol 72(2):1534-41

Pawson T and Gish GD. (1992) SH2 and SH3 domains: from structure to function. Cell 71(3):359-62

Pawson T. (1995) Protein modules and signalling networks. Nature 373(6515):573-80

Pelicci G, Lanfrancone L, Grignani F, McGlade J, Cavallo F, Forni G, Nicoletti I, Grignani F, Pawson T, Pelicci PG. (1992) A novel transforming protein (SHC) with an SH2 domain is implicated in mitogenic signal transduction. Cell 70(1):93-104

Pilch PF and Czech MP. (1979) Interaction of cross-linking agents with the insulin effector system of isolated fat cells. Covalent linkage of 125I-insulin to a plasma membrane receptor protein of 140,000 daltons. J Biol Chem 254(9):3375-81

Pilch PF and Czech MP. (1980) Hormone binding alters the conformation of the insulin receptor. Science 210(4474):1152-3

Porte D Jr. (1991) Banting lecture 1990. Beta-cells in type II diabetes mellitus. Diabetes 40(2):166-80

Pronk GJ, McGlade J, Pelicci G, Pawson T, Bos JL. (1993) Insulin-induced phosphorylation of the 46- and 52-kDa Shc proteins. J Biol Chem 268(8):5748-53

Radermacher M, Wagenknecht T, Grassucci R, Frank J, Inui M, Chadwick C, Fleischer S. (1992) Cryo-EM of the native structure of the calcium release channel/ryanodine receptor from sarcoplasmic reticulum. Biophys J 61(4):936-40

Rafaeloff R, Patel R, Yip C, Goldfine ID, Hawley DM. (1989) Mutation of the high cysteine region of the human insulin receptor alpha-subunit increases insulin receptor binding affinity and transmembrane signaling. J Biol Chem 264(27):15900-4

Roach P, Zick Y, Formisano P, Accili D, Taylor SI, Gorden P. (1994) A novel human insulin receptor gene mutation uniquely inhibits insulin binding without impairing posttranslational processing. Diabetes 43(9):1096-102

Rosenberg MF, Callaghan R, Ford RC, Higgins CF. (1997) Structure of the multidrug resistance P-glycoprotein to 2.5 nm resolution determined by electron microscopy and image analysis. J Biol Chem 272(16):10685-94

Roth RA, Cassell DJ, Wong KY, Maddux BA, Goldfine ID. (1982) Monoclonal antibodies to the human insulin receptor block insulin binding and inhibit insulin action. Proc Natl Acad Sci U S A 79(23):7312-6

Sasaoka T, Takata Y, Kusari J, Anderson CM, Langlois WJ, Olefsky JM. (1993) Transmembrane signaling by an insulin receptor lacking a cytoplasmic beta-subunit domain. Proc Natl Acad Sci U S A 90(10):4379-83

Schwabe C, Bullesbach EE. (1994) Relaxin: structures, functions, promises, and nonevolution. FASEB J 8(14):1152-60

Seino S, Bell GI. (1989) Alternative splicing of human insulin receptor messenger RNA. Biochem Biophys Res Commun 159(1):312-6

Seino S, Seino M, Bell GI. (1990) Human insulin-receptor gene. Diabetes 39(2):129-33

Schaefer EM, Siddle K, Ellis L. (1990) Deletion analysis of the human insulin receptor ectodomain reveals independently folded soluble subdomains and insulin binding by a monomeric alpha-subunit. J Biol Chem 265(22):13248-53

Schaefer EM, Erickson HP, Federwisch M, Wollmer A, Ellis L. (1992) Structural organization of the human insulin receptor ectodomain. J Biol Chem 267(32):23393-402

Schaffer L, Ljungqvist L. (1992) Identification of a disulfide bridge connecting the alpha-subunits of the extracellular domain of the insulin receptor. Biochem Biophys Res Commun 189(2):650-3

Schaffer L, Kjeldsen T, Andersen AS, Wiberg FC, Larsen UD, Cara JF, Mirmira RG, Nakagawa SH, Tager HS. (1993) Interactions of a hybrid insulin/insulin-like growth

factor-I analog with chimeric insulin/type I insulin-like growth factor receptors. J Biol Chem 268(5):3044-7

Schaffer L. (1994) A model for insulin binding to the insulin receptor. Eur J Biochem 221(3):1127-32

Schrag JD, Prasad BV, Rixon FJ, Chiu W. (1989) Three-dimensional structure of the HSV1 nucleocapsid. Cell 56(4):651-60

Schumacher R, Soos MA, Schlessinger J, Brandenburg D, Siddle K, Ullrich A. (1993) Signaling-competent receptor chimeras allow mapping of major insulin receptor binding domain determinants. J Biol Chem 268(2):1087-94

Serysheva II, Orlova EV, Chiu W, Sherman MB, Hamilton SL, van Heel M. (1995) Electron cryomicroscopy and angular reconstitution used to visualize the skeletal muscle calcium release channel. Nat Struct Biol 2(1):18-24

Shaw AL, Samal SK, Subramanian K, Prasad BV. (1996) The structure of aquareovirus shows how the different geometries of the two layers of the capsid are reconciled to provide symmetrical interactions and stabilization. Structure 4(8):957-67

Skolnik EY, Batzer A, Li N, Lee CH, Lowenstein E, Mohammadi M, Margolis B, Schlessinger J. (1993) The function of GRB2 in linking the insulin receptor to Ras signaling pathways. Science 260(5116):1953-5

Sciacca L, Costantino A, Pandini G, Mineo R, Frasca F, Scalia P, Sbraccia P, Goldfine ID, Vigneri R, Belfiore A. (1999) Insulin receptor activation by IGF-II in breast cancers: evidence for a new autocrine/paracrine mechanism. Oncogene 18(15):2471-9

Shalev A. (1999) Hope for insulin mimetic oral antidiabetic drugs. Eur J Endocrinol 141(6):561-2

Shier P, Watt VM. (1989) Primary structure of a putative receptor for a ligand of the insulin family. J Biol Chem 264(25):14605-8

Shoelson SE, White MF, Kahn CR. (1988) Tryptic activation of the insulin receptor. Proteolytic truncation of the alpha-subunit releases the beta-subunit from inhibitory control. J Biol Chem 263(10):4852-60

Shoelson SE, Lee J, Lynch CS, Backer JM, Pilch PF. (1993) BpaB25 insulins. Photoactivatable analogues that quantitatively cross-link, radiolabel, and activate the insulin receptor. J Biol Chem 268(6):4085-91

Siddle K, Soos MA, Field CE, Nave BT. (1994) Hybrid and atypical insulin/insulin-like growth factor I receptors. Horm Res Suppl 2:56-64; discussion 65

Sissom J, Ellis L.(1989) Secretion of the extracellular domain of the human insulin receptor from insect cells by use of a baculovirus vector. Biochem J 261(1):119-26

Sparrow LG, McKern NM, Gorman JJ, Strike PM, Robinson CP, Bentley JD, Ward CW. (1997) The disulfide bonds in the C-terminal domains of the human insulin receptor ectodomain. J Biol Chem 272(47):29460-7

Staubs PA, Reichart DR, Saltiel AR, Milarski KL, Maegawa H, Berhanu P, Olefsky JM, Seely BL. (1994) Localization of the insulin receptor binding sites for the SH2 domain proteins p85, Syp, and GAP. J Biol Chem 269(44):27186-92

Steiner DF, Tager HS, Chan SJ, Nanjo K, Sanke T, Rubenstein AH. (1990) Lessons learned from molecular biology of insulin-gene mutations. Diabetes Care 13(6):600-9

Sutherland C, Campbell DG, Cohen P. (1993) Identification of insulin-stimulated protein kinase-1 as the rabbit equivalent of rskmo-2. Identification of two threonines phosphorylated during activation by mitogen-activated protein kinase. Eur J Biochem 212(2):581-8

Sun XJ, Rothenberg P, Kahn CR, Backer JM, Araki E, Wilden PA, Cahill DA, Goldstein BJ, White MF. (1991) Structure of the insulin receptor substrate IRS-1 defines a unique signal transduction protein. Nature 352(6330):73-7

Sun XJ, Crimmins DL, Myers MG Jr, Miralpeix M, White MF. (1993) Pleiotropic insulin signals are engaged by multisite phosphorylation of IRS-1. Mol Cell Biol 13(12):7418-28

Sun XJ, Wang LM, Zhang Y, Yenush L, Myers MG Jr, Glasheen E, Lane WS, Pierce JH, White MF. (1995) Role of IRS-2 in insulin and cytokine signalling. Nature Sep 14;377(6545):173-7

Sung CK, Wong KY, Yip CC, Hawley DM, Goldfine ID. (1994) Deletion of residues 485-599 from the human insulin receptor abolishes antireceptor antibody binding and influences tyrosine kinase activation. Mol Endocrinol 8(3):315-24

Sweet LJ, Wilden PA, Pessin JE. (1986) Dithiothreitol activation of the insulin receptor/kinase does not involve subunit dissociation of the native alpha 2 beta 2 insulin receptor subunit complex. Biochemistry 25(22):7068-74

Sweet LJ, Morrison BD, Wilden PA, Pessin JE. (1987) Insulin-dependent intermolecular subunit communication between isolated alpha beta heterodimeric insulin receptor complexes. J Biol Chem 262(34):16730-8

Tager H, Thomas N, Assoian R, Rubenstein A, Saekow M, Olefsky J, Kaiser ET. (1980) Semisynthesis and biological activity of porcine [LeuB24]insulin and [LeuB25]insulin. Proc Natl Acad Sci U S A 77(6):3181-5

Taouis M, Levy-Toledano R, Roach P, Taylor SI, Gorden P. (1994) Rescue and activation of a binding-deficient insulin receptor. Evidence for intermolecular transphosphorylation. J Biol Chem 269(44):27762-6

Tavare JM, Siddle K. (1993) Mutational analysis of insulin receptor function: consensus and controversy. Biochim Biophys Acta 1178(1):21-39

Taylor R. (1991) Insulin action 1991. Clin Endocrinol (Oxf) Feb;34(2):159-71

Taylor SI, Cama A, Accili D, Barbetti F, Quon MJ, de la Luz Sierra M, Suzuki Y, Koller E, Levy-Toledano R, Wertheimer E, et al. (1992) Mutations in the insulin receptor gene. Endocr Rev 13(3):566-95

Taouis M, Levy-Toledano R, Roach P, Taylor SI, Gorden P. (1994) Rescue and activation of a binding-deficient insulin receptor. Evidence for intermolecular transphosphorylation. J Biol Chem 269(44):27762-6

Tanasijevic MJ, Myers MG Jr, Thoma RS, Crimmins DL, White MF, Sacks DB. (1993) Phosphorylation of the insulin receptor substrate IRS-1 by casein kinase II. J Biol Chem 268(24):18157-66

Trus BL, Roden RB, Greenstone HL, Vrhel M, Schiller JT, Booy FP. (1997) Novel structural features of bovine papillomavirus capsid revealed by a three-dimensional reconstruction to 9 A resolution. Nat Struct Biol 4(5):413-20

Turner R, Hattersley A, Cook J. (1992) Type II diabetes: search for primary defects. Ann Med 24(6):511-6

Ullrich A, Berman CH, Dull TJ, Gray A, Lee JM. (1984) Isolation of the human insulin-like growth factor I gene using a single synthetic DNA probe. EMBO J 3(2):361-4

Ullrich A, Bell JR, Chen EY, Herrera R, Petruzzelli LM, Dull TJ, Gray A, Coussens L, Liao YC, Tsubokawa M, et al. (1985) Human insulin receptor and its relationship to the tyrosine kinase family of oncogenes. Nature 313(6005):756-61

Ullrich A, Gray A, Tam AW, Yang-Feng T, Tsubokawa M, Collins C, Henzel W, Le Bon T, Kathuria S, Chen E, et al. (1986) Insulin-like growth factor I receptor primary structure: comparison with insulin receptor suggests structural determinants that define functional specificity. EMBO J 5(10):2503-12

Ullrich A, Schlessinger J. (1990) Signal transduction by receptors with tyrosine kinase activity. Cell 61(2):203-12

Unwin N. 1995 Acetylcholine receptor channel imaged in the open state. Nature 373(6509):37-43

Unwin N. 1998 The nicotinic acetylcholine receptor of the Torpedo electric ray. J Struct Biol 121(2):181-90

Van Horn DJ, Myers MG Jr, Backer JM. (1994) Direct activation of the phosphatidylinositol 3'-kinase by the insulin receptor. J Biol Chem 269(1):29-32

van der Geer P, Hunter T, Lindberg RA.(1994) Receptor protein-tyrosine kinases and their signal transduction pathways. Annu Rev Cell Biol 10:251-337

Van Heel M. (1987) Angular reconstruction: a posteriori assignment of projection directions for 3D reconstruction. Ultramicroscopy 21:111-24

Wagenknecht T, Berkowitz J, Grassucci R, Timerman AP, Fleischer S. (1994) Localization of calmodulin binding sites on the ryanodine receptor from skeletal muscle by electron microscopy. Biophys J 67(6):2286-95

Walz T, Hirai T, Murata K, Heymann JB, Mitsuoka K, Fujiyoshi Y, Smith BL, Agre P, Engel A.(1997) The three-dimensional structure of aquaporin-1. Nature 387(6633):624-7

Ward CW. (1999) Members of the insulin receptor family contain three fibronectin type III domains. Growth Factors 16(4):315-22

Waugh SM, DiBella EE, Pilch PF. (1989) Isolation of a proteolytically derived domain of the insulin receptor containing the major site of cross-linking/binding. Biochemistry 28(8):3448-55

Wedekind F, Baer-Pontzen K, Bala-Mohan S, Choli D, Zahn H, Brandenburg D. (1989) Hormone binding site of the insulin receptor: analysis using photoaffinity-mediated avidin complexing. Biol Chem Hoppe Seyler 370(3):251-8

Wells JA. (1996) Hormone mimicry. Science 273(5274):449-50

White MF. (1994) The IRS-1 signaling system. Curr Opin Genet Dev 4(1):47-54

White MF. (1996) The IRS-signalling system in insulin and cytokine action. Philos Trans R Soc Lond B Biol Sci 351(1336):181-9

White MF, Kahn CR. (1994) The insulin signaling system. J Biol Chem 269(1):1-4

White MF, Maron R, Kahn CR. (1985) Insulin rapidly stimulates tyrosine phosphorylation of a Mr-185,000 protein in intact cells. Nature 318(6042):183-6

White MF, Livingston JN, Backer JM, Lauris V, Dull TJ, Ullrich A, Kahn CR. (1988) Mutation of the insulin receptor at tyrosine 960 inhibits signal transmission but does not affect its tyrosine kinase activity. Cell 54(5):641-9

White MF, Kahn CR. (1994) The insulin signaling system. J Biol Chem 269(1):1-4

Whittaker M, Wilson-Kubalek EM, Smith JE, Faust L, Milligan RA, Sweeney HL. (1995) A 35-A movement of smooth muscle myosin on ADP release. Nature 378(6558):748-51

Wilden PA, Kahn CR, Siddle K, White MF. (1992) Insulin receptor kinase domain autophosphorylation regulates receptor enzymatic function. J Biol Chem 267(23):16660-8

Wilden PA, Boyle TR, Swanson ML, Sweet LJ, Pessin JE. (1986) Alteration of intramolecular disulfides in insulin receptor/kinase by insulin and dithiothreitol: insulin potentiates the apparent dithiothreitol-dependent subunit reduction of insulin receptor. Biochemistry 25(15):4381-8

Whittaker J, Okamoto AK, Thys R, Bell GI, Steiner DF, Hofmann CA. (1987) High-level expression of human insulin receptor cDNA in mouse NIH 3T3 cells. Proc Natl Acad Sci U S A 84(15):5237-41

Whittaker J, Okamoto A. (1988) Secretion of soluble functional insulin receptors by transfected NIH3T3 cells. J Biol Chem 263(7):3063-6

Williams JF, McClain DA, Dull TJ, Ullrich A, Olefsky JM. (1990) Characterization of an insulin receptor mutant lacking the subunit processing site. J Biol Chem 265(15):8463-9

Wilkinson DA, Marion TN, Tillman DM, Norcum MT, Hainfeld JF, Seyer JM, Carlson GM. (1992) An epitope proximal to the carboxyl terminus of the alpha-subunit is located near the lobe tips of the phosphorylase kinase hexadecamer. J Mol Biol 235(3):974-82

Williams PF, Mynarcik DC, Yu GQ, Whittaker J. (1995) Mapping of an NH2-terminal ligand binding site of the insulin receptor by alanine scanning mutagenesis. J Biol Chem 270(7):3012-6

Yang-Feng TL, Francke U, Ullrich A. (1985) Gene for human insulin receptor: localization to site on chromosome 19 involved in pre-B-cell leukemia. Science 228(4700):728-31

Yamada K, Goncalves E, Kahn CR, Shoelson SE. (1992) Substitution of the insulin receptor transmembrane domain with the c-neu/erbB2 transmembrane domain constitutively activates the insulin receptor kinase in vitro. J Biol Chem 267(18):12452-61

Yamauchi K, Pessin JE. (1994) Insulin receptor substrate-1 (IRS1) and Shc compete for a limited pool of Grb2 in mediating insulin downstream signaling. J Biol Chem 269(49):31107-14

Yamaguchi Y, Flier JS, Yokota A, Benecke H, Backer JM, Moller DE. (1991) Functional properties of two naturally occurring isoforms of the human insulin receptor in Chinese hamster ovary cells. Endocrinology 129(4):2058-66

Yeung CW, Moule ML, Yip CC. (1980) Photoaffinity labeling of insulin receptor with an insulin analogue selectively modified at the amino terminal of the B chain. Biochemistry 19(10):2196-203

Yip CC. (1991) Insulin receptor: aspects of its structure and function. Adv Exp Med Biol 334:79-88

Yip CC. (1992) The insulin-binding domain of insulin receptor is encoded by exon 2 and exon 3. J Cell Biochem 48(1):19-25

Yip CC. (1993) The insulin-binding domain of insulin receptor is encoded by exon 2 and exon 3. J Cell Biochem 1992 48(1):19-25

Yip CC, Yeung CW, Moule ML. (1978) Photoaffinity labeling of insulin receptor of rat adiopocyte plasma membrane. J Biol Chem 253(6):1743-5

Yip CC, Yeung CW, Moule ML (1980) Photoaffinity labeling of insulin receptor proteins of liver plasma membrane preparations. Biochemistry 19(1):70-6

Yip CC, Moule ML, Yeung CW. (1982) Subunit structure of insulin receptor of rat adipocytes as demonstrated by photoaffinity labeling. Biochemistry 21(12):2940-5

Yip CC, Hsu H, Patel RG, Hawley DM, Maddux BA, Goldfine ID. (1988) Localization of the insulin-binding site to the cysteine-rich region of the insulin receptor alpha-subunit. Biochem Biophys Res Commun 157(1):321-9

Yip CC, Grunfeld C, Goldfine ID. (1991) Identification and characterization of the ligand-binding domain of insulin receptor by use of an anti-peptide antiserum against amino acid sequence 241-251 of the alpha subunit. Biochemistry 30(3):695-701

Yip CC, Jack E. (1992) Insulin receptors are bivalent as demonstrated by photoaffinity labeling. J Biol Chem 267(19):13131-4

Yonezawa K, Roth RA. (1991) Assessment of the in situ tyrosine kinase activity of mutant insulin receptors lacking tyrosine autophosphorylation sites 1162 and 1163. Mol Endocrinol 5(2):194-200

Zhang B, Roth RA. (1991) A region of the insulin receptor important for ligand binding (residues 450-601) is recognized by patients' autoimmune antibodies and inhibitory monoclonal antibodies. Proc Natl Acad Sci U S A 88(21):9858-62

Zhang B, Salituro G, Szalkowski D, Li Z, Zhang Y, Royo I, Vilella D, Diez MT, Pelaez F, Ruby C, Kendall RL, Mao X, Griffin P, Calaycay J, Zierath JR, Heck JV, Smith RG, Moller DE. (1999) Discovery of a small molecule insulin mimetic with antidiabetic activity in mice. Science 284(5416):974-7

Zhou ZH, He J, Jakana J, Tatman JD, Rixon FJ, Chiu W. (1995) Assembly of VP26 in herpes simplex virus-1 inferred from structures of wild-type and recombinant capsids. Nat Struct Biol 2(11):1026-30

Zhou ZH, Prasad BV, Jakana J, Rixon FJ, Chiu W. (1994) Protein subunit structures in the herpes simplex virus A-capsid determined from 400 kV spot-scan electron cryomicroscopy. J Mol Biol 242(4):456-69

Zhou ZH, Macnab SJ, Jakana J, Scott LR, Chiu W, Rixon FJ. (1998) Identification of the sites of interaction between the scaffold and outer shell in herpes simplex virus-1 capsids by difference electron imaging. Proc Natl Acad Sci U S A 95(6):2778-83